Nanocarbons syntheses for advanced electrical and thermal applications

Rosangela Piscitelli

Unione Europea

Ministero dell'Istruzione, dell'Università e della Ricerca

UNIVERSITÀ DEGLI STUDI DI SALERNO

FONDO SOCIALE EUROPEO

Programma Operativo Nazionale 2000/2006
"Ricerca Scientifica, Sviluppo Tecnologico, Alta Formazione"
Regioni dell'Obiettivo 1 – Misura III.4
"Formazione superiore ed universitaria"

Department of Industrial Engineering

Ph.D. Course in Chemical Engineering
(XV Cycle-New Series, XXIX Cycle)

NANOCARBONS SYNTHESES FOR ADVANCED ELECTRICAL AND THERMAL APPLICATIONS

Supervisor
Prof. Maria Sarno

Ph.D. student
Rosangela Piscitelli

Scientific Referees
Prof. Paolo Ciambelli
Prof. Claudio Ampelli
Dott. Sergio Galvagno

Ph.D. Course Coordinator
Prof. Ernesto Reverchon

A Claudio

Ringraziamenti

Desidero ringraziare tutti coloro che hanno contribuito alla realizzazione di questo lavoro.

Un ringraziamento speciale alla Prof.ssa Maria Sarno che ha creduto in me fin dal primo momento e mi ha sostenuta con grande energia determinazione e professionalità dal primo all'ultimo giorno di questo difficile ed agognato percorso.

Ringrazio sentitamente il Prof. Paolo Ciambelli per avermi fatto da guida, per la sua visione di insieme e per la professionalità che da sempre lo contraddistingue.

Grazie alla Dott.ssa Claudia Cirillo per il suo fondamentale contributo nella realizzazione di questa tesi. Grazie per la disponibilità, la lealtà e l'amicizia che mostra sempre nei miei confronti.

Ringrazio inoltre il gruppo del dipartimento "Ambiente Cambiamenti Globali e Sviluppo Sostenibile" dell'ENEA che si occupa della preparazione del carburo di silicio per avermi consentito di poter lavorare su questo materiale così interessante.

Ringrazio Claudio per essere stato al mio fianco in ogni momento di questo percorso, per la pazienza, l'aiuto e la disponibilità che non mi fa mai mancare.

Ringrazio mia madre per aver avermi spronata in ogni momento di difficoltà.

Pubblicazioni

"Supercapacitor electrodes made of exhausted activated carbon derived SiC nanofilamment coated by graphene" Sarno M., Galvagno S., Piscitelli R., Portofino S., Ciambelli P. Industrial Engineering Chemistry Reserch 55 (20) 2016

"New Designed procedure for G/SiO2/SiC Nano-heterojunctions growth on recycled 3C-SiC powder" Sarno M., Galvagno S., Piscitelli R., Portofino S., Cirillo C., Ciambelli P. Chemical Engineering Transaction Vol. 57 2017 Accepted

"Experimental, Moodelling and theoretical study of CNT growth and connection on a flip- chip Device to improve thermal management performances" Sarno M., Piscitelli R., Marra F., Cirillo C., Ciambelli P. Chemical Engineering Transaction Vol. 57 2017 Accepted

"Raman Spectroscopy to measure carbon nanotubes thermal conductivity" M. Sarno, R Piscitelli, C. Cirillo, 2017 Carbon Submitted

"Microsupercapacitor based on graphene". "International Conference on Advanced Energy Materials" M. Sarno, R. Piscitelli. September 2017, England Submitted.

Index

List of Figures

Abstract

Carbon nanotubes are unique nanostructure with remarkable electronic, mechanical and thermal properties, some stemming from the close relation between carbon nanotubes and graphite, and some from their one-dimensional structure. Since their exceptional and suitable properties (high thermal and electrical conductivity, high thermal stability, relevant mechanical and field emission properties) they have soon attracted great attention.

Graphene is the first two-dimensional (2D) atomic crystal available to us. Since its discovery in 2004, graphene has captured the attention and the imagination of worldwide researchers thank to its supreme properties.

Carbon nanotubes and graphene are considered today the building blocks of nanotechnology.

In such light, this thesis work has been focused to develop industrial scalable processes, starting from research at lab scale on carbon nanotubes and graphene formation, to explore their potentialities for electrical and thermal applications, e.g. microelectronic devices.

In particular, graphene has been obtained at atmospheric pressure and low temperature on exhausted activated carbon-derived SiC nanoparticles (Chapter II). The graphene's growth, traced by online analyzers, has been obtained from an external source of carbon, in particular by methane/hydrogen chemical vapor deposition (CVD). Recycled SiC has been chosen as growth substrate to carry out a convenient process and to increase the added value of the recycled, combining the favorable properties of different substances. Therefore, the SiC powder and the composite material obtained have been carefully characterized by the combined use of different techniques and tested for energy storage applications, e.g. due to their "fine pitch" for microsupercapacitor. The results show a very high capacitances up to 114.7 F/g for SiC alone and three times higher in the presence of graphene with an excellent cycle stability

Moreover, few layer graphene/SiO_2/SiC (G/SiO_2/SiC) core-layers-sheath nano-heterojunctions were obtained (Chapter II) by a new easy and cheap designed procedure by thermal annealing at atmospheric pressure and low temperature on the SiC powder. The advanced materials obtained were carefully characterized by the combining use of different techniques: transmission electron microscopy (TEM) with EDAX probe, scanning electron microscopy (SEM), X-ray diffraction analysis, Raman spectroscopy, thermogravimetric analysis coupled with quadrupole mass detector (TG-DTG-MASS).

Finally, in Chapter III an experimental, modelling and theoretical study of CNT growth and connection on a chip device with a flip chip

configuration used to improve thermal management performances, in order to elaborate board design analysis, was reported. CNTs growth was obtained for the first time on AlN substrate typically used in high power electronic. An innovative technique was developed to measure thermal conductivity, of 1698,5 W/mK, for an isolated CNT. Moreover, the aim of the work was to study the role of the design parameters to mitigate the effects of a non-correct thermal management obtained with the help of high thermal conductive CNT connections bumps.

With the support of a COMSOL MULTIPHYSICS simulator we evaluated thermal performances to help in a preliminary phase the board design. We worked on a configuration that would allow the direct integration into flip-chip devices in order to reduce the thermal contact resistance at interfaces from the die through the heat spreader and the junction temperature and thermal crosstalk.

Introduction

Carbon nanomaterials such as carbon nanotubes (CNT) or graphene, are interesting materials for future microelectronics due to their outstanding electrical, mechanical and optical properties as well as their high surface area.

Carbon nanotubes (CNTs) are an allotrope of carbon, consisting in a graphene rolled into a tube.

Carbon Nanotubes can be achieved by several techniques, e.g. Arc discharge and Laser ablation, Plasma arc Jet, Chemical Vapor deposition (CVD).

Graphene is a flat monolayer of carbon atoms tightly packed into a two-dimensional (2D) honeycomb lattice, and is a basic building block for graphitic materials of all other dimensionalities.

Graphene can be achieved through different methods, like mechanical exfoliation using "scotch tape method", liquid-phase exfoliation of graphite exposing the materials to a solvent, epitaxial growth on SiC.

Starting from research at lab scale on carbon nanotubes and graphene a large scale and economical synthesis of three different nano-materials for several microelectronic applications was carried out.

In particular, the studies were focused on:

- The realization of graphene on recycled SiC to achieve a nano composite material tested for energy storage applications, e.g. due to their "fine pitch" for microsupercapacitor.
- The development of a nano-heterojunctions made of few layer graphene/SiO_2/SiC core-layers-sheath obtained by a new easy and cheap designed procedure by thermal annealing at atmospheric pressure and low temperature on the 3C-SiC powder derived from exhausted activated carbon.
- An experimental, modelling and theoretical study of CNT growth and connection on a chip device with a flip chip configuration used to improve thermal management performances, in order to elaborate board design analysis. Thermal performances of this device have been evaluated with the support of COMSOL MULTIPHYSICS simulator. An innovative technique to measure thermal conductivity for an isolated CNT was developed.

Objectives

The goal of the research has been to develop industrial scalable processes starting from research at lab scale on carbon nanotubes and graphene formation, to explore their potentialities for electrical and thermal applications, e.g. microelectronic devices.

In particular, the targets have been:

- The preparation of graphene at atmospheric pressure and low temperature on exhausted activated carbon-derived SiC nanoparticle, for supercapacitor applications.

- The preparation of few layer graphene/SiO_2/SiC core-layers-sheath nano-heterojunctions.

- The CNT growth and connection on a high power amplifier device with a flip chip configuration to improve thermal management performances using an experimental, modeling and theoretical study with COMSOL MULTIPHYSICS simulator.

- To develop an innovative technique to measure thermal conductivity for an isolated CNT.

Chapter I

Nanocarbons synthesis

Carbon is the element in the periodic table that provides the basis for life on Earth. It is also important for many technological applications, ranging from drugs to synthetic materials. This role is a consequence of carbon's ability to bind to itself and to nearly all elements in almost limitless variety. The resulting structural diversity of organic compounds and molecules is accompanied by a broad range of chemical and physical properties.

Carbon, one of the most common element on Earth, occurs naturally in many forms and as a component in countless substances.

Carbon has long been known to exist in three forms, namely, amorphous carbon, graphite, and diamond (Figure I.1) "Dai et al. (2012)".

Depending on how the carbon atoms are arranged, their properties vary. For example, graphite is soft and black and the stable, common form of carbon with strong covalent bonding in the carbon plane and the much weaker van der Waals interactions in the transverse direction between the layers (Figure I.1 a). Graphite's common usage is as the core of a pencil, where flakes of graphite slide off the bulk material and remain as a mark on paper.

Diamond is hard and transparent with each carbon atom bound to four other carbon atoms in a regular lattice (Figure I.1 b). It is constituted by a crystal lattice of carbon atoms arranged in a tetrahedral structure. Each carbon atom thus forms four covalent bonds with four neighboring atoms, completely filling its outer electron shell and resulting in one of the hardest and most valued substances in human history.

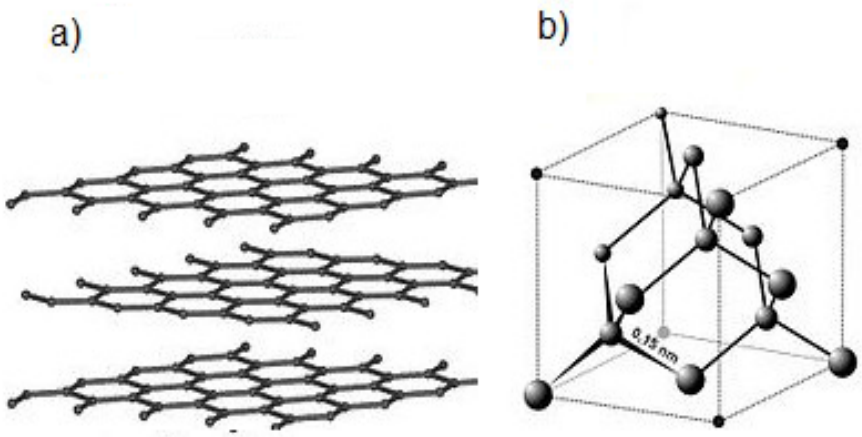

Figure I.1 *Images of crystal structure of: graphite (a) and diamond (b)*

But, in the last decade, three nanoscale forms of carbon have attracted widespread attention because of their novel properties: buckyballs, carbon nanotubes, and graphene.

A buckyball is created by collapsing yet another dimension. A buckyball is a small segment of a carbon nanotube that has been pinched together at both ends to form a hollow sphere of carbon atoms. The 60-carbon buckyball was the first carbon nanomaterial to gain widespread attention.

Carbon-60 (C60) is probably the most studied individual type of nanomaterial. The spherical shape of C60 is constructed from twelve pentagons and twenty hexagons and resembles a soccer ball. Buckyballs have many proposed uses, such as for example encapsulation of reactive compounds in chemistry.

Carbon nanotubes (CNTs) are another allotrope of carbon. They can be thought of as ribbons of graphene that have been rolled into a tube. Due to the strength of the bonds in a hexagonal carbon lattice, nanotubes are one of the strongest fibers ever discovered.

Actually the most recent carbon nanomaterial to be widely studied is graphene. Its basic structure is very simple: it is formed by a 6-carbon ring of atoms, and then tessellate that hexagon to form a two dimensional (2D) hexagonal honeycomb lattice. Such a 2D sheet is known as graphene.

Graphene's properties are striking in a number of respects, but probably most notable is that a single graphene sheet is quite stable and mechanically resilient, as well as very electrically conductive.

Graphene is the building block for carbon nanotubes and buckyball "Geim and Novoselov (2007)".

Fullerene, or buckyball, is formed by wrapping up graphene into zero dimensional (0D) buckyball; carbon nanotube is formed by rolling up graphene into 1D cylinder and graphite is formed by stacking graphene into 3D structure (Figure I.2). For example, the crystalline form of graphite consists of many graphene sheets stacked together.

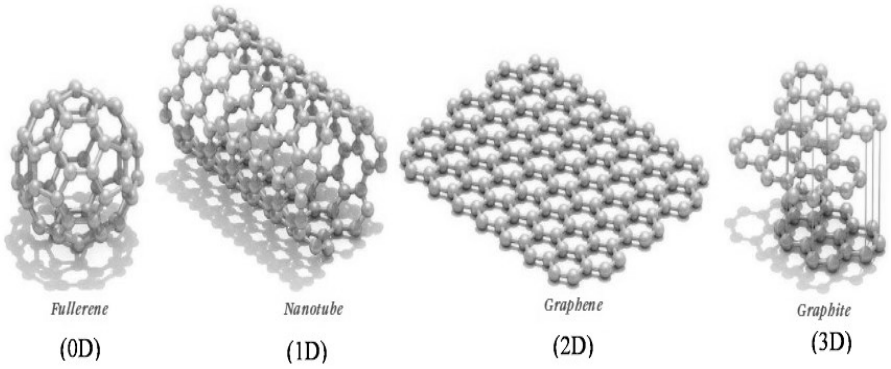

Figure I.2 *Carbon allotropes from 0D to 3D*

Graphene-like structures were already known of since the 1960's "Boehm et al. (1962), Van Bommel et al. (1975), Forbeaux et al. (1998), Oshima et al. (2000)" but there were experimental difficulties in isolating single layers in such a way that electrical measurements could be performed on them, and there were doubts that this was practically possible.

It is interesting to consider that everyone who has used an ordinary pencil has probably produced graphene-like structures without knowing it. A pencil contains graphite, and when it is moved on a piece of paper, the graphite is cleaved into thin layers that end up on the paper and make up the text or drawing that we are trying to produce. A small fraction of these thin layers will contain only a few layers or even a single layer of graphite, *i.e.* graphene.

Thus, the difficulty was not to fabricate the graphene structures, but to isolate sufficiently large individual sheets in order to identify and characterize the graphene and to verify its unique two-dimensional (2D)

properties. This is what Geim, Novoselov, and their collaborators succeeded in doing .

Ever since the discovery of the carbon nanotubes, several ways of preparing them have been explored. In particular, besides multi wall (MWNTs) and single wall (SWNTs) nanotubes have been prepared.

This chapter summarizes the progress made in recent years in growing carbon nanotubes by various methods such as arc-discharge, laser ablation and chemical vapour deposition (CVD). The growth of nanotubes materials by CVD will be focused on, because CVD is a highly promising technique in order to achieve defect-free materials by controlling the growing process during the synthesis operation.

Graphene is the name given to a flat monolayer of carbon atoms tightly packed into a two-dimensional (2D) honeycomb lattice, and is a basic building block for graphitic materials of all other dimensionalities (Figure II.1) “Geim and Novoselov (2007)”.

The term graphene was coined in 1962 as a combination of graphite and the suffix -ene by Hanns-Peter Boehm and described single-layer carbon foils. The crystalline or "flake" form of graphite consists of many graphene sheets stacked together.

In 2004 physicists at the University of Manchester and the Institute for Microelectronics Technology, Chernogolovka, Russia, first isolated individual graphene planes by using adhesive tape. They also measured electronic properties of the obtained flakes and showed their unique properties.

The Royal Swedish Academy of Sciences has awarded the Nobel Prize in Physics for 2010 to Andre Geim and Konstantin Novoselov, both of the University of Manchester, "*for groundbreaking experiments regarding the two-dimensional material graphene*".

A thin flake of ordinary carbon, just one atom thick, lies behind Nobel Prize in Physics. Geim and Novoselov have shown that carbon in such a flat form has exceptional properties that originate from the remarkable world of quantum physics.

Geim and Novoselov extracted the graphene from a piece of graphite such as is found in ordinary pencils. Using regular adhesive tape they managed to obtain a flake of carbon with a thickness of just one atom. This at a time when many believed it was impossible for such thin crystalline materials to be stable.

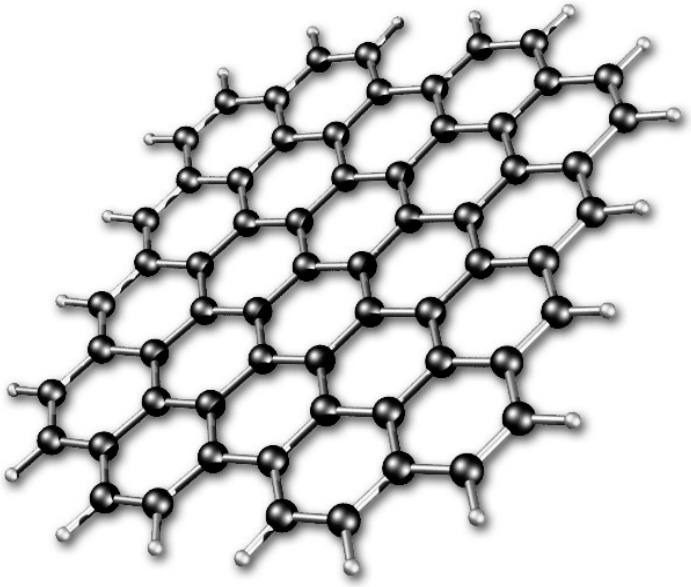

Figure I.3 *Structure of graphene: an atomic-scale honeycomb lattice made of carbon atoms*

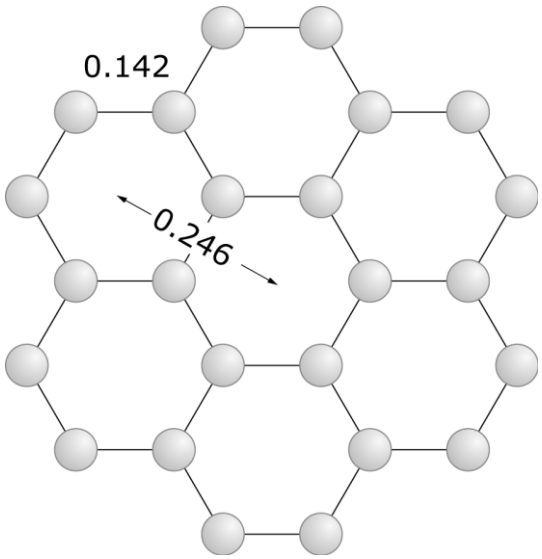

Figure I.4 *The honeycomb atomic lattice structure*

However, with graphene, it's possible to study a new class of two-dimensional materials with unique properties. Also a vast variety of practical applications now appear possible including the creation of new materials and the manufacture of innovative electronics.

Since it is practically transparent and a good conductor, graphene is suitable for producing transparent touch screens, light panels, and maybe even solar cells.
When mixed into plastics, graphene can turn them into conductors of electricity while making them more heat resistant and mechanically robust. This resilience can be utilized in new super strong materials, which are also thin, elastic and lightweight. In the future, satellites, airplanes, and cars could be manufactured out of the new composite materials.

Atomic Structure

In graphene, carbon atoms are arranged in a honeycomb lattice with angles of 120° as shown in Figure II.2. The carbon-carbon bond length in graphene is about 0.142 nanometers. We can see this atomic arrangement as a combination of benzene rings with a center-to-center distance of 0.246 nanometers.

Graphene sheets stack to form graphite with an interplanar spacing of 0.335 nm, which means that a stack of three million sheets would be only one millimeter thick.

Properties of graphene

Properties of graphene are determined mainly by its structural conformation, in particular by two unique features that affect its properties and material make it truly extraordinary. The first is the structural perfection: it is formed only by carbon atoms joined together by strong bonds and at the same time flexible, forming a crystalline structure practically, completely free of defects such as atoms out of place or missing. The second peculiarity is that the electrons behave as massless particles, such as photons, with an extremely high electron mobility (μ), equal to 15000 $cm^2 \cdot V^{-1} \cdot s^{-1}$ at room temperature. This makes this unique nanomaterial and suitable for many innovative applications “Geim and Novoselov et al. (2007)”.

Density of graphene

The unit hexagonal cell of graphene contains two carbon atoms and has an area of 0.052 nm^2. Thus, its density is 0.77 mg/m^2 “Nobel Physics Laureates (2010)”.

Electronics properties

One of the most useful properties of graphene is that it is a zero-overlap semimetal (with both holes and electrons as charge carriers) with very high electrical conductivity. Carbon atoms have a total of 6 electrons; 2 in the inner shell and 4 in the outer shell. The 4 outer shell electrons in an individual carbon atom are available for chemical bonding, but in graphene, each atom is connected to 3 other carbon atoms on the two dimensional plane, leaving 1 electron freely available in the third dimension for electronic conduction. These highly-mobile electrons are called pi (π) electrons and are located above and below the graphene sheet. These pi orbitals overlap and help to enhance the carbon to carbon bonds in graphene. Fundamentally, the electronic properties of graphene are dictated by the bonding and anti-bonding (the valance and conduction bands) of these pi orbitals.

Combined research over the last 50 years has proved that at the Dirac point in graphene, electrons and holes have zero effective mass. This occurs because the energy – movement relation (the spectrum for excitations) is linear for low energies near the 6 individual corners of the Brillouin zone. These electrons and holes are known as Dirac fermions, or Graphinos, and the 6 corners of the Brillouin zone are known as the Dirac points. Due to the zero density of states at the Dirac points, electronic conductivity is actually quite low. However, the Fermi level can be changed by doping (with electrons or holes) to create a material that is potentially better at conducting electricity than, for example, copper at room temperature "Geim and Novoselov (2007)".

Mechanical Properties

Another of graphene's stand-out properties is its inherent strength. Due to the strength of its 0.142 Nm-long carbon bonds, graphene is the strongest material ever discovered, with an ultimate tensile strength of 130,000,000,000 Pascals (or 130 gigapascals), compared to 400,000,000 for A36 structural steel, or 375,700,000 for Aramid (Kevlar). Not only is graphene extraordinarily strong, it is also very light at 0.77 milligrams per square metre (for comparison purposes, 1 square metre of paper is roughly 1000 times heavier). It is often said that a single sheet of graphene (being only 1 atom thick), sufficient in size enough to cover a whole football field, would weigh under 1 single gram.
What makes this particularly special is that graphene also contains elastic properties, being able to retain its initial size after strain. In 2007, atomic force microscopic (AFM) tests were carried out on graphene sheets that were

suspended over silicone dioxide cavities. These tests showed that graphene sheets (with thicknesses of between 2 and 8 Nm) had spring constants in the region of 1-5 N/m and a Young's modulus (different to that of three-dimensional graphite) of 0.5 TPa. Again, these superlative figures are based on theoretical prospects using graphene that is unflawed containing no imperfections whatsoever and currently very expensive and difficult to artificially reproduce, though production techniques are steadily improving, ultimately reducing costs and complexity "Geim and Novoselov (2007)".

Optical Properties

Graphene's ability to absorb a rather large 2.3% (97.7% transmittance) of white light is also a unique and interesting property, especially considering that it is only 1 atom thick. This is due to its aforementioned electronic properties; the electrons acting like massless charge carriers with very high mobility. A few years ago, it was proved that the amount of white light absorbed is based on the Fine Structure Constant, rather than being dictated by material specifics. Adding another layer of graphene increases the amount of white light absorbed by approximately the same value (2.3%). Due to these impressive characteristics, it has been observed that once optical intensity reaches a certain threshold (known as the saturation fluence) saturable absorption takes place (very high intensity light causes a reduction in absorption). This is an important characteristic with regards to the mode-locking of fibre lasers. Due to graphene's properties of wavelength-insensitive ultrafast saturable absorption, full-band mode locking has been achieved using an erbium-doped dissipative soliton fibre laser capable of obtaining wavelength tuning as large as 30 nm.
In terms of how far along we are to understanding the true properties of graphene, this is just the tip of the iceberg. Before graphene is heavily integrated into the areas in which we believe it will excel at, we need to spend a lot more time understanding just what makes it such an amazing material. Unfortunately, while we have a lot of imagination in coming up with new ideas for potential applications and uses for graphene, it takes time to fully appreciate how and what graphene really is in order to develop these ideas into reality. This is not necessarily a bad thing, however, as it gives us opportunities to stumble over other previously under-researched or overlooked super-materials, such as the family of 2D crystalline structures that graphene has born "Bonaccorso et al. (2010)".

Thermal Properties

Graphene is a perfect thermal conductor. Its thermal conductivity was measured recently at room temperature and it is much higher than the value

observed in all the other carbon structures as carbon nanotubes, graphite and diamond (> 5000 W/mK).
The ballistic thermal conductance of graphene is isotropic, i.e. same in all directions. Similarly to all the other physical properties of this material, its 2 dimensional structure make it particularly special. Graphite, the 3D version of graphene, shows a thermal conductivity about 5 times smaller (1000 W m^{-1} K^{-1}). The phenomenon is governed by the presence of elastic waves propagating in the graphene lattice, called phonons.
The study of thermal conductivity in graphene may have important implications in graphene-based electronic devices. As devices continue to shrink and circuit density increases, high thermal conductivity, which is essential for dissipating heat efficiently to keep electronics cool, plays an increasingly larger role in device reliability "Zhu et al. (2010b)"

Chemical properties

Similar to the surface of graphite, graphene can adsorb and desorb various atoms and molecules (for example, NO_2, NH_3, K, and OH).
Weakly attached adsorbates often act as donors or acceptors and lead to changes in the carrier concentration, so graphene remains highly conductive. This can be exploited for applications as sensors for chemicals.
Other than weakly attached adsorbates, graphene can be functionalized by several chemical groups (for instances OH^-, F^-) forming graphene oxide and fluorinated graphene. It has also been revealed that single-layer graphene is much more reactive than 2, 3 or higher numbers or layers.
Also, the edge of graphene has been shown to be more reactive than the surface. Unless exposed to reasonably harsh reaction conditions, graphene is a fairly inert material, and does not react readily despite every atom being exposed and vulnerable to its surrounding "Bonaccorso et al. (2010)"

Applications of graphene

The extraordinary properties of graphene, carbon sheets that are only one atom thick, have caused researchers to consider using this material in many technology areas. Some of these are:

(i) Graphene-based electronics and optoelectronics, partially replacing conventional siliconbased electronics, because graphene has ultrafast terahertz electron mobility that gives it a very bright future for building smaller, faster, cheaper electronic devices such as ballistic transistors "Liang et al. (2007)", spintronics "Yazyev et al. (2008)", field effect transistors "Meric et al. (2008)", and optoelectronics "Bonaccorso et al. (2010)".

(ii) Graphene filled polymer composites with high electrical and thermal conductivity, good mechanical strength, and low percolation threshold, which, in combination with low-cost and largescale production, allow a variety of performance-enhanced multifunctional use in electrically conductive composites, thermal interface materials, etc. “Dikin et al. (2007), Stankovich et al. (2006)”.
Large-area CVD-grown graphene that is suitable to replace indium tin oxide (ITO) as cheaper, transparent conducting electrodes in various display applications such as touch screens, which is considered to be one of the immediate applications in a few years “Kim et al. (2009), Bae et al. (2010)”.

(iii) Another advantage over ITO is that ITO suffers from being brittle and is incapable of bending, which does not allow it to meet the requirements for flexible devices, while graphene is a more competitive solution for flexible, transparent and processable electrodes.

(iv) Graphene-based electrochemical storage energy devices such as high-performance Lithium Ion Batteries (LIBs) and ElettroCapacitors (ECs) because of their greatly improved electrochemical performance of capacity, cyclability and rate capability due to its unique 2D structure and excellent physiochemical properties “Chen et al. (2008)”.

(v) Recent research indicates many other potential applications in bio-, electrochemical, and chemical sensors “Pumera (2009)”, dye-sensitized solar cells “Wang et al. (2008)”, organic solar cells “Wang et al. (2008)”, field emission devices “Wu et al. (2009)”, catalysts “Lightcap et al. (2010)” and photocatalysts “Williams et al. (2008)”, nanogenerators “Choi et al. (2010)”, hydrogen storage “Ma et al. (2009)”, etc.
Graphene may offer other advantageous properties that outperform those of CNT and graphite, resulting in the development of new and unexpected applications.

Graphene production

The methods of preparation for graphene can be divided into two categories, top-down and bottom-up ones. The top-down methods include (i) mechanical exfoliation and (ii) chemical oxidation/exfoliation. The bottom-up methods include (i) epitaxial growth on SiC and other substrates, (ii) Chemical vapor deposition.
Each of these methods has some advantages and limitations. Among them chemical synthesis of graphene using graphite, graphite oxide (GO) is a scalable process but it leads to more defect in the graphene layer.
Currently, there are probably a dozen methods being used and developed to prepare graphene of various dimensions, shapes and quality.
The main synthesis techniques are described in the following.

Micromechanical Cleavage

The reason for the popularity of graphene in the last few years lies in how simple it is to make. Anyone with a pencil, a roll of scotch tape and a silicon wafer can start doing original experiments. In the same way that a pencil can be used to draw on paper, very thin graphite flakes can be exfoliated onto a substrate.
This technique, shown in Figure III.1 (a,b,c), involves the repeated pealing of layers of graphite. An adhesive tape is used to peel off layers from the surface of HOPG and subsequent peeling eventually leads to a single layer of graphite on the surface of a substrate like silicon oxide. Single layers of sizes up to 10 μm in size and thicker multilayer films (two or more layers) of around 100μm have been reported "Novoselov (2004)".
The yield of single layers obtained by this technique is very low (a few graphene monolayers per mm^2 of substrate area). Research on improving the yield of exfoliated single layers have led to many variants of the exfoliation technique "Liang et al. (2007)", "Song et al. (2009)". However, the size and yield of single layer graphene still remains a bottleneck in this process.

Epitaxial Graphene from Silicon Carbide

Growth of graphitic thin films on silicon carbide is well known "Van Bommel et al. (1975), Mrtensson and Owman (1996)".
Specifically they grow on the 0001 (silicon-terminated) and 0001 (carbonterminated) faces of 4H- and 6H-SiC crystals upon heating to about 1300 °C in ultra-high vacuum (UHV). It is also possible to grow these films under less demanding vacuum conditions using ovens with controlled background gas. This technique, however, does not produce atomically thin single graphene layers, rather it produces epitaxially ordered stacks of graphene.
Although the graphene obtained in the way is not structurally perfect, it shows electrical properties comparable to that of mechanically exfoliated graphene "Berger et al. (2006)".
In order to grow homogeneous mono- and few-layer graphene on SiC(0001), a suitable approach is to anneal the SiC samples at temperatures above 1600°C in an Ar atmosphere in a quartz glass reactor "Emtsev et al. (2009)".
Furthermore, it has recently been demonstrated that it is also possible to grow graphene on both SiC faces with an additional carbon supply similar to molecular beam epitaxy using relatively low temperatures of around 950°C "Al-Temimy et al. (2009)".

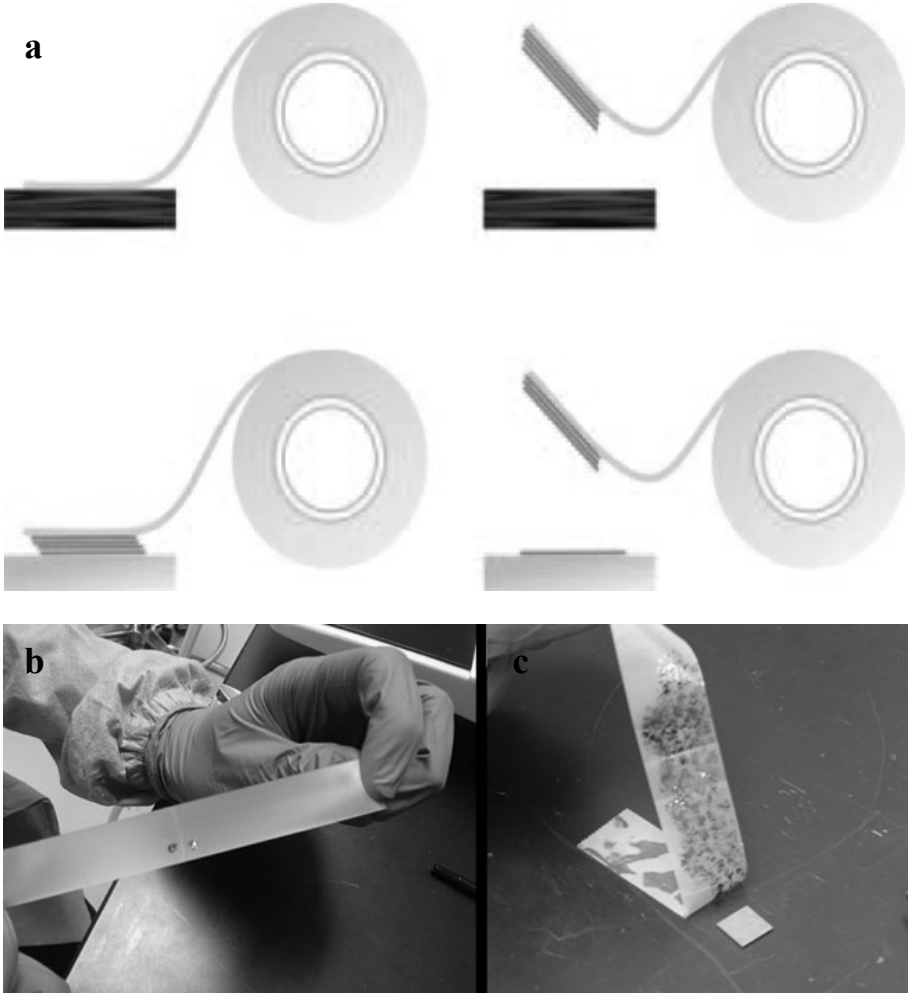

Figure I.5 *Scheme of the micromechanical cleavage technique ('Scotch tape' method) for producing graphene "Novoselov (2011)"(a), Images of: graphite flake cleaved by Scotch tape (b) tape covered with graphite pressed down on silicon wafer (c)*

Chemical Exfoliation

To achieve high quality results using a process that could be mass produced, chemical exfoliation of graphite to produce graphene monolayers have been explored "Hernandez et al. (2008)".
Liquid-phase exfoliation is based on exposing the materials to a solvent with a surface tension that favours an increase in the total area of graphite

crystallites. Typically, the solvent is non-aqueous, but aqueous solutions with surfactant can also be used.
The role of the solvent is crucial, since n-Methyl-Pyrrolidone (NMP) has a strong interaction with the honeycomb lattice, thus easily infiltrating between the planes facilitating their exfoliation. Other similar solvents were tried by the group, but NMP resulted the one with the highest yield of single layer flakes. The method (Figure III.3) is really simple and clean, since it does not involve modification of the chemical composition of graphite, and residual solvent evaporates without remarkable traces. Produced solutions provide a ratio of mono-layers over multilayers of ~ 1 wt%, ending in relatively large flakes.
Previously, other methods such as intercalation (injecting atoms between graphite layers to peel them apart) "Viculis et al. (2003)", ultrasonic heating "Chen et al. (2004)" and acid treatment "Li et al. (2008)" have produced monolayer hexagonal carbon, generally produced nanoribbons (thin flat graphene wires), not full graphene sheets.

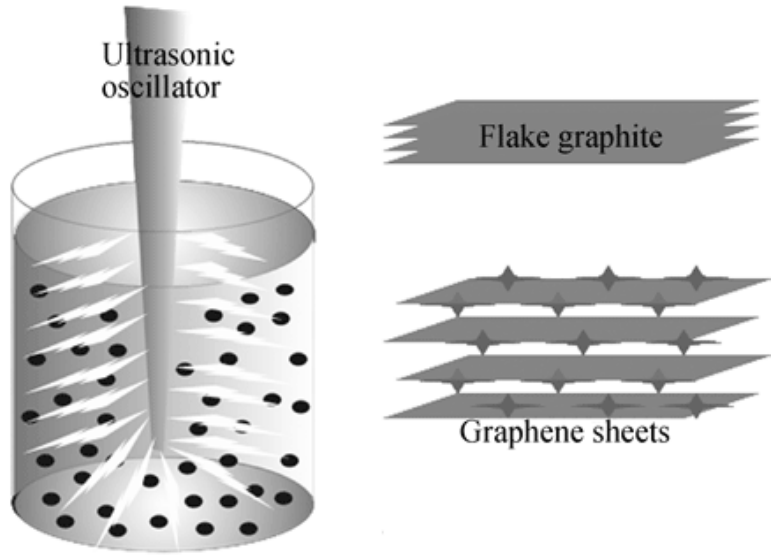

Figure I.6 *Liquid-phase exfoliation of graphite method*

Graphene grown on transition metal surfaces using Chemical Vapour Deposition (CVD)

Chemical vapor deposition (CVD) is an alternative method to mechanical exfoliation and it's used to obtain high quality graphene for large-scale production of mono or few layer graphene films on metal substrate. CVD is widely used in the microelectronics industry in processes involving the

deposition of thin films of various materials. The deposition is made from precursors in the gas phase which adsorb on the target surface producing a condensed phase of a specific material. The attractiveness of the generation of graphene by CVD is based on the fact that this technique allows for scalability as well as low cost. A schematic experimental set-up is shown in Figure III.4. The process begins with an atomically flat surface of a transition metal substrate and an appropriate carbon precursor (like in methane or ethylene). The metal substrate plays the role of catalyst. This substrate is placed in a heated furnace and is attached to a gas delivery system. The precursor molecules will be brought into contact with the substrate surface from the gas phase or from liquid phase at elevated temperature. Upon contact with the surface, the precursor molecules are cracked to form carbon atoms and form gas-phase species, leaving the carbon atoms (which are free of functionalities) attached to the substrate surface. Graphene is formed when carbon atoms after diffusion on the metal surface, encounter other carbon atoms and form bonds.
Optimization of this process over the years has triggered interest in growth of graphene on relatively inexpensive polycrystalline Ni "Kim et al. (2009)", "Obraztsov et al. (2007)", "Reina et al. (2009)" and Cu "Li et al. (2009)". substrates.

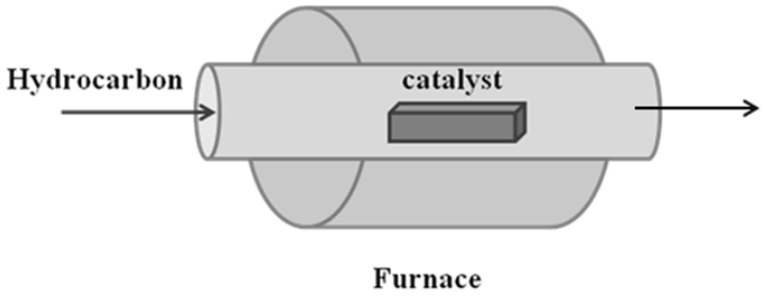

Figure I.7 *Scheme of the growth process for the synthesis of graphene using CVD*

Transfer of graphene grown on metals

Bae et al. "Bae et al. (2010)", in 2010, first reported the transfer of single layer graphene (SLG) and few layer graphene (FLG) grown on Ni, by depositing a PMMA sacrificial layer and subsequently etching the underlying Ni by aqueous HCl solution "Bae et al. (2010)". Li et al. transferred films grown by CVD on Cu, etched by iron nitrate "Li et al. (2009)". Kim et al. introduced etching by aqueous $FeCl_3$ in order to remove Ni without producing hydrogen bubbles, which may damage graphene when acid etching is used "Kim et al. (2009)".

They also reported a technique where PDMS stamps are attached directly to the graphene surface. Ni is then chemically etched by $FeCl_3$ leaving graphene attached to the Polydimethylsiloxane (PDMS). Graphene is then transferred to SiO_2 by pressing and peeling the PDMS stamp. Bae et al. "Bae et al. (2010)" also introduced roll-to-roll transfer of graphene grown by CVD on Cu foils as large as 30 x 30in^2, guided through a series of rolls: a thermal release tape was attached to the Cu+graphene foil, and then an etchant, an aqueous 0.1 M ammonium persulphate solution $(NH_4)_2S_2O_8$, removed Cu (Fugure III.5).
The tape+graphene film was then attached to a (flexible) target substrate and the supporting tape removed by heating, thus releasing graphene onto the target substrate "Bae et al. (2010)".
To avoid Fe contamination caused by $FeCl_3$ etching, ammonium persulfate $[(NH_4)_2S_2O_8]$ was used "Aleman et al. (2010)". To avoid mechanical defects caused by roll to roll transfer, a hot pressing process was developed "Kang et al. (2012)": similar to a roll-to-roll process, the Cu+graphene foil is first attached to thermal release tape and then Cu is chemically etched. The tape+graphene foil is then placed on the target substrate and both are subsequently inserted between two hot metal plates with controlled T and pressure. This results in the detachment of the adhesive tape with very low

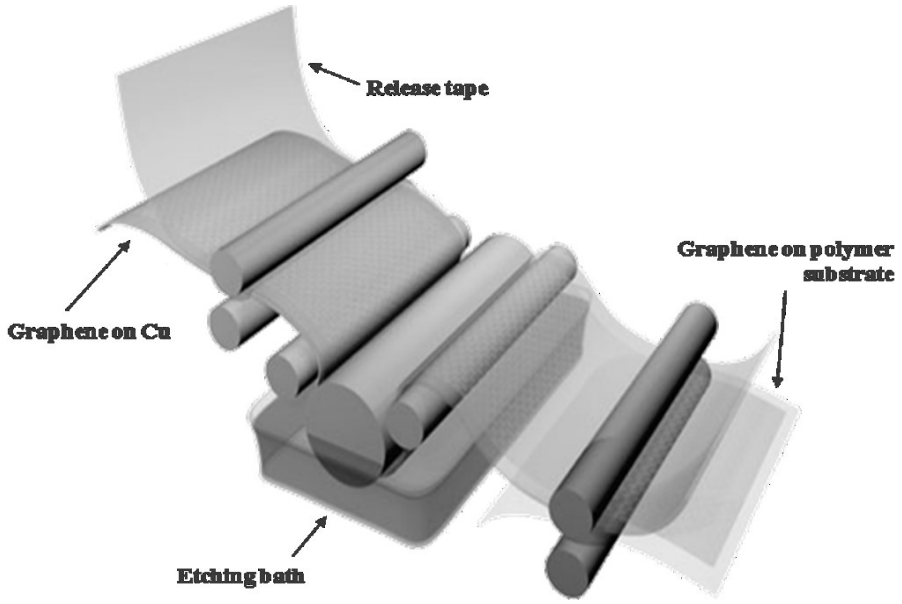

Figure I.8 *Scheme of the graphene transfer process to a substrate "Bae et al.(2010)"*

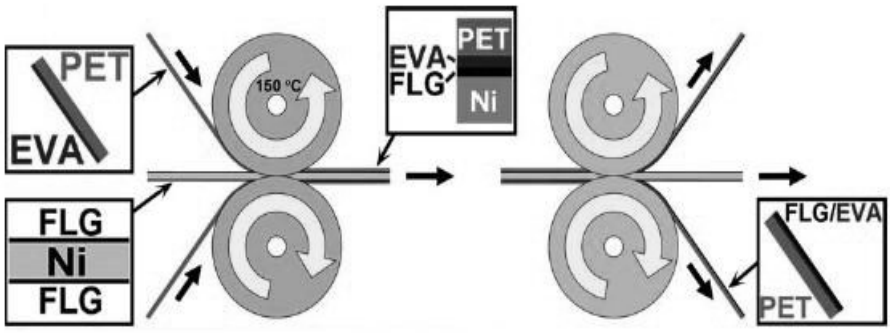

Figure I.9 *Scheme of roll-to-roll process for the transfer of FLG from Ni foil to EVA/PET substrates "Juang et al. (2010)"*

frictional stress, therefore less defects, than a roll-to-roll process "Kang et al. (2012)".
According to Juang et al. "Juang et al. (2010)" roll-to-roll process is an ideal production choice when a very low cost per unit area of deposition is required. In the process for the transfer of few layer graphene to various flexible substrates, shown in Figure III.6, commercial ethylene-vinyl acetate copolymer (EVA) coated transparent polyethylene terephthalate (PET) sheets were used as the target substrate.
At a temperature of 150°C, the EVA/PET and FLG/Ni sheets were pressed together with hot rollers to form a double-sided PET/EVA/FLG/Ni sheet. The EVA layer here plays a role of viscose between the PET and FLG. After the hot rolling step, the sheet was passed onto cold rollers at room temperature. The purpose of the cold rolling step is to separate the PET/EVA/FLG layers from the Ni surface in a uniform manner with a controlled, constant rolling speed

Multi-Walled Carbon Nanotubes

Arc discharge and Laser ablation

Arc discharge and laser ablation methods for growth of nanotubes have been actively pursued in the past ten years. Both methods involve the condensation of carbon atoms generated from evaporation of solid carbon sources. The temperature involved in these methods are close to the melting point of graphite, 3000-4000°C.

Arc discharge

In the arc discharge carbon atoms are evaporated by plasma of helium gas ignited by high currents passed through opposing carbon anode and cathode (Fig. I.1). Carbon nanotubes can be obtained by controlling the growth conditions such as the pressure of inert gas in the discharge chamber and the arcing current.

In 1992, a breakthrough in MWNTs growth by arc-discharge was first made by Ebbesen and Ajayan "Ebbesen *et al.* (1992)" who achieved growth and purification of high quality MWNTs. The syntheses were conducted in helium flow in the range of 2-3 atm, considerably higher than the pressure of gas used in the production of fullerene. A current of 60 - 100 A across a potential drop of about 25 V gives high yields of carbon nanotubes. The synthesised MWNTs have lengths on the order of ten microns and diameters in the range 5-30 nm. The nanotubes are typically bound together by strong van der Walls interactions and form tight bundles. MWNTs produced by arc-discharge are very straight, indicative of their high crystallinity. For as grown materials, there are few defects such as pentagons or heptagons existing on the sidewalls of nanotubes.

In the arc-discharge growth process the product contains carbon nanotubes and also others carbon species mainly constituted by multi-layered graphitic particles in polyhedron shapes. Purification of the tubes can be achieved by heating the as grown material in an oxygen environment to oxidise away the graphitic particles "Ebbesen end Ajayan (1992)". The polyhedral graphitic particles exhibit higher oxidation rate than MWNTs; nevertheless, the oxidation purification process also removes an appreciable amount of nanotubes. A typical example of nanotubes so obtained is shown in Fig. I.2.

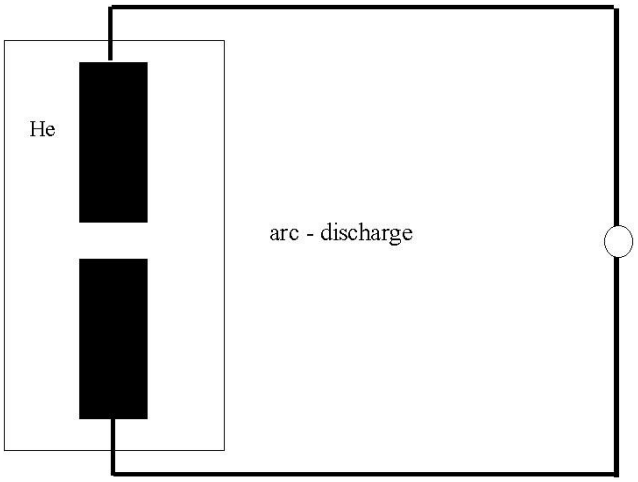

Figure I.10 *Arc-discharge schematic experimental setup*

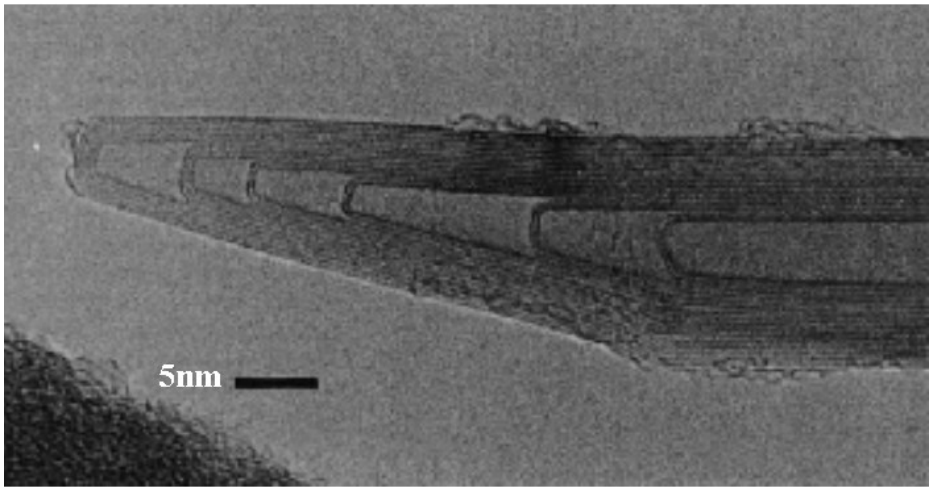

Figure I.11 *TEM image of carbon nanotubes produced by arc discharge*

Plasma arc Jet

Carbon nanotubes have been produced also by plasma arc jets "Hatta and Murata (1994)", and in large quantities, by optimizing the quenching process in an arc between a graphite anode and a cooled copper electrode "Colbert *et al.* (1994)". The product of these processes is a mixture of carbon nanotubes with different percents of amorphous carbon, fullerene. The tubes, so produced, are straight and show a small amount of structural defects.

Laser ablation

Laser ablation technique (Fig. I.3) is able to produce carbon nanotubes with the highest degree of purity. The method utilised intense laser pulses to ablate a carbon target containing a percent of nickel and/or cobalt. The target was placed in a tube-furnace heated to 1200°C. During laser ablation, a flow of inert gas was passed through the growth chamber to carry the grown nanotubes downstream to be collected on a cold finger. In contrast to the arc method, direct vaporisation allows far greater control over growth conditions, permits continuous operation, and produces nanotubes in higher yield and better quality.

By vaporisation of graphite rod with the addition of Co or Ni, it is possible to obtain materials containing until 80% of pure SWNTs with the same diameter "Guo *et al.* (1995), Thess et al. (1996)", see Fig. I.4.

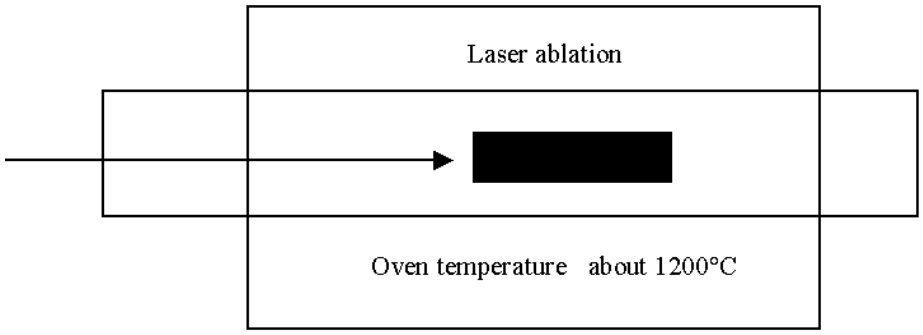

Figure I.12 *Laser ablation schematic experimental setup*

Chemical Vapour deposition (CVD)

One more effective method of generating carbon nanotubes is based on the chemical vapour deposition (CVD) of hydrocarbons over supported transition metal particles, that constitute the active species.

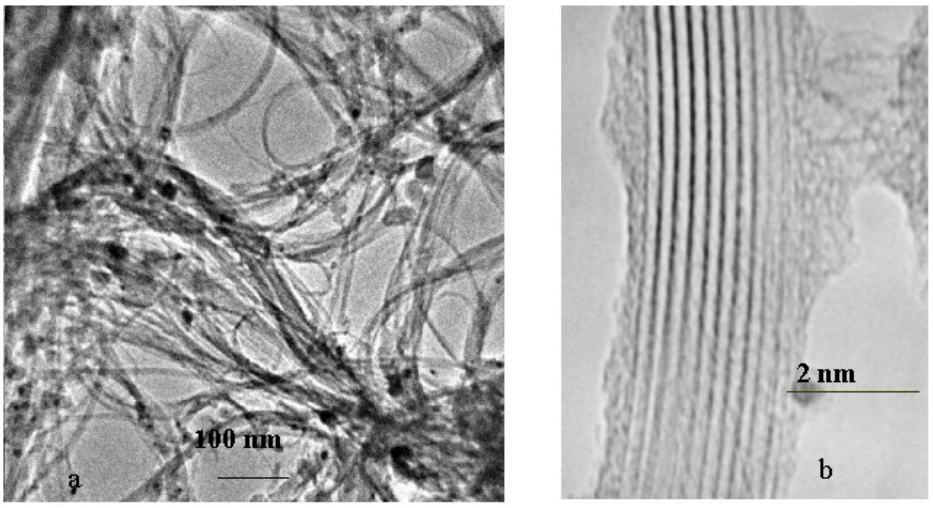

Figure I.13 *TEM images of carbon nanotubes produced by laser ablation method (a); tube wall particular (b).*

This is a successful way to synthesize carbon nanotubes, because of the lower growth temperature (below 1000°C) compared to arc-discharge or laser vaporization methods and of the possibility to control inner diameter and length of the tubes.

A schematic experimental setup for CVD growth is depicted in Fig. I.5.

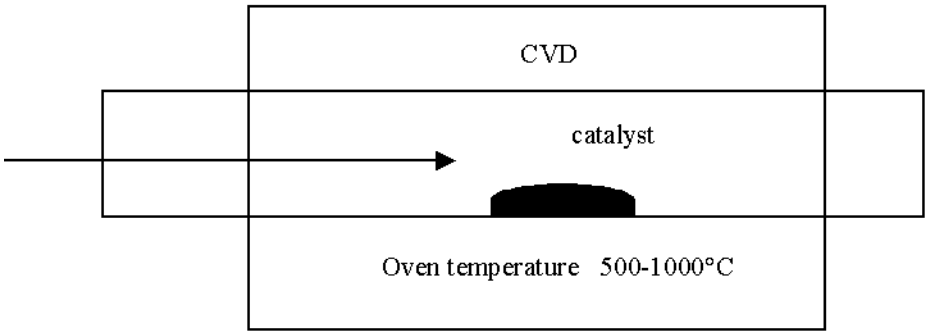

Figure I.14 *CVD schematic experimental setup*

The growth process involves heating a catalyst material to high temperatures in a tube furnace and flowing a hydrocarbon vapour through the tube reactor for a period of time. Materials grown over the catalyst are collected upon cooling the system to room temperature.

The general nanotube growth mechanism in a CVD process (see Chapter IV), involves the dissociation of hydrocarbon molecules catalysed by a transition metal, and the dissolution and saturation of carbon atoms in the metal nanoparticles. The precipitation of carbon from the saturated metal leads to the formation of tubular carbon solids in sp^2 structure. Tubule formation is favoured over other forms of carbon such as graphitic sheets with open edges. This is because a tube contains no dangling bonds and therefore is in a low energy form.

The key parameters in nanotube CVD growth are the nature of hydrocarbon and catalyst and the reaction temperature.

For MWNT growth, most of the CVD methods employ ethylene or acetylene as carbon feedstock and the growth temperature is typically in the range of 550-750°C "Ivanov *et al.* (1994), B.Nagy *et al.* (2000b), Hernadi *et al.* (1996)".

The catalytic system consists of transition metals, such as Fe, Ni, Cu and Co of several nanometers in size, used as catalysts, dispersed on a support constituted in general of metal oxides, but in some cases of zeolites.

The presence of transition metal particles is essential for the formation of nanotubes by the pyrolysis process. It has been suggested that the nanotube diameter is determined by the size of the metal particles "Rodriguez (1993)".

The length of nanotubes varies from several micrometers to several tens of micrometers.

The rationale for choosing these metals as catalyst for CVD growth of nanotubes lies in the phase diagram of the system metal-carbon.

At high temperature carbon has finite solubility in these metals, which leads to the formation of metal-carbon solutions (see Chapter IV). Iron,

cobalt and nickel are the favoured catalytic metals in laser ablation and arc-discharge too.

This simple fact may hint that laser, arc and CVD growth methods may share a common nanotubes growth mechanism, although very different approaches are used to provide carbon feedstock.

The CVD method permitting to generate the nanotubes in a wide range of their physical characteristics was gathering force in the set of works "Yacaman *et al.* (1993), Ivanov *et al.* (1994), B.Nagy *et al.* (2000b), Hernadi *et al.* (1996)".

However, these syntheses gave rise, together with carbon nanotubes, to different carbon structures, mostly amorphous generated in the support porosity or coating the outside surface of carbon nanotubes. Therefore, different methods for purification, consisting essentially in thermal and chemical oxidations, have been studied. For example, amorphous carbon can be burned away by heating the nanotubes in air "Shi at al. (1999b)".

The yield of nanotubes in a sample depends on the type of catalyst: in the presence of iron, for example, it is much higher than for cobalt. For copper catalyst a great part of carbon precipitates in an amorphous form "Chesnokov *et al.* (1994)".

The typical appearance is a tangle of tubes that after sonication exhibit the aspect shown in Fig. I.6.

Recent interest in CVD nanotube is also due to the idea that aligned and ordered nanotube structures can be grown on surface with a control that is not possible with arc-discharge or laser ablation techniques "Dai *et al.* (1999)".

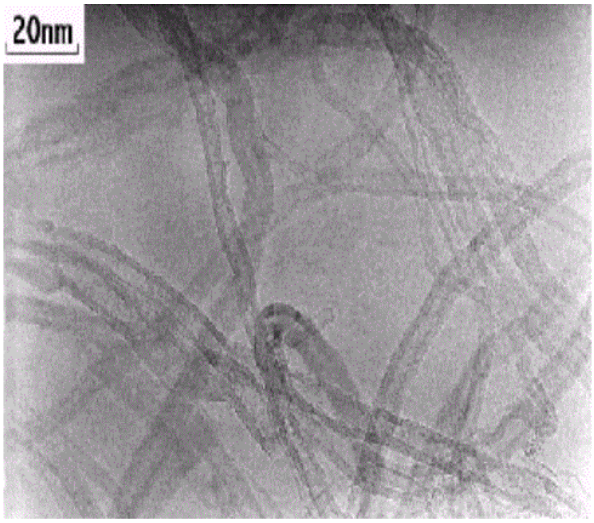

Figure I.15 *TEM images of carbon nanotubes produced by CVD method*

Methods that have been developed to obtain aligned MWNTs include CVD growth of nanotubes in the pores of mesoporous silica, an approach developed by Xie's group at the Chinese Academy of Science. The catalyst used in this case is iron oxide particles formed inside the pores of silica. The carbon feedstock is 9% acetylene in nitrogen at 180 torr pressure, and the growth temperature is 600°C. Remarkably, nanotubes with lengths up to millimetres are obtained "Li *et al.* (1996)".

Ren has grown relatively large-diameter, well-aligned MWNTs, for field emission display application, forming oriented "forest" on glass substrate using a plasma assisted CVD method with nickel as catalyst and acetylene as carbon source around 660°C "Ren *et al.* (1998)".

An extension of the method reported in "Li *et al.* (1996)" has produced self-oriented patterned arrays of CNTs on iron-coated porous silicon "Fan *et al.* (1999b)".

Dai's group has been devising growth strategies for ordered MWNTs architectures by CVD on catalytically patterned substrate. They have found that MWNTs can self-assemble into aligned structures as they grow, and the driving force for self-aligned is the van der Waals interaction between nanotubes "Dai *et al.* (2000)". The growth approach involves catalyst patterning and rational design of the substrate to enhance catalyst-substrate interactions and control the catalyst particle size. Porous silicon is found to be an ideal substrate for this approach and can be obtained by electrochemical etching of n-type silicon wafers in hydrofluoric acid/methanol solution. The resulting substrate consists of a thin nanoporous layer on the top of a macroporous layer.

The porous silicon substrate exhibit important advantages over plain silicon substrate in the synthesis of self-aligned nanotubes. Growth on substrates containing both porous silicon and plain silicon portions permits to obtain higher rate grow of nanotubes (in terms of length/min), than on porous substrate. This suggest that ethylene molecules can permeate through the macroporous silicon layer and thus efficiently feed the growth of nanotubes within the towers (Fig. I.7).

Ren et al. "Ren *et al.* (1998)" employed plasma-enhanced CVD on nickel-coated glass with acetylene and ammonia mixtures for this purpose. The mechanism of growth of nanotubes by this method and the exact role of the metal particles was investigated, a nucleation process involving the metal particles is considered to be important.

Fan et al. "Fan *et al.* (1999a)" have obtained aligned nanotubes by employing catalytic decomposition on porous silicon and plain silicon substrates patterned with iron films. Also in this case, the role of the metal particles is not completely known.

The role of the transition metal particles assumes importance in view of the report of Pan et al. "Pan *et al.* (1999)" that aligned nanotubes can be obtained by pyrolysis of acetylene over iron/silica catalytic surfaces.

In the light of the earlier work on the synthesis of carbon nanotubes by pyrolysis of mixtures of organometallic precursors and hydrocarbons, "Sen *et al.* (1997a, 1997b)" one would expect that the transition metal nanoparticles produced in situ in the pyrolysis may not only nucleate the formation of carbon nanotubes but also align them.

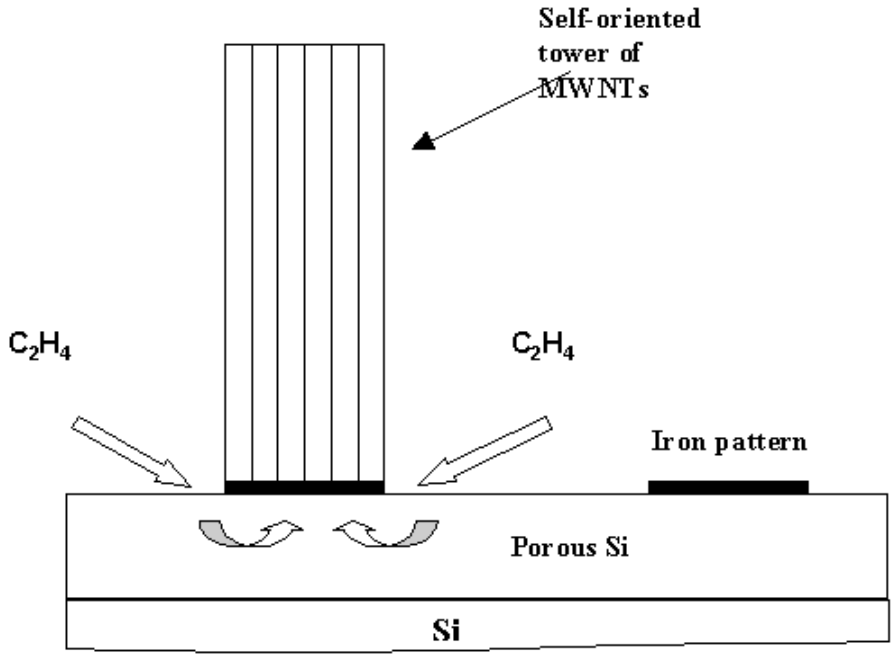

Figure I.16 *Schematic diagram of the growth process*

This aspect has been examined by carrying out the pyrolysis of metallocenes along with additional hydrocarbon sources in a suitably designed apparatus "Sen *et al.* (1997a, 1997b), Satishcumar *et al.* (1999), Rao *et al.* (1998b)". Scanning electron microscopy (SEM) images of aligned nanotubes obtained by pyrolysis of ferrocene are shown in Fig. I.8. Images a) and b) show views of the aligned nanotubes along and perpendicular to the axis of the nanotubes, respectively. Figure I.7a shows the top view of the aligned nanotubes, wherein the nanotube tips are seen, while the image in Figure I.7b shows the side view. The average length of these nanotubes is generally around 60 mm obtained either form methane and acetylene.

Recently, CVD conducted in the presence of inorganic structure-directed or templated structure have been explored to synthesize a wide variety of new carbon materials. During templated synthesis methods, substrate or precursor materials are included into the template framework in such a way that their final structure reflects shape and dimension of the templates.

Organic templates are commonly used to synthesize inorganic materials. For example, surfactants have been used to template the synthesis of MCM-41 "Asefa *et al.* (1999)", or other porous silicates "Sandi *et al.* (1999), Kresge *et al.* (1992)" and oxides "Bagshaw *et al.* (1995)".

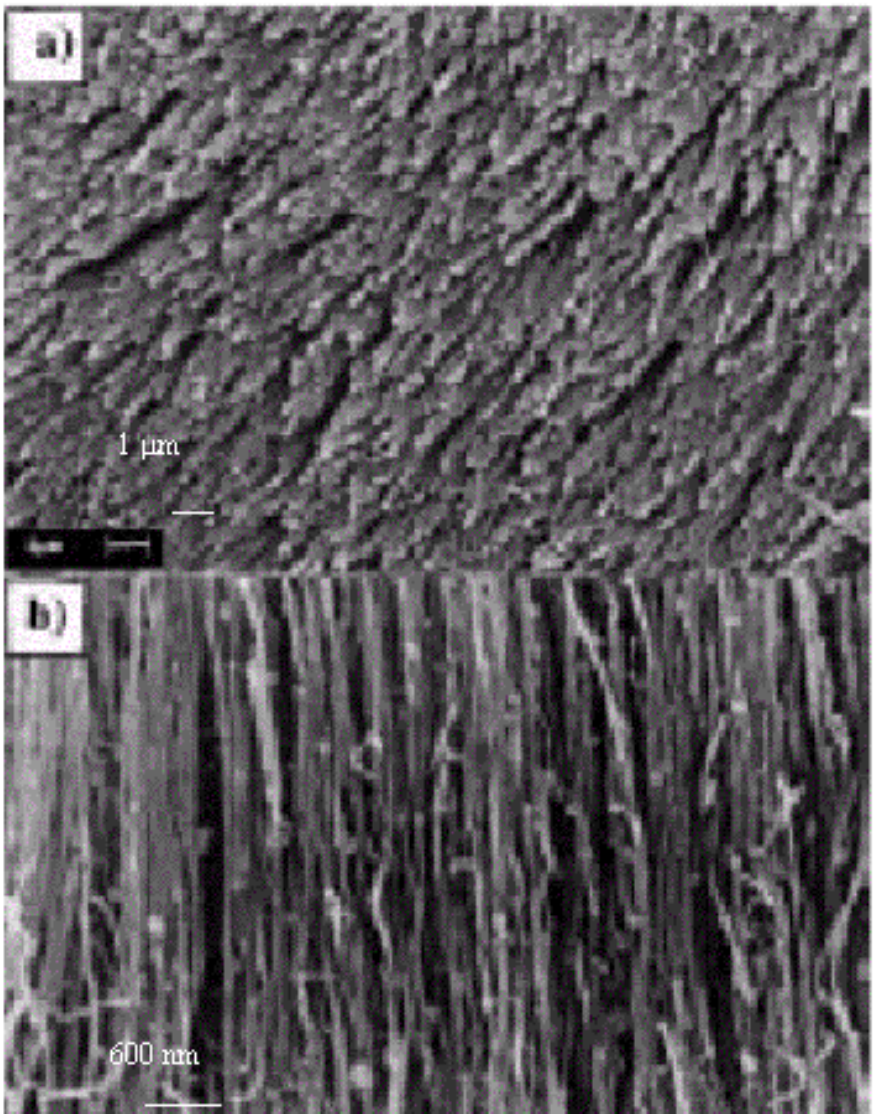

Figure I.17 *SEM images of aligned carbon nanotubes obtained by the pyrolysis of ferrocene, images a) and b) show views of the aligned nanotubes along and perpendicular to the axis of the nanotubes respectively*

In the templated synthesis method carbon nanotubes are obtained as a print of a directional structure. In this case addition of metal particles to the system is not necessary. It can lead to the production of aligned carbon nanotubes.

A major hurdle in applying CVD to template synthesis is the necessity to control the deposition rate. In fact, the pores can become blocked before the chemical vapour traverse the length of the pores.

First example of carbon nanotubes synthesis by CVD template-based method has been reported by Martin et al. "Hulteen and Martin (1997), Che *et al.* (1998)", using alumina membrane, with and without the additon of transition metal catalysts.

The use of micoporous zeolites, such as Y, ZSM-5, mordenite, L, as templates "Kyotani et al. (2003)", and only recently BEA, has been investigated. By propylene CVD carbon materials with a controlled microporosity have been obtained.

Single-Walled Carbon Nanotubes

The nanotubes obtained by the previously described methods are generally MWNTs having several graphitic sheets or layers. SWNTs can be also synthesised by using these methods.

For a long time, arc-discharge and laser–ablation have been the principal methods for obtaining nearly perfect SWNTs. Both methods are based on evaporating carbon atoms from solid carbon sources at about 3000°C, which is not efficient and limits the scale-up of SWNTs production. Recently, growth of SWNTs with structural perfection was achieved by CVD methods.

SWNTs have been first prepared by metal-catalysed direct-current arcing of graphite rods "Ichihashi and Iijima (1993), Bethune *et al.* (1993)" under helium atmosphere. The graphite anode was filled with metal powders (Fe, Co, Ni) and the cathode was pure graphite. SWNTs generally occur in the weblike material deposited behind the cathode. Various metal catalysts have been used to make SWNTs by this route.

Arc evaporation of graphite rods filled with nickel and yttrium under a helium atmosphere (660 Torr) gives rise to weblike deposits on the chamber walls near the cathode, which consist of SWNT bundles "Rao *et al.* (1998a)". HRTEM images show bundles consisting of 10 - 50 SWNTs forming highway junctions (Figure I.9). The average diameter of the SWNTs was around 1.4 nm and the length extended up to 10 mm.

SWNTs have been produced in more than 70% yield by the condensation of a laser-vaporized carbon - nickel - cobalt mixture at 1200°C "Thess *et al.* (1996)". These SWNTs were nearly uniform in diameter and self-assembled into ropes which consists of 100 to 500 tubes in a 2D triangular lattice.

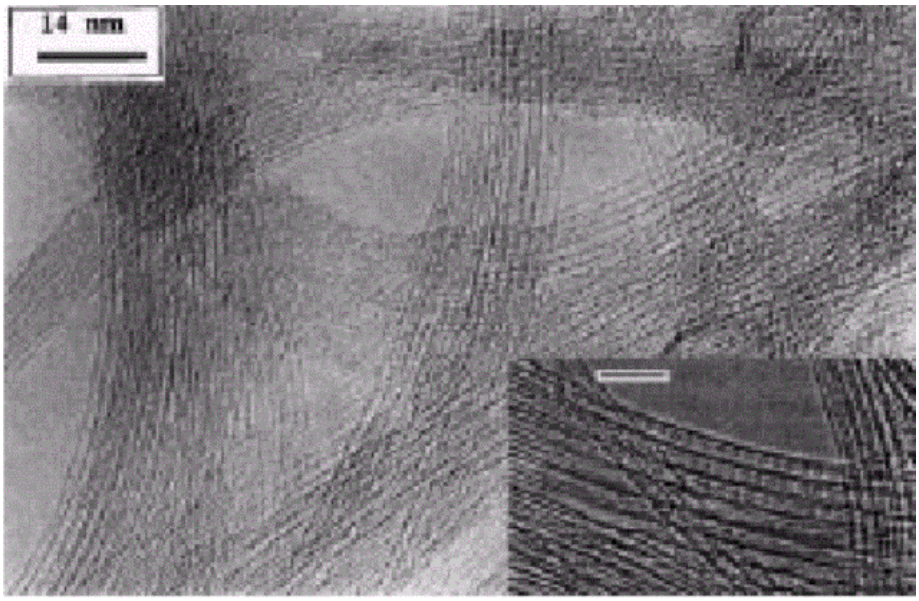

Figure I.18 *HRTEM image of SWNTs obtained by arcing graphite electrodes*

Cassel et al. (1999) found that by using methane as carbon source reaction temperatures in the range of 850-1000 °C, suitable catalyst materials and flow conditions, one can grow high quality SWNT materials by simple CVD process. High temperature is necessary to form SWNTs that have small diameters and thus high strain energies, and allow for nearly-defect free crystalline nanotubes structures. Among all hydrocarbon molecules, methane is the most stable at high temperatures against self-decomposition. Therefore, catalytic decomposition of methane by transition-metal catalyst particles is the dominant process in SWNT growth. The choice of carbon feedstock is one of the key elements to the growth of high quality SWNTs containing no defects and amorphous carbon over-coating.

Another CVD approach to SWNTs was reported by Smalley and coworkers who used ethylene as carbon feedstock and growth temperature around 800°C "Hafner *et al.* (1998)". In this case, low partial pressure ethylene was employed in order to reduce amorphous carbon formation due to self-pyrolysis/dissociatin of ethylene at high growth temperature.

Gaining an understanding of the chemistry involved in the catalyst and nanotube growth process is critical to enable materials production scale-up by CVD. The choice of many parameters in CVD requires to be rationalised in order to optimise the materials growth. Within the methane CVD approach for SWNT growth, it has been found high yield and quality SWNTs "Cassel *at al.* (1999)". Cassel at al. have developed a catalyst consisting of Fe/Mo bimetallic species supported on a sol-gel derived

alumina-silica multicomponent material. The catalyst exhibits a surface are of approximately 200 m^2/g and mesopore volume of 0.8 mL/g.

B.Nagy et al. " Colomer *et al.* (2000)" obtained SWNTs in high yield by the decomposition of methane over transition-metal-supported MgO substrates.

Different catalysts have been prepared by impregnation of MgO with ethanol solution of metal salts (Co, Ni, Fe) or a mixture of metal salts (Co-Fe) in the appropriate concentration. The used carbon source methane/hydrogen has been feed at 1000°C obtaining SWNTs with a diameter in the range 0.8-2 nm. The high resolution TEM imaging of he SWNTs synthesized by this method frequently shows closed tube ends free of encapsulated metal particles as observeed in Fig. I.10. The opposite ends were typically found embedded in the catalyst support particles, suggesting a base-growth process.

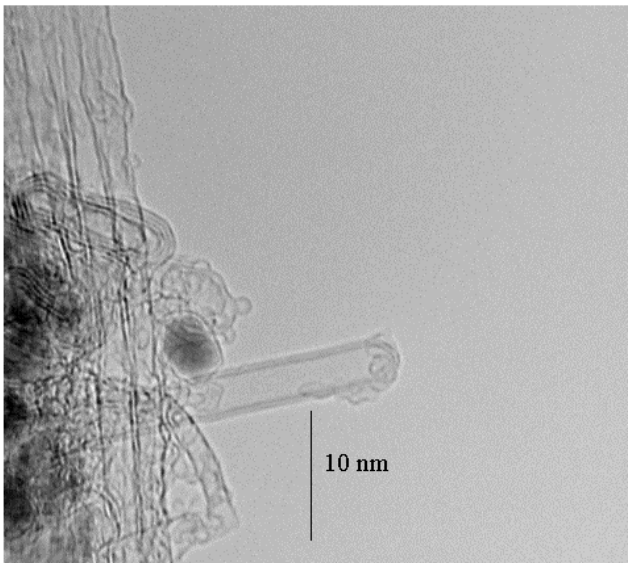

Figure I.19 *HRTEM image of the ends of SWNTS*

Considering the importance of the SWNTs, alternate synthesis strategies have been explored. Under controlled conditions of pyrolysis, dilute hydrocarbon - organometallic mixtures yield SWNTs "Satishkumar *et al.* (1998), Rao *et al.* (1998)".

Pyrolysis of a nickelocene - acetylene mixture at 1100 °C yields SWNTs, shown in TEM images in Figure I.11 "Satishkumar *et al.* (1998)". The diameter of the SWNT in Figure I.11a is 1.4 nm. It may be recalled that the pyrolysis of nickelocene mixed to benzene under similar conditions primarily yields MWNTs. Acetylene appears to be a better carbon source for the preparation of SWNTs, since it contains a smaller number of carbon

atoms per molecule. The bottom portion of the SWNT in Figure I.11b shows amorphous carbon coating around the tube. Many of the SWNT preparations show the presence of amorphous carbon. This can be avoided by reducing the concentration of hydrocarbon (C_2H_2) and mixing hydrogen in the argon stream.

Pyrolysis of acetylene in mixture with [$Fe(CO)_5$] at 1100 °C gives good yields of SWNTs (Figure I.12). Table I.1 summarizes the nature of products obtained by pyrolysis of hydrocarbon - organometallic mixtures at 1100°C in a stream of argon and hydrogen.

Pyrolysis of ferrocene - thiophene mixtures also yield SWNTs but the yield appears to be somewhat low. Pyrolysis of benzene and thiophene along with ferrocene gives a high yield of SWNTs "Cheng, H. M. *et al.* (1998)".

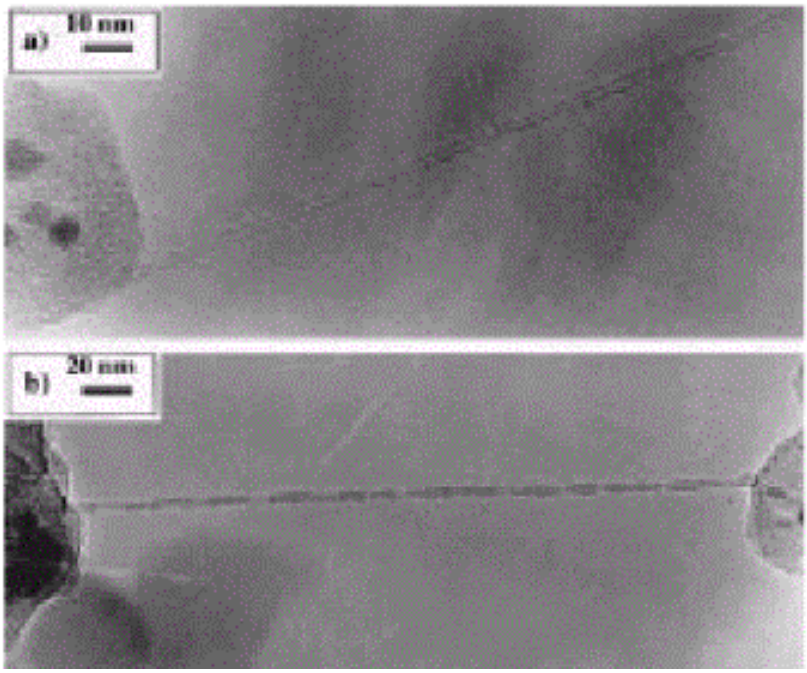

Figure I.20 *HRTEM image of SWNTs obtained by the pyrolysis of nickelocene and C_2H_2. (flow rate= 50cm^3/min) at 1100°C in a flow Ar (1000 cm^3/min)*

Laplaze et al. have demonstrated that concentrated solar energy can be employed to vaporize graphite to synthesize SWNTs "Laplaze *et al.* (1998)".

Dai et al. have prepared SWNTs by the disproportionation of CO at 1200°C over molybdenum particles of a few nanometers diameter dispersed in a fumed alumina matrix "Dai *et al.* (1996)".

Nikolaev et al. have obtained SWNTs using a gas-phase catalytic method involving the pyrolysis of [$Fe(CO)_5$] and CO "Nikolaev *et al.* (1999)". The

decomposition of CO on a silica-supported Co/Mo catalyst also yields SWNTs "Kitiyanan *et al.* (2000)".

SWNTs were also prepared by using various oxides (Y_2O_3, La_2O_3, CeO_2) as catalysts "Saito *et al.* (1995)".

Flahaut et al. have synthesized SWNTs by passing a H_2/CH_4 mixture over transition metal oxide spinels, obtained by the combustion route "Flahaut *et al.* (1999)". The transition metals studied include iron, cobalt, and nickel. These workers have characterized the quality of SWNTs on the basis of adsorption measurements.

Zeolites containing one-dimensional channels have also been investigated in a templated synthesis of SWNTs nanotubes. SWNTs synthesised by direct pyrolisis of tripropylamine molecules, contained in channels of $AlPO_4$-5 zeolite crystals "Wang *et al.* (2000) "Sun *et al.* (1999)", in turn used for zeolite synthesis, still constitute the only example of nanotubes production in microporous zeolite by templating method.

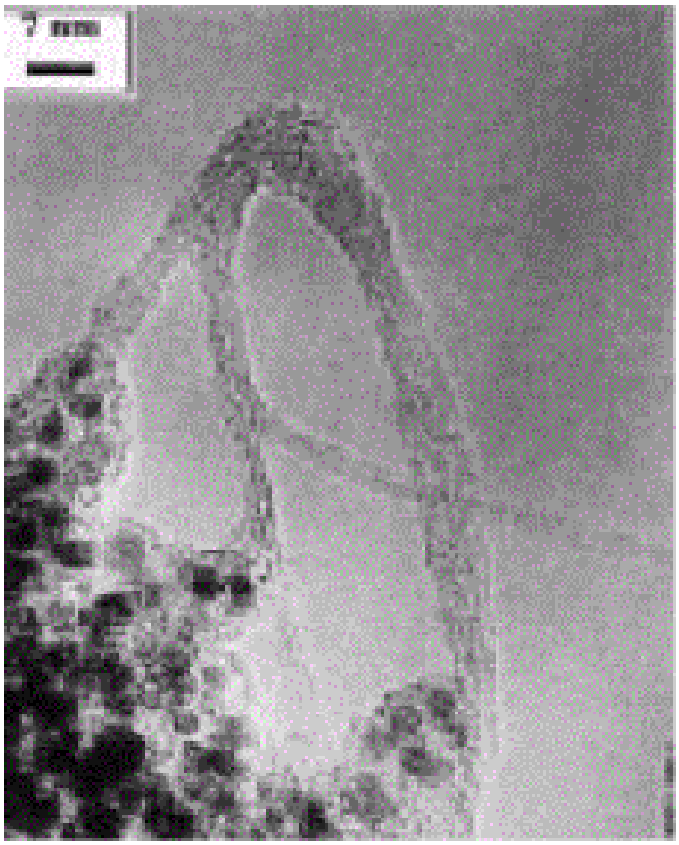

Figure I.21 *HRTEM image of SWNTs obtained by the prolysis of $Fe(CO)_5$ and C_2H_2 (flow rate= 50cm^3/min) at 1100°C in a flow Ar (1000 cm^3/min)*

Table I. 1 **Products obtained by pyrolysis of hydrocarbon - organometallic mixtures at 1100°C.**

Organometallic Precursor	Hydrocarbon	Inlet	Outlet
Ferrocene	Acetylene	Aligned MWNTs	Metal nanoparticles*
Nickelocene	Acetylene	MWNTs	SWNTs
Cobaltocene	Acetylene	MWNTs	SWNTs
Ferrocene+Nickelocene	Acetylene	Aligned MWNTs	SWNTs
Ferrocene+Cobaltocene	Acetylene	Aligned MWNTs	SWNTs
Nickelocene+Cobaltocene	Acetylene	MWNTs	SWNTs
$Fe(CO)_5$	Acetylene	MWNTs	SWNTs

* Metal nanoparticles covered with graphite layers

Very recently the synthesis of SWNTs with diameter of about 0.43 nm, using a floating catalyst method with zeolite particles has been reported "Hayashi *et al.* (2003)".

All as-prepared SWNTs contain several contaminants, such as amorphous carbon, graphitic nanoparticles and nanometer size catalyst particles coated with carbon, in different proportions depending on different preparation method. For example graphitic nanoparticles are present essentially in the products of laser ablation or arc-discharge.

In addition to purification, size separation has also been achieved. Since SWNTs occur as large bundles with lengths of the order of microns, it is desirable to break them from the bundles, for purposes of further manipulations.

Liu et al. "Liu et al. (1998)" have employed chemical processing based on ultrasound treatment, where in the SWNTs in an acidic medium were subjected to sonication so that the bundles break into open-ended small fragments of 100 - 300 nm length.

Chapter II

Graphene and graphene/SiO_2 composites on exhausted activated carbon derived 3C-SiC powders.

Graphene growth on SiC.

Graphene, a single monolayer of graphite, has attracted vast interest in recent years thanks to the very high number of application's fields. Graphene exhibits unconventional electronic properties, such as high and nearly equal mobilities at room temperature for both electron and hole conduction, which makes it a strong candidate for nanoelectronic devices and CMOS applications.

In view of the possible applications large scale syntheses are required. Single layer or few layer graphene can be prepared by several methods: micromechanical cleavage (MCP), or exfoliation from bulk graphite powders, thermal decomposition of commercial silicon carbide (SiC) substrates, or chemical vapour deposition of hydrocarbons on transition metal.

The preparation of graphene by SiC thermal decomposition is very promising for the possibility to growth graphene on a suitable surface that doesn't require further transfer process. In recent years there has been increased attention to SiC, thanks to its unique electrical and thermal properties. Silicon carbide is a wide-bandgap semiconductor with many interesting properties, such as high hardness, large thermal conductivity, low

coefficient of thermal expansion, and excellent resistance to erosion and corrosion.

Graphitization of SiC, studied since the mid 70's , has been widely explored in the last years, as a way of producing graphene films on semi-insulating substrates for both fundamental studies and applications. The epitaxial growth method requires high temperature, ultra-high vacuum and perfectly ordered silicon carbide. Current results show that the graphitization leads on the Si-terminated face, to the formation of a layer frequently called the buffer layer (the bottom graphitic layer does not contain exclusively sp^2 carbon atoms, some carbon atoms of this layer share covalent bonds with SiC surface) . Graphene above this layer results oriented at 30° with respect to the SiC surface. Whereas on the C terminated larger domains but of multilayered rotationally disordered graphene (graphene with different orientation coexist on the same substrate), have been produced. Recently, it has been shown that a soft annealing under hydrogen or air allows to break the coupling at the graphene/SiC interface, transforming the buffer layer into graphene.

To improve the film quality, Emtsev et al. suggested using unreactive argon at nearly ambient pressure to reduce the overall sublimation rate and to increase the graphitization temperature by several hundred degrees. The key factor in achieving an enhanced growth is the higher annealing temperature (1650°C), attainable for graphene formation under argon. In the presence of high pressure argon Si evaporation rate is reduced, since silicon atoms desorbing from the surface have a finite probability of being reflected back to the surface by collision with Ar atoms. Under Ar atmosphere Si sublimation is not observed at temperature up to 1500°C, whereas Si desorption begins at 1150°C in vacuum. This results in a faster surface diffusion such that the surface reconstruction is completed before graphene is formed.

Following the studies of graphene formation by SiC annealing, graphene growth on SiC from external sources of carbon has been explored. The first demonstrations have been done under ultra-high vacuum (UHV) environment with solid carbon source. Later, graphene growth on SiC by chemical vapor deposition (CVD) using propane as carbon source and argon or hydroge as carrier gas have been performed. It has been demonstrated that the graphene structure can be controlled by using propane hydrogen CVD, the result depends of the operating conditions, in particular of the couple carbon supply rate-growth temperature. It is worthwhile to notice that this temperature can be varied in a very large range, and also to lower values range. By using propane under CVD conditions and hydrogen as carrier gas, either IRD structure and the $6\sqrt{3}\times\sqrt{63}$-R30° can be obtained on the Si-face depending on the growth pressure and temperature.

Even if the growth of graphene is favoured on comparable lattice structure, recently graphene has been successfully grown, on cheaper 3C-SiC. In

Michon's work (Michon et al., 2013), the growth was obtained with an external source of carbon, in particular by propane/hydrogen CVD. In Michon'work (Michon et al., 2012), interstingly, a very weak interaction between the graphene layer and the substrate, crucial to preserve the astonishing intrinsic properties of graphene, has been demonstrated.

C/SiO_2/SiC core layers sheath nanofilaments

During the fast development of nanotechnology in the past decade, research effort has been focused on the preparation, thought different approaches, of nanometer-sized functional electronic devices. By combining different types of nanomaterials, nanoscaled electronic devices with a variety of functions may be realized. For the intrinsic characteristic of SiC and graphitic carbon, and the possibility to obtain a metallic-insulator-semiconductor geometry, coaxial nanocable of SiC-SiO_2–carbon (Zhang et al., 1998; Li et al., 2004) and chains of carbon nanotubes-SiC, have been also prepared by CVD or reactive laser ablation (Panda et al., 2010; Cai et al., 2007). On the other hand, the formation of a SiO_2 layer on SiC can be obtained via a simple oxidation method. In the preparation of electronic devices, in analogy with the Si/SiO_2 technology, to obtain a metal-oxide-semiconductor field-effect-transistors (FET), one of the major advantages of SiC is the ability to thermally oxidize to SiO_2, that is thus a common and know procedure . However, thermal oxidation of SiC is rather complicated if compared with Si oxidation, and product could results in mixed oxides containing C species. Numerous paper have been published on this theme (Schürmann et al., 2006), one of the key aspect was the diffusion of CO and CO_2 molecules in SiO_2 during SiC oxidation, whereas a challenging goal was to avoid carbon intermixing in the SiO_2 interlayer and covering the outer surface by a carbon layer.

Here we report, for the first time, the growth of graphene by methane/hydrogen CVD, and the preparation of few layer carbon/SiO_2/SiC composite by thermal annealing under few percents of oxygen in nitrogen, on 3C-SiC powder (Sarno et al., 2016) at atmospheric pressure and low temperature for their intrinsic advantages. SiC, which was derived from exhausted activated carbon, was prepared and chosen as substrate. Activated carbon is widely used as adsorbent for the removal of organics in water and wastewater treatment. The economics of the adsorption process greatly depends of the possibility of reusing the adsorbent along several operation cycles. Regeneration refers to removal of the adsorbate and restoration of previous adsorptive capacity of the original activated carbon. The currently available regeneration methodologies which include thermal desorption, wet air oxidation, steam, infrared radiation, and solvent extraction have been extensively reviewed but very often the efficiency of the regeneration

techniques is not high enough and decreases with the number of regenerations. So the possibility of reusing this material for a new application appear the most economical method. Recycled SiC was chosen as growth substrate to realize a convenient process and to increase the added value of the recycled, combining the favourable properties of different substances. SiC powder and the composite materials obtained were carefully characterized by the combining use of different techniques: transmission electron microscopy (TEM) coupled with an EDAX probe, scanning electron microscopy (SEM), Raman spectroscopy, thermogravimetric analysis (TG-DTG) coupled with a quadrupole mass detector and X-ray diffraction analysis.

Experimental

Material and methods

Preparation of SiC from exhausted activated carbon

Silicon carbide powder was synthesized in ENEA from exhausted activated carbon and inexpensive silicon dioxide, by means of a carbothermal reduction reaction which involves the following fundamental steps:

$$SiO_2(s)+C(s) \rightarrow SiO(g)+CO(g) \quad (1)$$

$$SiO(g)+2C(s) \rightarrow SiC(s)+CO(g) \quad (2)$$

The carbon matrix was milled into particles up to 1 mm in diameter, mixed with commercial silica gel (Carlo ERBA silica gel 60 230-400 mesh ASTM) in a mixer drum for 2h, fixing the powder weight ratio SiO2/C at 1.514. After being ground, samples were maintained under ambient conditions.

The reactions (1) and (2) were conducted at temperature ranging from 1500-1800 °C in a tubular furnace (Nabertherm 120/300/1800), with a residence time of nearly 1 hour, in argon atmosphere (flow rate of 50 l/h). At these experimental conditions, β-phase prevails on α-SiC and the product yields are very close to the theoretical value (nearly 35%).

SiC powder was purified from the residual carbon by treating the samples at 700°C in oxidizing atmosphere and from the residual silica by dissolving the samples in hydrofluoric acid (HF) 50 wt % solution and by subsequently washing the residues with alcohol.

The exploitation of solid by-products for the production of high added value materials, such as SiC powder, has been conducted in the frame of a wider research line which is devoted to the matter recovery from the waste treatment and that has got its main goals into the ceramic production.

Preparation of Graphene/SiC and few layer carbon/SiO2/SiC

Graphene (G/SiC) and few layer carbon/SiO_2 on SiC (C/SiO_2/SiC) were prepared in a laboratory apparatus consisting of a continuous flow microreactor, loaded with SiC and fed by pure argon, nitrogen, hydrogen, methane or their mixtures. A constant flow rate of each gas was provided by mass flow controllers. The temperature of SiC bed was measured with a K thermocouple located inside an internal coaxial quartz tube (4 mm internal diameter). The reactor was heated by an electrical oven, whose temperature was controlled by a temperature programmer–controller (Eurotherm 2408).

On-line analyzers permit the monitoring of the concentrations of CH_4 and hydrogen in the reactor outlet gas.

For the graphene synthesis hydrogen was used as carrier gas and methane as carbon source. The substrate was previously annealed for 10 min under argon at 1200°C in order to uniform the surface by removing residual polishing damage. Such treatments do change the surface morphology and typically cause significant step bunching.

SiC powder was put on a removable support inside the quartz reactor, and the gas mixture flow horizontally invests the substrate. Cylinder gases (99.998 pure methane and 99.9990 pure hydrogen) were mixed to obtain the methane/hydrogen stream (3000 ppm of methane in 100 cc(stp)/min total flow rate) fed to the reactor. After a temperature ramp-up to 1250°C, graphene growth was started by adding methane to hydrogen. After 5 min, the reacting gas stream was stopped, and hydrogen was fed to the reactor. Finally, the reactor was extracted from the furnace and allowed to cool under ambient temperature conditions.

For the G/SiO_2/SiC growth, Oxygen 50 ppm in nitrogen was fed to the reactor heated from room temperature to 1150°C, then kept 1 hour at this constant temperature, and finally 15 min under pure hydrogen. Finally, the sample was treated for 30 min in argon to allow residual CO to diffuse out.

Characterization Methods

For the characterization: transmission electron microscopy (TEM) images were acquired using a 200 kV FEI Tecnai microscope, equipped with an EDX probe; scanning electron microscopy (SEM) images were obtained with a LEO 1525 microscope.

Raman spectra were obtained with a micro-Raman spectrometer Renishaw inVia (514 nm excitation wavelength-laser power 100 mW). The laser spot diameter was about 10 μm.

XRD measurements were performed with a Bruker D8 X-ray diffractometer using CuKαradiation; thermogravimetric analysis (TG-DTG) at a 10 K/min in flowing air was performed with a SDTQ 500 analyzer (TA Instruments) coupled with a mass spectrometer (MS); N_2 adsorption−desorption isotherms at 77 K, on powder samples previously outgassed in He flow at 523 K for 4 h, were obtained with a Thermoquest Sorptomatic 1900.

Conductivity measurements of SiC and G/SiC thin films (~3μm thick, SEM evaluation), obtained by drop-casting from ethanol powder suspensions onto mica substrates followed by a pressing, were obtained with a four- point probe surface resistance Keithley 4200 source meter.

Before electrical and electrochemical measurements, SiC was dipped into 5% HF solution for 3 h to remove SiO_2 followed by a washing in distilled water until the pH of the leaching water reached a value of 7−8. For the electrochemical measurements, a homogeneous ink was prepared by dispersing 4 mg of SiC or G/

SiC in 80 μL of 5 wt % Nafion solution. Then, the ink was dropcast onto a 6 mm diameter glassy carbon electrode. Linear sweep voltammetry was obtained using a potentiostat from Amel Instruments in 0.1 M H_2SO_4.

Saturated calomel, graphite, and a loadable glassy carbon electrode were the reference, the counter, and the working electrodes, respectively. EIS measurements were obtained in AC by applying a voltage

of 5 mV amplitude in a frequency range 0.1−105Hz at open circuit potential.

Results and discussion

SiC characterization

The characteristic XRD pattern of the synthesized SiC is shown in Figure 1.

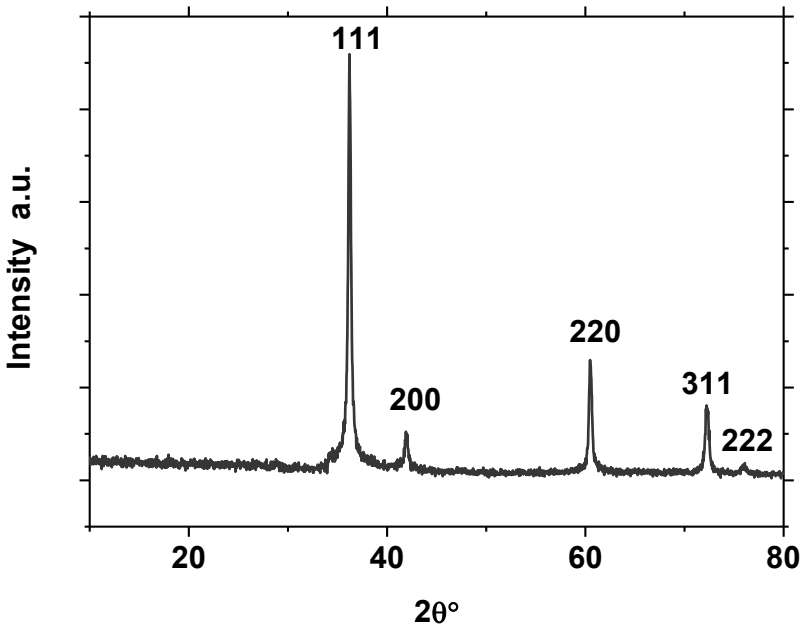

Figure II.1 *X-ray diffraction pattern of the synthesized 3C-SiC*

The major diffraction peaks can be indexed as the (111), (200), (220), (311), and (222) reflections of 3C-SiC (cubic β-phase of SiC, unit cell a = 0.4370 nm), as confirmed by the Raman analysis (Figure 5). No peaks are observed in the range 2θ=20°-30°, indicating the absence of residual carbon and SiO_2 (see also Figure 1 and relative comments).

Three SEM images of SiC at increasing magnification are reported in Figure 2. The powder consists mainly of a texture of presumable curved filaments with a diameter in the range 15-80 nm.

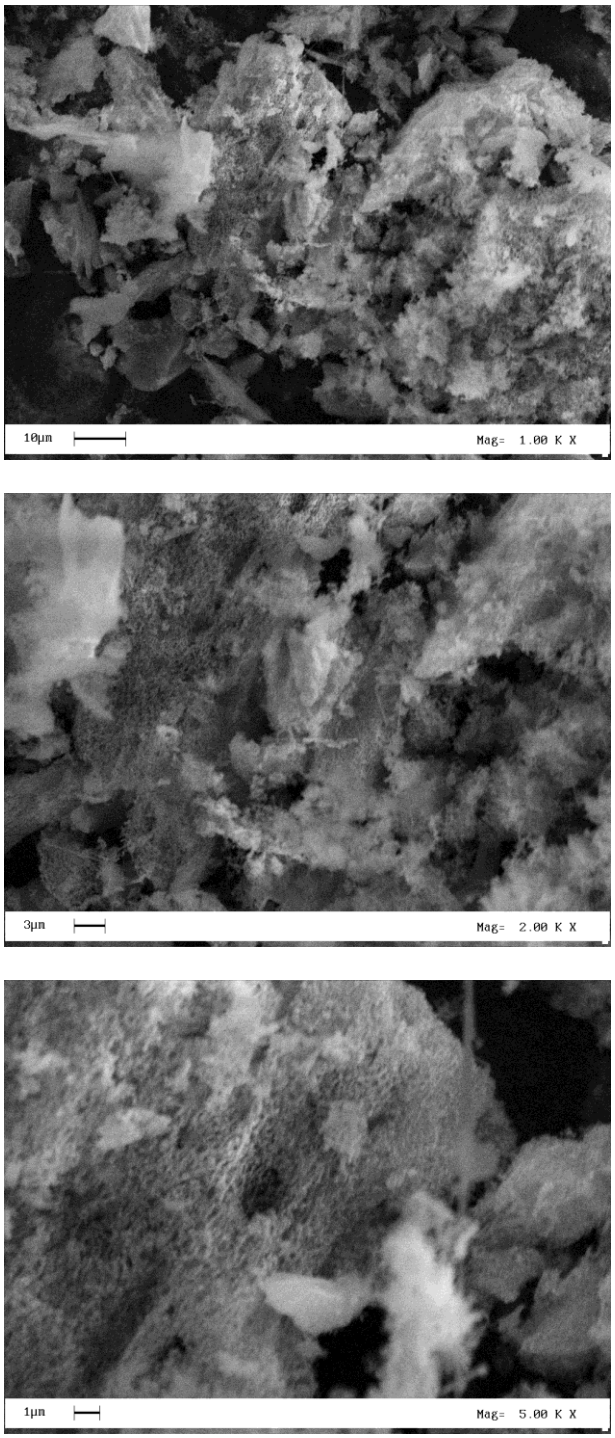

Figure II.2 *SEM images of the produced SiC at increasing magnification*

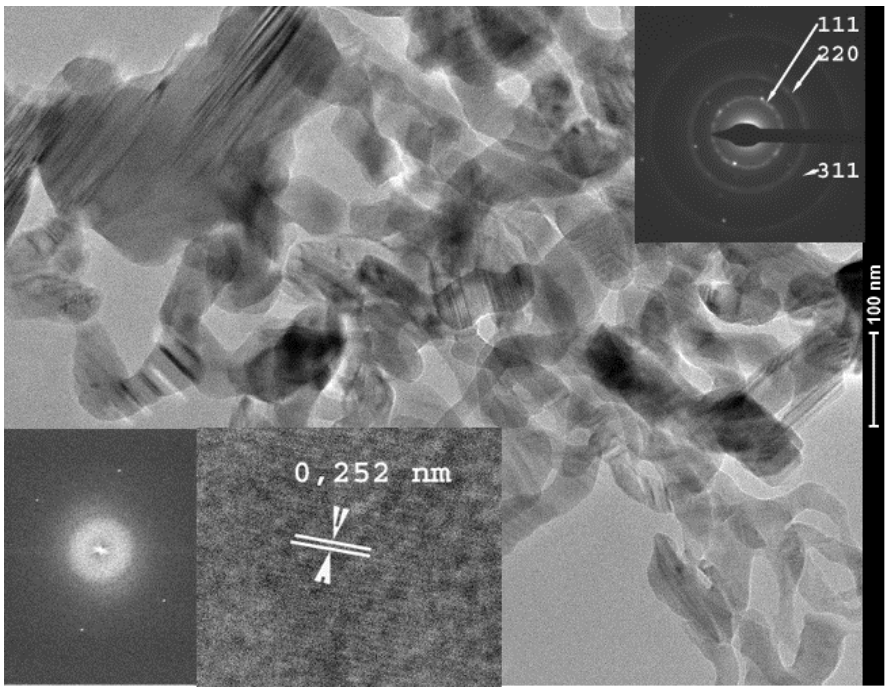

Figure II.3 *TEM image of the SiC nanofilaments. The inserts show: an higher-magnification image, an FFT and electron diffraction patter*

The TEM image in Figure 3 reveals that the most powder consists of nanofilaments of about 1 μm in length and tens of nanometers in diameter; a small number of larger particles is also present.

The corresponding selected-area electron diffraction (SAED) pattern (area in red of Figure 3) indicates a cubic structure of the SiC sample. The fast Fourier transform (FFT) evidences two different orientations of packed SiC with the typical 0.252 nm interlayer spacing (see the high resolution TEM image).

In particular, in Figure 4 the EDS spectrum highlighted the background of the spectrum evidencing the presence of Ca, K, Ti, Cr and Fe coming from the exhausted activated carbon. By EDS analysis it has been found that these metals correspond to less than 0,5% of the total sample weight (this level of impurities reduces the electric band gap for this SiC, up to values around the unit about the half of the typical values reported for 3C-SiC, results not shown here, this aspect is under investigation).

The Raman spectrum of the SiC is shown in Figure 5. The transverse optical (TO) at 795 cm^{-1} and longitudinal optical (LO) between 870 and 995 cm^{-1} bands indicate the presence of β-SiC phase [Chaika, (2013), Schürmann

(2006), Di Bartolomeo (2009)-Handa (2011)]. Shoulders are present at both sides of the TO and LO bands, likely due to the 6H or other SiC polytypes. The other features observed at 1515 and 1710 cm^{-1} are ascribed to the second order optical phonon modes

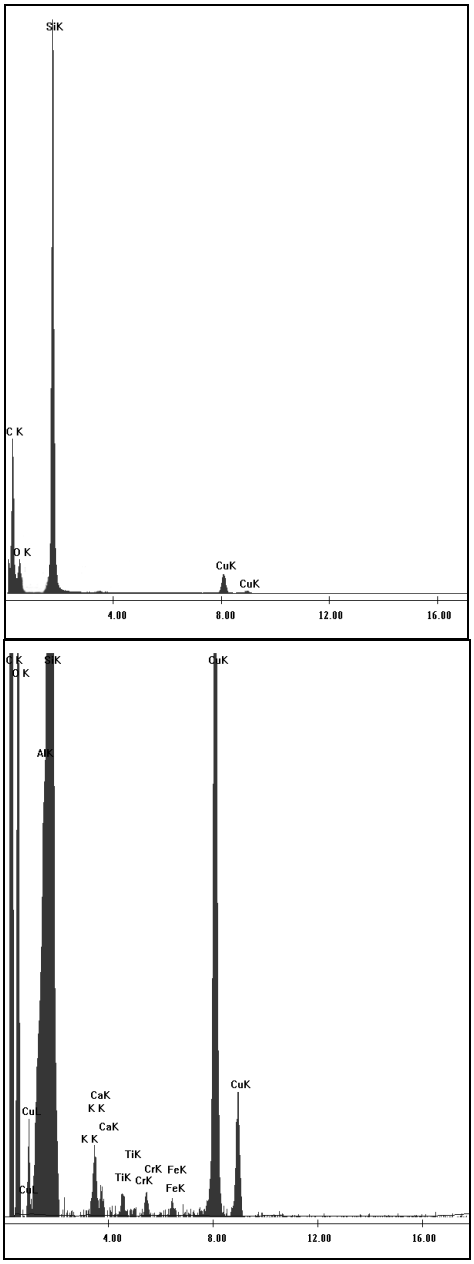

Figure II.4 *EDX spectrum collected on the all image*

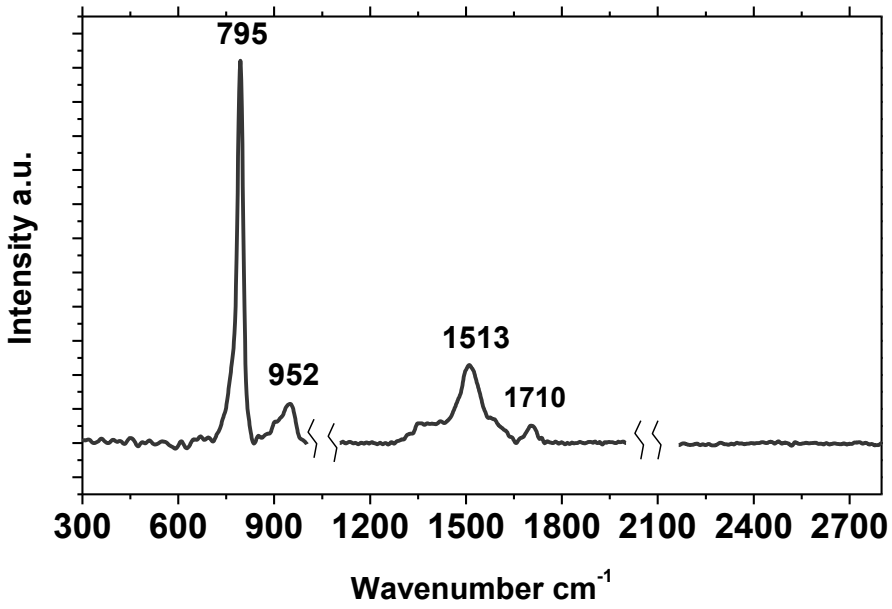

Figure II.5 *Raman spectrum of the synthesized 3C-SiC*

The thermal stability, and the absence of additional carbon in the produced SiC, have been evaluated by a thermogravimetric test from room temperature to 1200°C in air flow. After a very small mass loss (lower than 0,3 wt.%, see Figure 6), a mass gain occurs, due to the formation of SiO_2 by the reaction of SiC and oxygen , "Guerét, (1997)". The oxidation of SiC begins at about 700 °C and proceeds via diffusion in a surface limited process (amorphous silica is formed below 1100°C, while above this temperature cristobalite forms at increasing temperature and time, "Holmen (1995)".

The XRD spectrum of the powder after the thermogravimetric test (Figure 7) shows the peaks from 3C-SiC together with a broad and weak peak at $2\theta=20°–23°$ that can be attributed to amorphous silicon oxide.

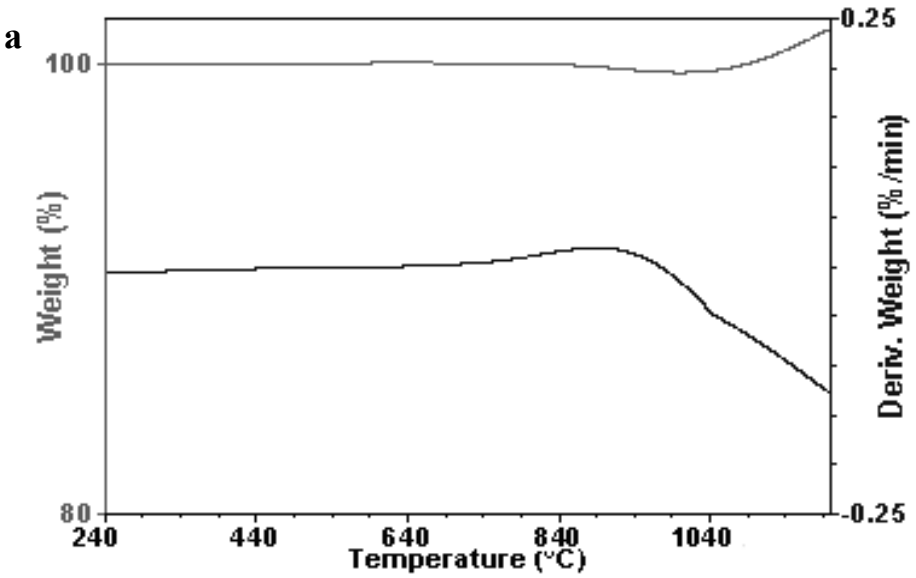

Figure II.6 *Thermogravimetric test on the synthesized SiC: TG in green, DTG in blue*

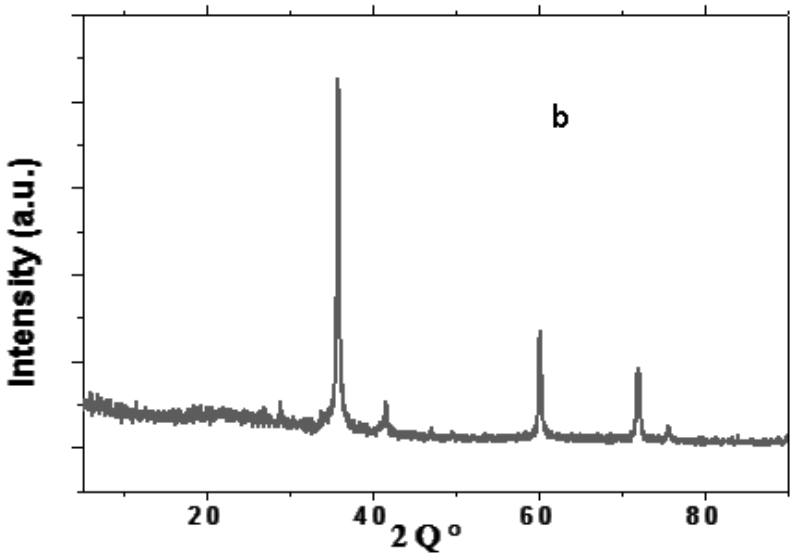

Figure II.7 *XRD spectrum obtained on the powder after the thermo gravimetrical test*

Figure 8 shows the N_2 adsorption-desorption isotherms for the SiC nanofilaments. The measured BET surface area is 500.45 m^2/g, with a micropore surface area of 238,2 m^2/g, the total pore volume and the microporous volume are 0.43 cm^3/g of 0,083 cm^3/g, respectively.

The multimodal pore size distribution (BJH (Barrett-Joyner- Halenda) Desorption pore distribution) centered at 2.3, 8.1, 11,1 and 19.7 nm, due to pores between exposed surface filaments, which agree with nanofilaments packaging observed in SEM and TEM images, is shown in Figure 9.

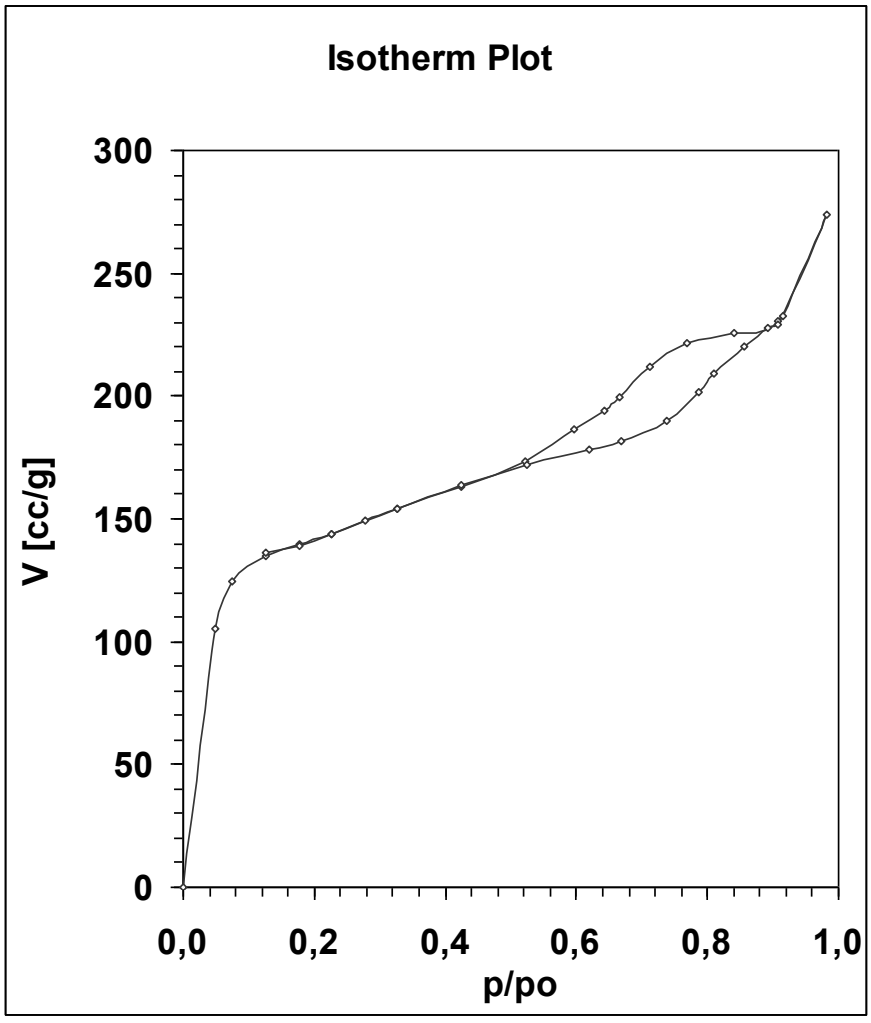

Figure II.8 *Nitrogen adsorption-desorption isotherm for SiC nanofilament*

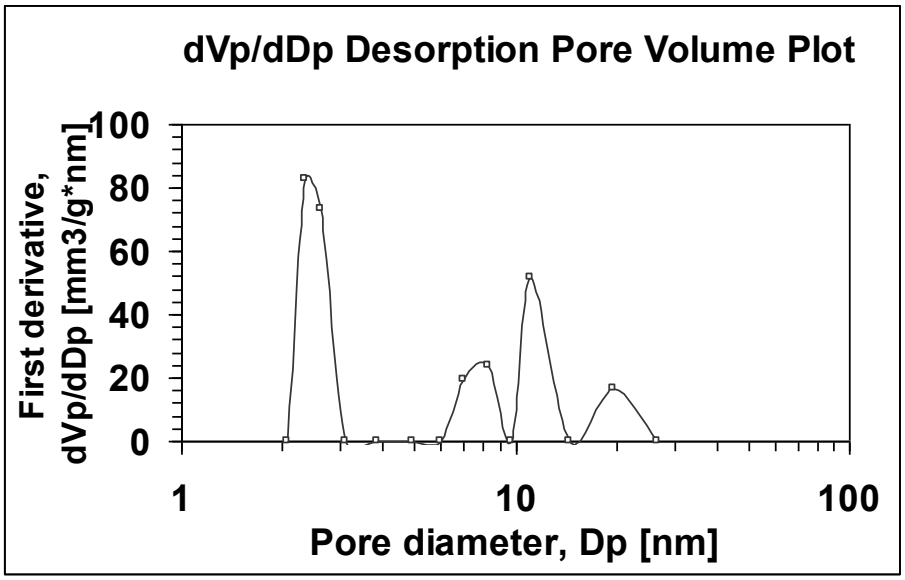

Figure II.9 *Pore-diameter distribution curves of the synthesized SiC*

G/SiC and FLG/SiO2/SiC characterization

G/SiC characterization

The key Raman results are displayed in Figure 10, to be compared with the reference spectrum measured on bare 3C-SiC of Figure 5. Transverse optical (TO) at 795 cm^{-1} and longitudinal optical (LO) between 870 and 995 cm^{-1} bands indicate the presence of 3C-SiC (β-SiC) phase.

Shoulders are present at both sides of the TO and LO bands, probably due to the 6H or other SiC polytypes.

The well isolated G, D and 2D bands near 1350, 1590 and 2700 cm^{-1}, due to carbon, jump into the eye.

In particular, we can see the so-called G band and the 2D band at about 2700 cm^{-1}, that suggests the generation of graphitic domains, indeed it is a representative characteristic feature of undisturbed or highly ordered graphitic lattice that can be fitted with six Lorentzian lines, as it is typical of three layer graphene.

On the other hand, the multiple components nature of the 2D Raman bands support the hypothesis of an interlayer coupling absence between graphene and the SiC surface, likely due not only to the SiC crystalline orientation but also to the graphene formation from carbon addition.

We can also see the so-called disorder-induced D-band that is assigned to a typical characteristic for disordered graphite or crystal defects, corresponding to a graphitic lattice vibration mode with A1g symmetry.

We can also see the so-called disorder-induced D-band, at about half of the frequency of the G band, typically due to disorder and edge, but in this case also due to the curvature imposed to the graphene layers.

Figure 11 shows a TEM image of a SiC nanofilaments after graphene formation.

The high resolution TEM images in the inserts of Figure 11 evidence the interface between the graphene formed and the 3C-SiC surface. Three graphene layers are visible in the image with interlayer distance of 0.35 nm.

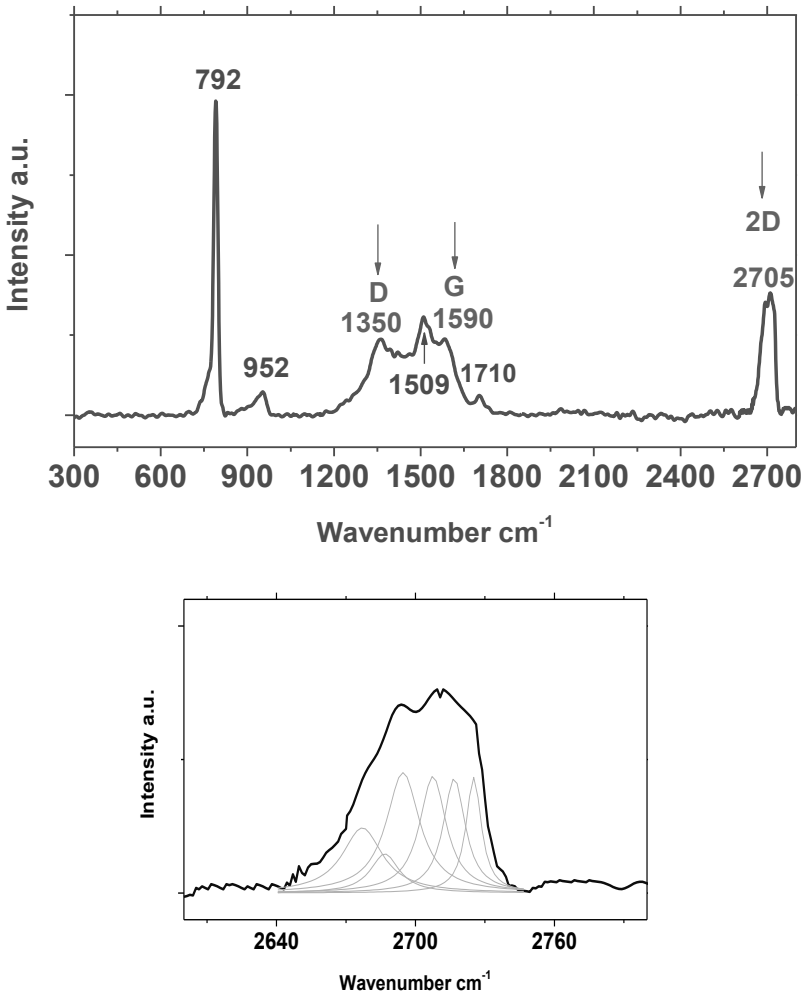

Figure II.10 *Raman spectrum of graphene SiC, 2D peaks deconvolution*

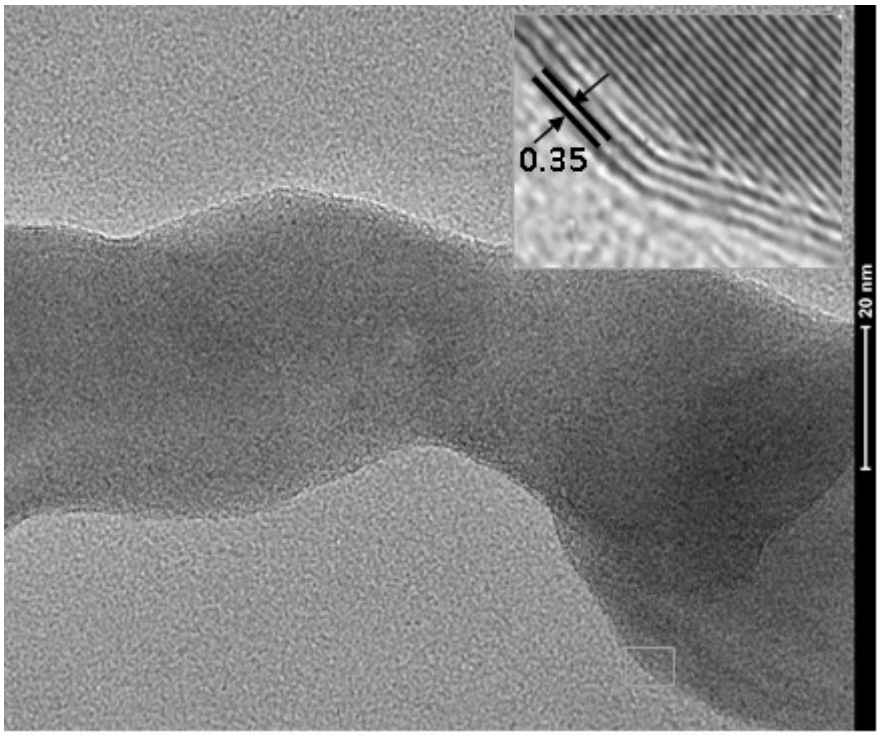

Figure II.11 *TEM image of three layers graphene on SiC*

To better understand this result the evolution of the concentration profiles of H_2 and CH_4 during the synthesis has been recorded. Typical concentration profiles of H_2 and CH_4 during graphene synthesis test is shown in Figure 12.

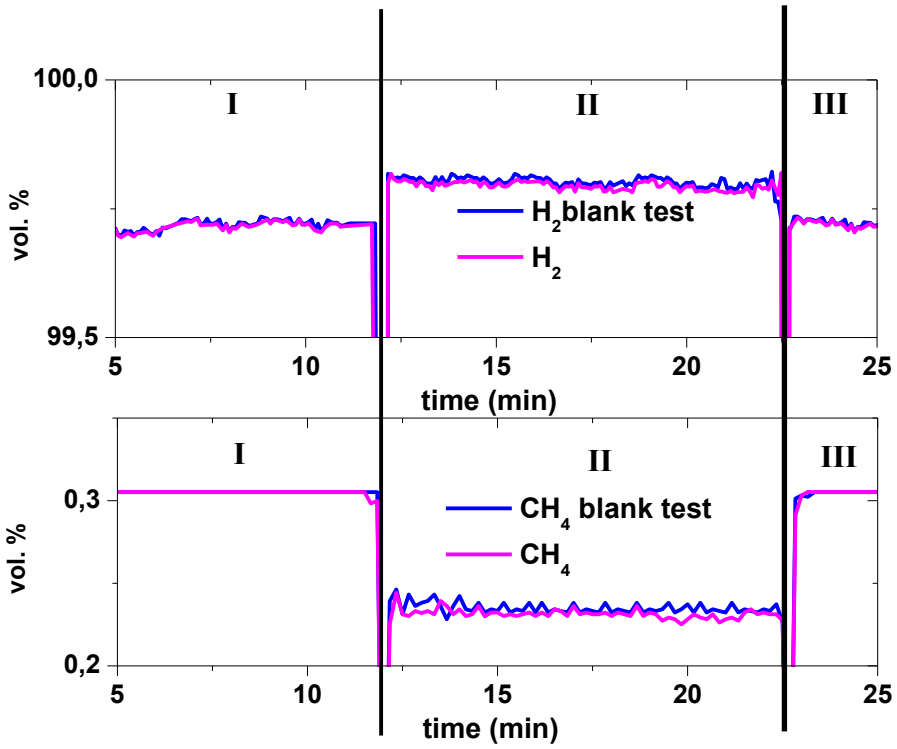

Figure II.12 *Concentration profiles of H_2 and CH_4 during the graphene synthesis test*

We can distinguish three temporal phases: (I) Pre-reaction phase: H_2 and CH_4 are fed to the analyzer; (II) Reaction phase: H_2 and CH_4 are fed to the reactor, reaching the analyzer after passing over the SiC powder; (III) Post-reaction phase: the reaction has ended, and the gases are sent directly back to the analyzer (bypassing the reactor), the concentration is the same as that in the pre-reaction phase.

Considering, the methane decomposition to give carbon and hydrogen (CH_4 → C + $2H_2$), the initial feed composition and the expansion volume factor (εCH4), we calculate the methane conversion and hydrogen yield as:

$$X_{CH4} = \frac{1 - \frac{C_{CH4}}{C^0_{CH4}}}{1 + \frac{\varepsilon_{CH4} \times C_{CH4}}{C^0_{CH4}}} \quad (1)$$

$$R_{H2} = \frac{(1+\varepsilon_{CH4} X_{CH4}) \times C_{H2}}{2C^{0}_{CH4}} \quad (2)$$

where C is the concentration and C0 the initial concentration of a single component, finding that the two values are in disagreement, indicating that the methane decomposition to carbon is not the only reaction that occurs in the reactor.

This is not an unexpected result, it is well known that starting with methane, the pyrolysis is represented as occurring stepwise:

$$CH_4 \rightarrow C_2H_6 \rightarrow C_2H_4 \rightarrow C_2H_2 \rightarrow C \quad (3)$$

At the highest temperature >1000°C, the ethane and ethylene are short lived. In particular, the thermal decomposition of methane, over the range of 1000°-1630°C, follows two main parallel reactions.

$$2\ CH_4 \rightarrow C_2H_2 + 3\ H_2 \quad (4)$$

$$CH_4 \rightarrow C + 2H_2\ (2) \quad (5)$$

At a temperature lower than 1200°C the main reaction products of methane pyrolysis are hydrogen and carbon, though very small amounts of higher hydrocarbons, including aromatic hydrocarbons are formed. The maximum acetylene concentration in the reaction product, as well as aromatic hydrocarbons, especially benzene and naphthalene, increased with temperature.

The carbon formation can be limited using short reaction times and low partial pressures of methane preferably by hydrogen dilution of the feed. Obviously, one needs to distinguish between thermodynamic equilibrium conversion and conversion limited by kinetics in a finite reactor. Moreover, the methane cracking was a heterogeneous, autocatalytic reaction, with the initiation step of

$$CH4 \rightarrow CH3 + H, \quad (6)$$

and with an acceleration step of $CH_3 \rightarrow CH_2 + H$ occurring on the carbon surface.

so it is necessary to take into account that the deposition of successive carbon atoms is accelerated by the presence of those already deposited. Finally, in our reaction conditions, 1250 °C and high hydrogen

concentration, it is expected that most of the byproduct is acetylene, and the presence of aromatic hydrocarbons traces cannot be excluded.

Moreover, by observing the reaction chamber, we can conclude that carbon covers not only the SiC surface but also the reactor filter that is slightly gray after synthesis. Definitely, the process is quite complex and a quantification of the deposited carbon, even more than that deposited on the SiC, is not possible, since it is necessary to know the amount of all the species involved.

On the other hand, an important consideration can be done considering what happens during a blank test, performed by recording the evolution of the hydrogen and methane composition, to determine the behavior of the system in the absence of SiC powder. The concentration of methane practically overlapped that found in the presence of SiC. In the case of hydrogen profiles, even if the hydrogen concentration variation is very small in both cases, it stays at a slightly higher value during all the test time, indicating the occurrence of an interaction between H_2 and the SiC surface and/or the gas phase.

This observation is a direct confirmation of what is understood, downstream of numerous experimental analysis.

Graphene growth on SiC has been mainly studied using sublimation methods under UHV or argon pressure conditions. In both cases the growth involves Si sublimation, that under UHV conditions happens at considerably lower temperature ~1200°C (Si sublimation begins at 1150°C) compared with the 1650°C (Si sublimation begins at 1600°C due to the argon molecules) of the atmospheric growth, that leads to more uniform and larger terraces and carbon graphitization.

The situation is different in the case of a methane/H_2 CVD. First of all, H_2 passivate the SiC surface, as in the detaching of the buffer layer. In Michon work, (2012b), in which graphene was grown by hydrogen/propane CVD, it has been found, due to presence of hydrogen, the IRD structure also on the Si terminated surface. On the other hand the presence of hydrogen determines the formation of a new number of species (SiH_2, CH_4, C_2H_2 etc…) absent in the other cases, that could led to a silicon etching together with a methane direct supply. It has been demonstrated, in all the operating conditions explored, that no graphene can be observed feeding pure hydrogen, even if SiC etching occurs, but silicon and carbon released sublimate from the surface. In a number of operating conditions the graphene formation results by the combination of the carbon addition by the hydrocarbon and the SiC etching, the additional carbon results necessary to create a carbon overpressure and the subsequent segregation on the surface. Finally, we want to point out, that recycling can be used considering the very high level of hydrogen and the very low conversion of methane.

C/SiO2/SiC characterization

A typical TEM image of the synthesized sample is reported in Figure 13, showing around the nanofilaments a layer of different colour of about 20 nm. An enlarged image of the sample is shown in Figure 14, it displays a characteristic dark core and lighted sheath, with the nanofilament sheath about 20-30 nm thick.

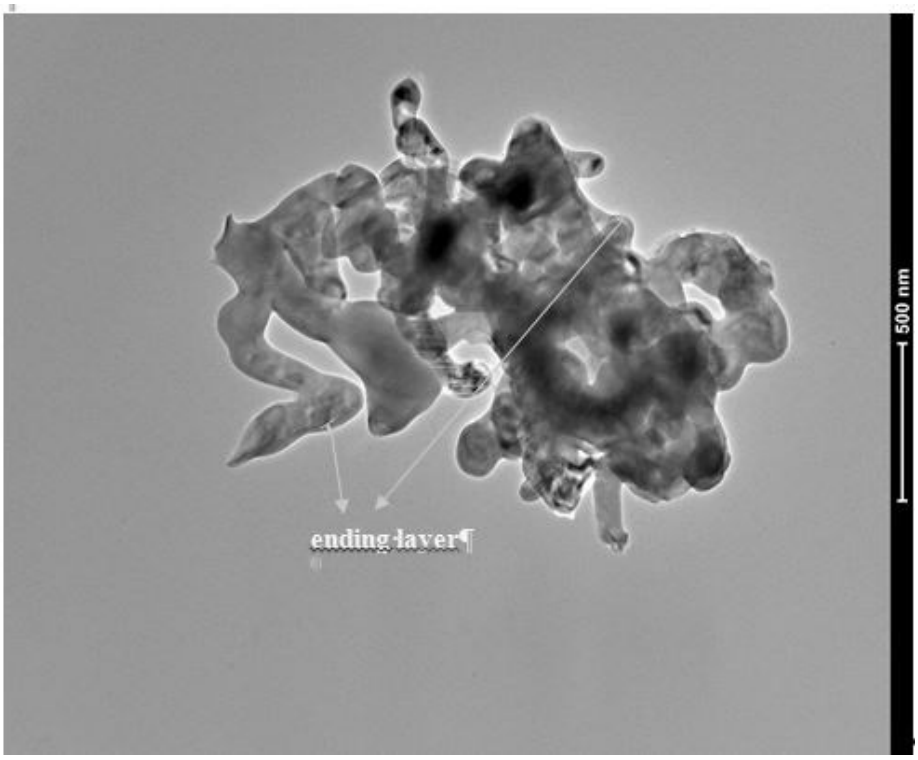

Figure II.13 *TEM image of C/SiO_2/SiC*

Chemical composition microanalysis, evidences the outer C sheath and the increased oxygen amount in the intermediate layer with respect to the core. Typical EDS spectra taken from three different zones (indicated as A, B, C in the inserts of Figure 14) of a nanofilaments are depicted in Figure 14. The EDS results were confirmed by the high resolution TEM image observations. They showed that the nanowhiskers are indeed composed of a 3C-SiC core, a SiO_2 intermediate layer, and an outer layer of graphitic carbon. Twisted graphene layers (about 13 are counted in the insert of Figure 11) with the typical (002) stacking of graphitic carbon are clearly visible for the outermost nanowhisker layers.

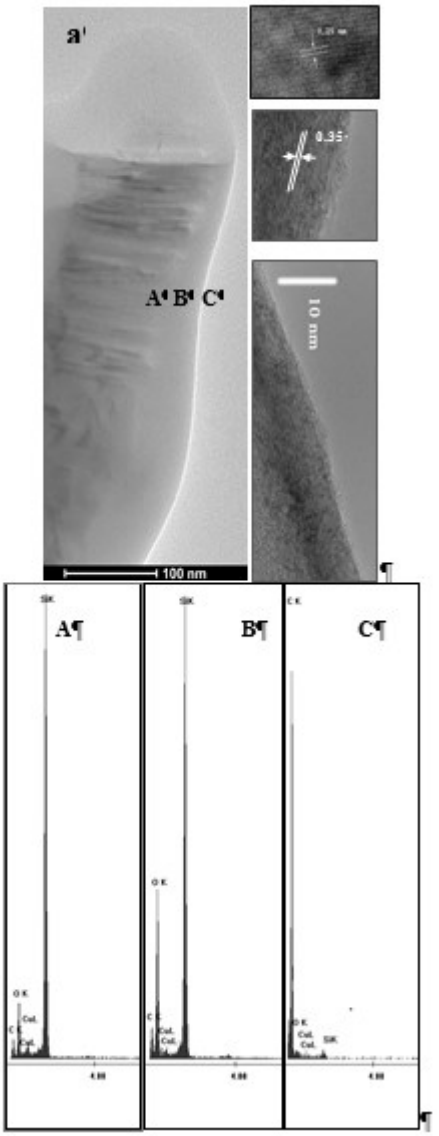

Figure II.14 *Representative TEM images of the prepared nanofilaments of C/SiO_2/SiC composite. High resolution TEM images of coaxial nanowhiskers, displaying single crystalline 3C-SiC core, SiO_2 intermediate layer and outer graphitic carbon sheaths. Energy dispersion spectra taken from different zones of the nanofilament as marked in the insert of (a) with A, B and C*

The Raman Spectrum reported in Figure 15, collected on the C/SiO_2/SiC, clearly shows the multiphase nature of the sample, the band between 400

cm-1 and 500 cm^{-1} are due to SiO_2, on the other hand at higher cm^{-1} the spectrum results from the superimposition of SiC and sp2 carbon. In particular, in the range 1200-3200 cm^{-1}, three additional bands appear at about 1346, 1588 and 2700 cm^{-1}, which are attributed respectively to the D, G and 2D carbon bands [Chaika et al 2013]. The presence of a single G and 2D bands indicates the thin thickness of the carbon layer. The appearance of the D band indicate structural defect of edge in the few layers graphene formed. All the TO and LO are shifted towards low wavenumber region if compared with pristine 3C-SiC, the red shift of the Raman bands might be due to the confinement effect, stacking faults and stress form the heterostructure of core shell $C/SiO_2/SiC$ structure ["Schürmann et al (2006)"].

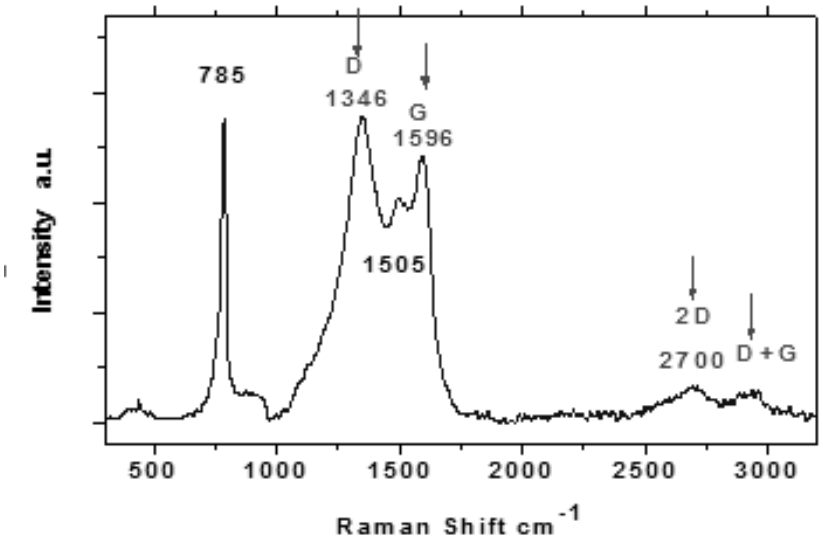

Figure II.15 *Raman spectrum of $C/SiO_2/SiC$*

In addition to the typical peaks of SiC in the XRD spectrum of the $C/SiO_2/SiC$ (Figure 16) the strong peak at 21,9° due to SiO_2 is also visible. The spectrum in the range 20-30° is characterized by a more noise than that of pristine 3C-SiC, on the other hand the (002) peak due to carbon stacking is no visible, suggesting a thin structure of few graphene and disorder for the carbon layers.

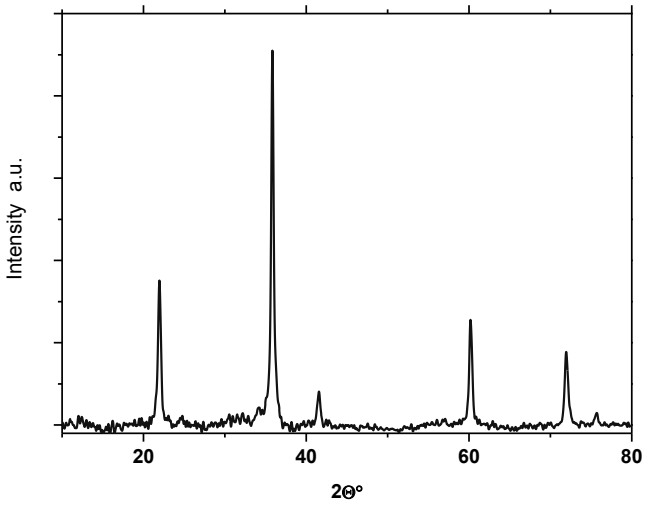

Figure II.16 *X-ray diffraction spectrum of C/SiO_2/SiC*

This study was focused on the preparation of few layer carbon/SiO_2/SiC composite by thermal annealing under few percents of oxygen in nitrogen, on 3C-SiC powder, at atmospheric pressure and low temperature for their intrinsic advantages and on the preparation of few layer carbon on 3C-SiC powder.

Silicon carbide is a promising semiconductor to be used in metal-oxide-semiconductor devices, for this applications it is most advantageous that the oxidation of SiC leads to SiO_2 passivated surface.

Therefore, numerous studies as per "Schmeiber et al (2001)", "Htun et al. (2002)", Vathulya at al (1998) have been conducted on the oxidation of 4H- and 6H-SiC samples, and several models reported to explain it.

Compared to oxidation of Si, thermal oxidation of SiC is considerably more complicated. The oxidation process of silicon carbide is governed by the transport of molecular oxygen to the reaction front, the reaction of oxygen with SiC at the interface and the out diffusion of gases through the growing silicon oxide film.

There are five steps (see the scheme 1) in the thermal oxidation of SiC:

- transport of molecular oxygen gas to the oxide surface;
- in-diffusion of oxygen through the oxide film;

- reaction with SiC at the oxide SiC interface;
- out-diffusion of product gases through the oxide film; and
- removal of product gases away from the oxide surface.

The first and last steps are rapid and are not rate-controlling steps. Among the different other steps the rate limiting step is still uncertain as discussed in several articles. Depending on the oxidation conditions, various limiting processes are possible, which can also influence the characteristics of the oxidation process. Four different reactions are predicted to be dominant, depending on $P(O_2)$ and T, producing four different results (the experiments have been performed in the temperature range 1150-1600°C in pure oxygen P=0,001-100Pa).

At low partial pressure of oxygen and high temperature the reaction:
$(2+x)SiC(s)+ O_2(g) \rightarrow (2+x)Si(g)+2CO(g)+xC(s)$ (1)

is dominant, corresponding to an etching along with the formation of a carbon layer.

The reaction:

$2SiC(s)+ O2(g) \rightarrow 2Si(g)+2CO(g)$ (2)

is predominant in the boundary conditions, between those of reaction (1) and (3).this reaction corresponds to the simultaneous vaporization and etching of SiC.

At increasing partial pressure of oxygen and lower temperature, the reaction:

$2SiC(s)+ O_2(g) \rightarrow SiO(g)+CO(g)$ (3)

happens, leading to an active oxidation or etching of the SiC.

At still higher $P(O_2)$ and lower temperature, the dominant reaction is

2SiC(s)+ 3O This study was focused on the preparation of few layer carbon/SiO_2/SiC composite by thermal annealing under few percents of oxygen in nitrogen, on 3C-SiC powder, at atmospheric pressure and low temperature for their intrinsic advantages and on the preparation of few layer carbon on 3C-SiC powder.

Silicon carbide is a promising semiconductor to be used in metal-oxide-semiconductor devices, for this applications it is most advantageous that the oxidation of SiC leads to SiO_2 passivated surface.

Therefore, numerous studies as per "Schmeiber et al (2001)", "Htun et al. (2002)", Vathulya at al (1998) have been conducted on the oxidation of 4H- and 6H-SiC samples, and several models reported to explain it.

Compared to oxidation of Si, thermal oxidation of SiC is considerably more complicated. The oxidation process of silicon carbide is governed by the transport of molecular oxygen to the reaction front, the reaction of oxygen with SiC at the interface and the out diffusion of gases through the growing silicon oxide film.

There are five steps (see the scheme 1) in the thermal oxidation of SiC:

- transport of molecular oxygen gas to the oxide surface;
- in-diffusion of oxygen through the oxide film;
- reaction with SiC at the oxide SiC interface;
- out-diffusion of product gases through the oxide film; and
- removal of product gases away from the oxide surface.

The first and last steps are rapid and are not rate-controlling steps. Among the different other steps the rate limiting step is still uncertain as discussed in several articles. Depending on the oxidation conditions, various limiting processes are possible, which can also influence the characteristics of the oxidation process. Four different reactions are predicted to be dominant, depending on $P(O_2)$ and T, producing four different results (the experiments have been performed in the temperature range 1150-1600°C in pure oxygen P=0,001-100Pa).

At low partial pressure of oxygen and high temperature the reaction:

$$(2+x)SiC(s)+ O_2(g) \rightarrow (2+x)Si(g)+2CO(g)+xC(s) \quad (1)$$

is dominant, corresponding to an etching along with the formation of a carbon layer.

The reaction:

$$2SiC(s)+ O2(g) \rightarrow 2Si(g)+2CO(g) \quad (2)$$

is predominant in the boundary conditions, between those of reaction (1) and (3).this reaction corresponds to the simultaneous vaporization and etching of SiC.

At increasing partial pressure of oxygen and lower temperature, the reaction:

$$2SiC(s)+ O_2(g) \rightarrow SiO(g)+CO(g) \quad (3)$$

happens, leading to an active oxidation or etching of the SiC.

At still higher $P(O_2)$ and lower temperature, the dominant reaction is

$$2SiC(s)+ 3O2(g) \rightarrow 2SiO_2(s)+2CO(g) \quad (4)$$

which product is commonly the desired product, ie the passivation of the SiC surface.

Although, at even higher partial pressure of O_2 than that used in the case of reaction (4), it has been predicted that solid SiO_2 and C can be the only products.

Reaction (4) is the fundamental in the passivation of SiC.

Most of the paper published, regarding the SiC oxidation, deal specifically on this reaction, in particular because during the SiC oxidation carbon contaminations can be easily observed either at the interface or incorporated in the silicon dioxide layer. Carbon atoms from the silicon carbide substrate leave the sample during the oxidation process.

This happens via out-diffusion of CO molecules through the growing oxide film. These CO molecules determine the formation of carbon clusters or graphitic regions. Basically, a CO molecules, generated at the advancing interface and diffusing through the oxide can bind weakly to a O site in the SiO_2 network. A second CO molecules, however, can bind to the first forming a new very stable complex. Additional CO molecules can extend the cluster. The process is helped by a passing CO that takes an O atom from the cluster and effuses as CO_2. The net result is O-deficient cluster of carbon.

In particular, looking to scheme 1, the oxygen flux to the vicinity and in the SiO_2 bulk, can be written as:

$$F_{O_2} = h_{O_2}(C^*_{O_2} - C^S_{O_2})$$
$$F_{O_2} = D_{O_2}\frac{(C^S_{O_2} - C_{O_2})}{W} \quad (5)$$

where hO_2 is the gas phase transport coefficient, DO_2 the oxygen diffusivity in the metal bulk, and those for CO:

$$F_{CO} = h_{CO}(C^S_{CO} - C^*_{CO})$$
$$F_{CO} = D_{CO}\frac{(C_{CO} - C^S_{CO})}{W} \quad (6)$$

finally the flux corresponding to the oxidation rate are:

$$F = K_f C_{O,} - K_r C_{CO} \quad (7)$$

where Kf and Kr are the rate constant of the forward and reverse reactions, respectively.

For the SiC oxidation, it has been reported, that the thermal growth kinetics is governed by linear parabolic law of Deal and Grove, as derived for Silicon.

$$W + AW = B\,t + \tau \quad (8)$$

Where, W denotes the oxide thickness and t is oxidation time. The quantity τ corresponds to a shift in the time coordinate that correct for the presence of the initial layer of oxide thickness and A and B are constants (B parabolic and B/A linear rate constant). The above equation is a quadratic equation.

The solution of equation (8) can be written as:

$$\frac{W}{A/2} = (1 + \frac{t + \tau}{A^2/4B})^{1/2} - 1 \quad (9)$$

where A and B can be expressed as:

$$A = \frac{1 + \frac{1{,}5K_f}{h_{O_2}} + \frac{K_r}{h_{CO}}}{\frac{1{,}5K_f}{D_{O_2}} + \frac{K_r}{D_{CO_2}}}$$

$$B = \frac{1 + \frac{1{,}5K_f}{h_{O_2}} + \frac{K_r}{h_{CO}}}{\frac{1{,}5K_f}{D_{O_2}} + \frac{K_r}{D_{CO_2}}} \qquad (10)$$

According with "Song et al (2004)", the oxidation kinetic results linear when the interface reaction is the rate-controlling step:

$$\frac{B}{A} \approx \frac{C^*_{O_2}}{N_0} K_f \qquad (11)$$

The kinetic is parabolic, if O_2 diffusion or CO out-diffusion are controlling:

$$B \approx \frac{C^*_{O_2}}{1.5N_0} D_{O_2} \qquad (12)$$

$$B \approx \frac{C^*_{O_2} K_f}{N_0 K_r} D_{CO} \qquad (13)$$

If oxygen diffusion is the rate limiting step, there may be the formation of an area rich in carbon in the SiO_2 near the surface of SiC, up to the formation of a carbon layer (limit case); if the out-diffusion of CO controlling, carbon can be formed in the SiO_2 layer more close to the outer surface.

We chose our operating conditions, on the base of the literature overview, experimental evidences and the following considerations: to obtain SiO_2 formation on the SiC surface, it is important to avoid that oxygen diffusion is the rate limiting step (O_2 pressure must not be too low, temperature must not be too high, since it favors the kinetics (which we want controlling) much more than the diffusion).

Moreover, the target is to form carbon layers on the outer surface, so the out-diffusion of CO should not be too favored, this is achieved by disfavoring further the reaction, in a sort of reaction/out-diffusion regime, and choosing a suitable reaction time to have a controlled SO_2 thickness.

We choose to operate at high oxygen partial pressure, and low temperature, in an operating conditions range that permits to cover SiC with SiO_2.

$$(g) \rightarrow 2SiO_2(s)+2CO(g) \qquad (4)$$

which product is commonly the desired product, ie the passivation of the SiC surface.

Although, at even higher partial pressure of O_2 than that used in the case of reaction (4), it has been predicted that solid SiO_2 and C can be the only products.

Reaction (4) is the fundamental in the passivation of SiC.

Most of the paper published, regarding the SiC oxidation, deal specifically on this reaction, in particular because during the SiC oxidation carbon contaminations can be easily observed either at the interface or incorporated in the silicon dioxide layer. Carbon atoms from the silicon carbide substrate leave the sample during the oxidation process.

This happens via out-diffusion of CO molecules through the growing oxide film. These CO molecules determine the formation of carbon clusters or graphitic regions. Basically, a CO molecules, generated at the advancing interface and diffusing through the oxide can bind weakly to a O site in the SiO_2 network. A second CO molecules, however, can bind to the first forming a new very stable complex. Additional CO molecules can extend the cluster. The process is helped by a passing CO that takes an O atom from the cluster and effuses as CO_2. The net result is O-deficient cluster of carbon.

In particular, looking to scheme 1, the oxygen flux to the vicinity and in the SiO_2 bulk, can be written as:

$$F_{O_2} = h_{O_2}(C^*_{O_2} - C^S_{O_2})$$
$$F_{O_2} = D_{O_2}\frac{(C^S_{O_2} - C_{O_2})}{W} \qquad (5)$$

where hO_2 is the gas phase transport coefficient, DO_2 the oxygen diffusivity in the metal bulk, and those for CO:

$$F_{CO} = h_{CO}(C_{CO}^{S} - C_{CO}^{*})$$
$$F_{CO} = D_{CO}\frac{(C_{CO} - C_{CO}^{S})}{W} \quad (6)$$

finally the flux corresponding to the oxidation rate are:

$$F = K_f C_{O,} - K_r C_{CO} \quad (7)$$

where Kf and Kr are the rate constant of the forward and reverse reactions, respectively.

For the SiC oxidation, it has been reported, that the thermal growth kinetics is governed by linear parabolic law of Deal and Grove, as derived for Silicon.

$$W + AW = B\,t + \tau \quad (8)$$

Where, W denotes the oxide thickness and t is oxidation time. The quantity τ corresponds to a shift in the time coordinate that correct for the presence of the initial layer of oxide thickness and A and B are constants (B parabolic and B/A linear rate constant). The above equation is a quadratic equation.

The solution of equation (8) can be written as:

$$\frac{W}{A/2} = (1 + \frac{t+\tau}{A^2/4B})^{1/2} - 1 \quad (9)$$

where A and B can be expressed as:

$$A = \frac{1 + \frac{1{,}5K_f}{h_{O_2}} + \frac{K_r}{h_{CO}}}{\frac{1{,}5K_f}{D_{O_2}} + \frac{K_r}{D_{CO_2}}}$$

$$B = \frac{1 + \frac{1{,}5K_f}{h_{O_2}} + \frac{K_r}{h_{CO}}}{\frac{1{,}5K_f}{D_{O_2}} + \frac{K_r}{D_{CO_2}}} \tag{10}$$

According with "Song et al (2004)", the oxidation kinetic results linear when the interface reaction is the rate-controlling step:

$$\frac{B}{A} \approx \frac{C^*_{O_2}}{N_0} K_f \tag{11}$$

The kinetic is parabolic, if O_2 diffusion or CO out-diffusion are controlling:

$$B \approx \frac{C^*_{O_2}}{1.5N_0} D_{O_2} \tag{12}$$

$$B \approx \frac{C^*_{O_2} K_f}{N_0 K_r} D_{CO} \tag{13}$$

If oxygen diffusion is the rate limiting step, there may be the formation of an area rich in carbon in the SiO_2 near the surface of SiC, up to the formation of a carbon layer (limit case); if the out-diffusion of CO controlling, carbon can be formed in the SiO_2 layer more close to the outer surface.

We chose our operating conditions, on the base of the literature overview, experimental evidences and the following considerations: to obtain SiO_2 formation on the SiC surface, it is important to avoid that oxygen diffusion is the rate limiting step (O_2 pressure must not be too low, temperature must not be too high, since it favors the kinetics (which we want controlling) much more than the diffusion).

Moreover, the target is to form carbon layers on the outer surface, so the out-diffusion of CO should not be too favored, this is achieved by disfavoring further the reaction, in a sort of reaction/out-diffusion regime, and choosing a suitable reaction time to have a controlled SO_2 thickness.

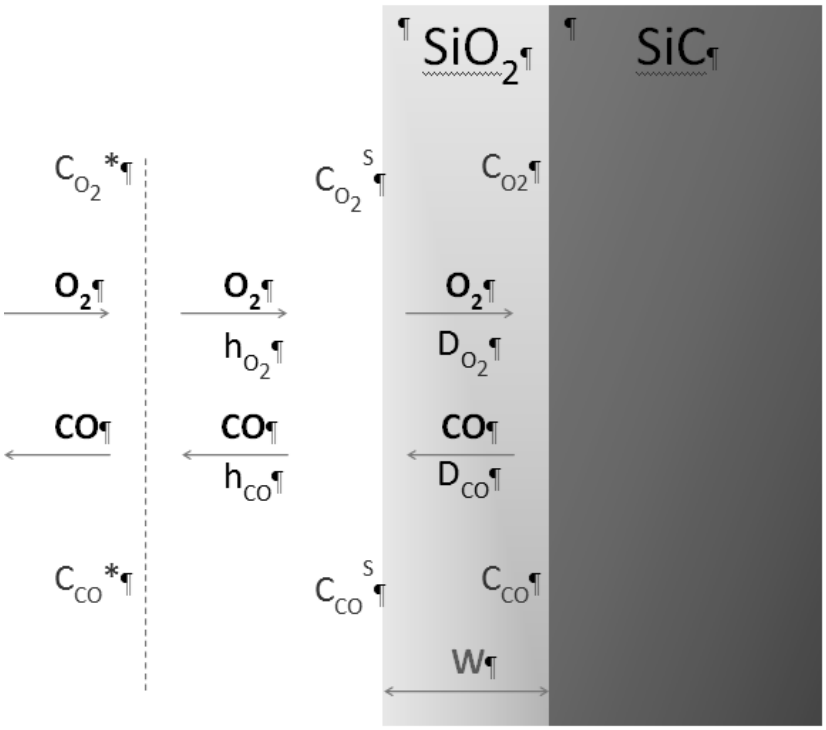

Scheme 1. The five steps during SiC oxidation

We choose to operate at high oxygen partial pressure, and low temperature, in an operating conditions range that permits to cover SiC with SiO_2.

For the SiC oxidation, it has been reported, that the thermal growth kinetics is governed by linear parabolic law of Deal and Grove, as derived for Silicon [Schmeiber et al., 2001].

According with the study of Afanasev et al 1996, the oxidation kinetic results linear when the interface reaction is the rate-controlling step: The kinetic is parabolic, if O2 diffusion or CO out-diffusion are controlling:

We evaluate the average oxide thickness as a function of time, see Figure 17, in the same operating conditions reported in the experimental section but temperatures (the tests were performed at 1150, 1200 and 1250°C), finding an activation energy of 2.74 eV, suggesting a CO-out diffusion/interface reaction limiting steps [Song et al 2004].

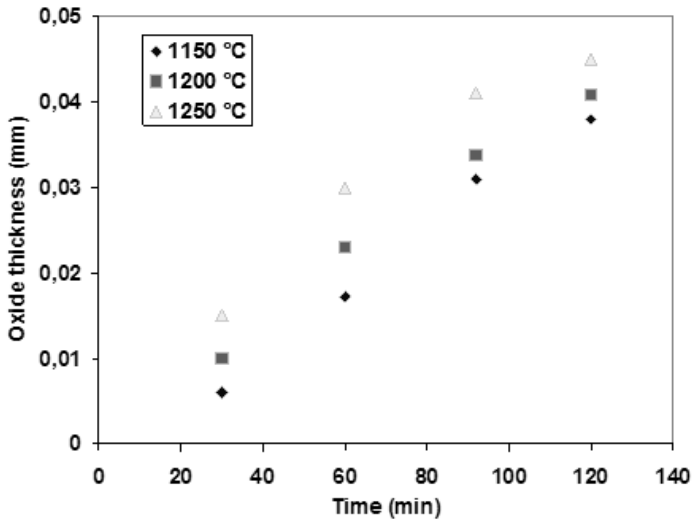

Figure II.17 *Oxide thickness vs reaction time*

Supercapacitors application

Supercapacitors are electrochemical energy storage devices which possess high specific capacitance, high power density and long and robust charge/discharge life time cycle. Depending on energy storage modes in supercapacitors, are classified as pseudocapacitors and electrical double layer capacitors (EDLC).

The pseudocapacitors or redox capacitors are based on fast, reversible faradic redox reactions which occur between the oxide and the electrolyte.

The energy storage mechanism involves the separation of electronic charges at the interface between electrode and electrolyte. For EDLC, no chemical reaction occurs in which only adsorption and desorption of electrolyte ions on electrode materials occur during the charge/discharge process. On the one hand, EDLC offer high power density than the pseudocapacitors due to large charge accumulation. Although the specific capacitance of pseudocapacitors is much larger than of EDLC, the former having a limited application due to their low electrical conductivity and poor cycling stability.

Carbon materials (activated carbons, carbon aerogels, and nanostructures) have been widely studied for EDLC electrodes, because they presents high surface area at the electrode/electrolyte interfaces [3-11].

In particular, graphene is a very attractive carbon-based material thanks to its open 2D structure and amazing electronic conductivity. In

supercapacitors, graphene-based materials have shown remarkable specific capacitances in aqueous electrolytes, organic electrolytes and ionic liquids.

Moreover, their low equivalent series resistances (ESR) and good electrochemical stability make of graphene an efficient substrate for pseudocapacitive and battery materials, significantly improving both energy and power capabilities of resulting composite electrodes. Most significantly, the intrinsic capacitance of graphene was found to be 21 $\mu F/cm^2$ which sets the upper limit of EDL capacitance for all carbon-based materials.

This study asserts that graphene is the ideal carbon electrode material for EDL supercapacitors because it can store an EDL capacitance value of up to 550 F/g, provided the entire 2675 m^2/g is fully utilised.

Recently, EDLC made of semiconductors, such as: silicon, silicon carbide, titanium nitride and titanium dioxide nanowires have attracted much attention because of their high specific surface area and electrical conductivity.

In particular, in recent years there has been increased attention to SiC, thanks to its unique electrical and thermal properties. Silicon carbide, as a promising electrode material, has attracted considerable industrial and scientific interest due to its wide band gap and high electron mobility. It has many interesting properties, such as high hardness, large thermal conductivity, low coefficient of thermal expansion, excellent resistance to erosion and corrosion, and biocompatibility.

Some papers related to the use of SiC in micro-supercapacitor, indeed current development trend towards miniaturized portable electronic devices shows a significant increase in the demand for compact power sources: this is particularly true for sensors operating in harsh environments.

In this regard, micro-supercapacitors based on:

(i) graphene arranged with a structured mesoporous, in 2D in-plane design (e.g. vertically oriented graphene stacked layers) to improve surface availability and thus the electrochemical performances;

(ii) planar supercapacitors of carbon inkjet–printed from bulk to micro.

In particular, Zinc blende (cubic) (3C-SiC) alone, that exhibits outstanding electronic conductivity because possesses the smallest band gab (~2.4 eV) and one of the highest electron mobility of all the known polytypes, has been tested in 0.1M H_2SO_4 as a thin film supercapacitor.

Approaching biosensing applications, it has been tested as nanowires grown on a graphite paper electrode in 0.1M H_2SO_4 and in the potential windows 0-0.5V, showing improved performances (a specific capacitances of about 30 mF/cm2). In particular, the authors conclude that the 3-dimension porous network structure of graphite paper-supported SiC in the form of high-aspect-ratio nanowires contributes to the high electrochemical performance. Besides, 3C-SiC had been previously tested in 1M H2SO4 solution in a form of thin film and after a nitrogen doping [25], finding

interesting electrochemical performance, ensured also by a low resistivity graphitized layer that avoid energy loss through the electrode.

"Gu et al. (2015)" report the performances of a supercapacitor electrodes in 2M KCl, with long cycle stability, made of SiC nanowires (SiCNWs) grown on a flexible carbon fabric. The excellent cycle stability of the electrodes is attributed to the thermal and chemical stability of SiC and carbon fibres, which provide a conductive and stable substrate.

A further improvement of the electrode capability in 1M KOH/PVA was obtained by the same author in 2015, by deposition of a $Ni(OH)_2$ layer on the surface of the SiCNWs. Hybrid materials, consisting of microspheres of silicon carbide/nanoneedle of MnO_2 composites in 1M Na_2SO_4 have displayed a significant capacitance values due to the combination of EDLCs and pseudo-capacitance materials. Silicon carbide nanowires (SiCNWs), produced via a chemical vapour deposition (CVD) process on oxidized silicon wafer, have demonstrated a relatively high capacitances values of about few hundred microfarads for square centimeters as supercapacitor electrode materials operating in 3.5M KCl ("Alper at al. 2013").

The same authors (Alper et al. 2012) have investigated SiNWs arrays as electrode material in 1M KCl, and compared the supercapacitors performances with that performed by an electrode made with SiNWS covered by a SiC layer. They have demonstrated that the application of the SiC coating avoids the undesired oxidation of silicon, responsible of no capacitive behavior, and permits to enhance the capacitances values up to about 1.7 mF/cm^2.

Although carbon stabilizing and potentiating effects on the performance of SiC as a supercapacitor are now clear, graphene has never been studied in combination with SiC for this application at the best of our knowledge. Indeed, among the different methods to synthesize graphene, this can be directly prepared on SiC by thermal decomposition.

G/SiC supercapacitor performance evaluation

Graphene and SiC have been used into the past for supercapacitor applications, most of the obtained results are summarized in Table 1. Data in Table 1 show the results obtained using graphene in different configuretion and with different electrolytes.

As far as SiC is concerned, it has been tested: (i) alone; (ii) in combination with carbonaceous materials; (iii) in combination with pseudocapacitive materials.

In the case of electrodes designed for applications in micro-supercapacitors or planar capacitors, the reported capacitance values have been typically measured as an areal capacitance in $\mu F/cm^2$.

In particular, the data expressed in $\mu F/cm^2$ refers to the geometrical area of the electrodes, which can be characterized by different thickness. In

general, the more the electrode thickness the more the areal capacitance increases. This is particular true in liquid electrolyte due to the ability to penetrate in the increased effective area of a thicker electrode.

The paper of "Xia et al. (2012)", reports a value of 21 μF/cm^2 (550 F/g) for a single graphene layer, setting the upper limit of EDL capacitance for all carbon-based materials.

When more graphenes constitute the electrode, the capacitance values, increase as more is made available the graphene surface, and from a ionic electrolyte, to organic and aqueous. A value of 247 F/g (electrode weight of 0.283 μg) in PVA-H_3PO_4 electrolyte, that yield almost the same double-layer capacitance measured in H_2SO_4, has been found for multilayer reduced graphene oxide in a 2D in-plane design obtained through an LBL deposition. The same authors reported a normalized capacitance by geometrical area of 394 μF/cm2 (electrode area 0.08465x2.1 cm^2), and a capacitance normalized by the accessible interfacial surface of 18.9 μF/cm^2, quite close to the limiting double-layer capacitance.

Regarding the SiC capacity, it increases from a film of SiC aggregated nanocrystals [Yang et al (2012)], to a substrate of parallel SiC nanowires, and furtherly for SiC supported on a carbon based material. In Yang et al work (2012) the electrode is a 1 μm thick film of nanocrystalline 3C-SiC with a roughness of 30 nm, this is important to take in account in the comparison with the performance of a single graphene layer.

It is worth noticing that: (i) because the micro-supercapacitor applications, at the best of our knowledge, the SiC capacitance has never been reported in F/g, (ii) the data showing the electrochemical performances in F/g, published to date, refer to SiC coupled with pseudocapacitive materials [Gu et al (2015)].

Conductivity measurements of SiC and G/SiC thin films (~3 μm thick, SEM evaluation), obtained by drop-casting from ethanol powder suspensions onto mica substrates followed by a pressing, were obtained with a four-point probe surface resistance Keithley 4200 source meter. Before measurements electrical and electrochemical measurement, for SiC a dipping into 5% HF solution for 3h to remove SiO_2 was performed, followed by a washing in distilled water until the pH of the leaching water reached a value of 7-8. For the electrochemical measurements, a homogeneous ink was prepared by disperding 4 mg of SiC or G/SiC in 80 μl of 5 wt.% Nafion solution. Then, the ink was drop casted onto 6 mm diameter glassy carbon electrode. Linear sweep voltammetry were obtained using a potentiostat from Amel Instruments in 0.1 M H_2SO_4. Saturated calomel, graphite and a loadable glassy carbon electrode as the reference, the counter and the working electrodes, respectively.

Table 1. Comparison of the Specific Capacitance of As Prepared SiC and G/SiC with for Graphene and SiC Reported in the Literature.

Sample	Electrolyte	C	C	Ref.
3C-SiC film[+]	0.1M H_2SO_4	30-35 μF/cm^2 at 100 mV/s	-	32
3C-SiC nanowire film on a graphite paper	0.1M H_2SO_4	28000 μF/cm^2 at 2mA/cm^2	-	34
Graphitic carbon on nitrogen-doped polycrystalline 3C-SiC	1M H_2SO_4	743 μF/cm^2 at 50 mV/s	-	35
Silicon carbide nanowires on a carbon fabric	2M KCl	23000 μF/cm^2 at 50 mV/s	-	36
Silicon carbide nanowires@$Ni(OH)_2$ on carbon fabric	1M KOH	-	1724 F/g at 2 A/g	37
Microsphere silicon carbide/nanoneedle manganese	1M Na_2SO_4	-	272 F/g at 10 mV/s	39
Microsphere silicon carbide-MnO_2 nanoneedles	1M Na_2SO_4	-	59.9 F/g at 2 mV/s	40
SiC nanowires	3.5 KCl	400 μF/cm^2 at 100 mV/s	-	41
SiC nanowires	3.5 KCl	240 μF/cm^2 at 100 mV/s	-	42
SiC coated silicon nanowires	1M KCl	1700 μF/cm^2 at 50 mV/s	-	43
SiC **nanoparticles**	1M H_2SO_4	40191 μF/cm^2 at 0.1 mA/cm^2	114.7 F/g at 0.12 A/g	This paper
Graphene coated SiC **nanoparticles**	1M H_2SO_4	115789 μF/cm^2 at 0.1 mA/cm^2	325.9 F/g at 0.12 A/g	This paper

[+] The film was 1 μm thick.

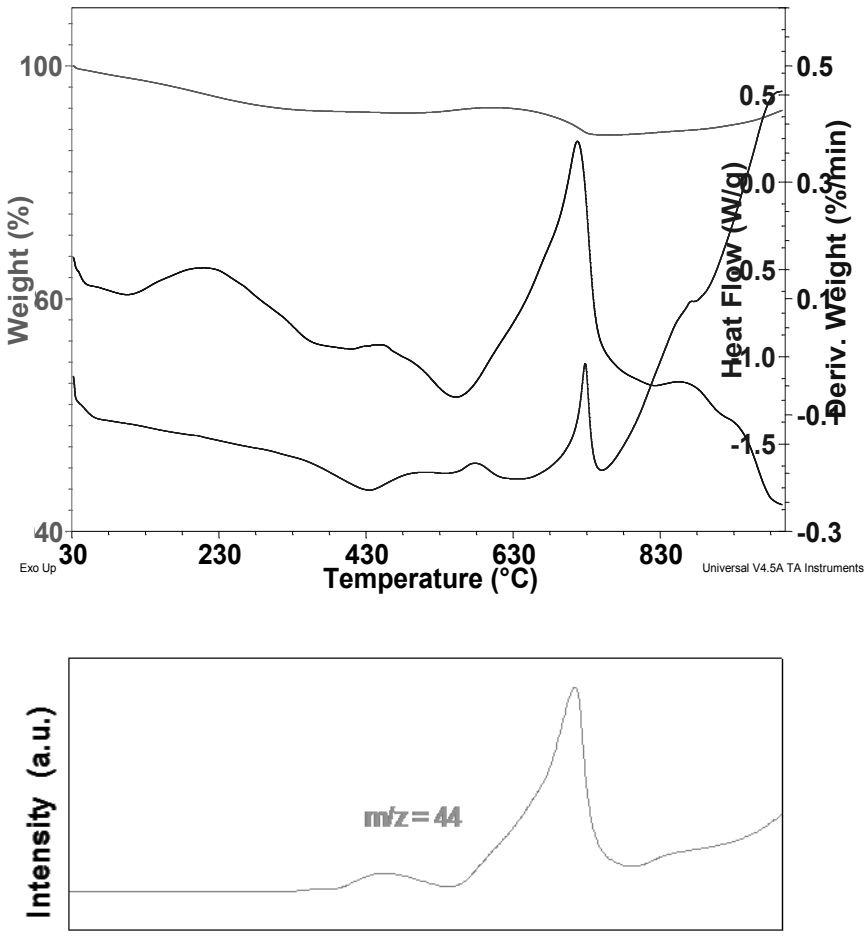

Figure II.18 *TG-DTG-MS of G/SiC: TG in green; DTG in blue; DSC in maroon; MS in orange*

EIS measurements were obtained in AC by applying a voltage of 5 mV amplitude in a frequency range 0.1-105 Hz at open circuit potential.

In order to evaluate the electrochemical properties of our SiC and G/SiC nanocomposite, cycling voltammetry (CV) and galvanostatic charge/discharge tests were performed.

The CV curves at 10-20-50-100 mV/s in the potential window of 0-1 V in 1M H_2SO_4 electrolyte are presented below for SiC and G/SiC, respectively. These curves, for G/SiC, subtend a larger area and are closer to a rectangular shape than for SiC alone.

The thermal stability of G/SiC has been evaluated by a thermogravimetric test from room temperature to 1000°C in air flow (Figure 18).

During the test, a weight loss, of about 5,3 wt.%, can be observed in the temperature range 430-750°C due to graphene oxidation, followed by a mass gain due to the formation of SiO_2 by the reaction of SiC and oxygen83 (see the mass fragment m/z=44 for thermogravimetric test on the synthesized SiC). Starting from 1 g of SiC nanoparticles with a mean diameter of 50 nm and the SiC density of 3.21 g/cm^3 2*1014 NPs have been calculated. A deposited carbon mass of 51.87 mg can be calculate by multiplying the number of NPs for the carbon volume (1.3*10-16 cm^3) and density, corresponding to the carbon weight loss in the range 430-750°C.

The nitrogen adsorption-desorption isotherm of G/SiC is shown in Figure 15. The total specific surface area of G/SiC is 528.6 m^2/g, with a micropore surface area of 221,2 m^2/g, the total pore volume and the microporous volume are 0.45 cm^3/g and 0,081 cm^3/g, respectively. All the results are very similar to those of the starting SiC, also the multimodal pore size distribution (BJH (Barrett-Joyner-Halenda) Desorption pore distribution centred at 2.3, 8.1, 11,1 and 19.7 nm (Figure 19).

Prior to electrochemical experiments, to evaluate the suitability of the materials prepared to be applied as electrode for electrochemical experiments, the electrical conductivities of SiC and G/SiC thin films (~3 μm thick) were measured by four-probe technique. SiC film possesses a surface resistance of 5540 Ω/sq due to defects in the films (e.g. planar defects, grain boundaries and amorphous phase),95 and probably metallic inclusions (see EDS analysis). On the other hand, it is known that 3C-SiC, that is the main component of our sample, possesses the smallest band gap (~2.4 eV) and one of the highest electron mobilities (~800 cm2/Vs).96 G/SiC film shows a lower surface resistance of 1500 Ω/sq likely due to graphene covering.
In order to evaluate the electrochemical properties of our SiC and G/SiC nanocomposite, cycling voltammetry (CV) and galvanostatic charge/discharge tests were performed. The CV curves at 2-10-20-30-60-120-240 mV/s in the potential window of 0-1 V in 1M H_2SO_4 electrolyte are presented in Figure 9a and 9b for SiC and G/SiC, respectively.

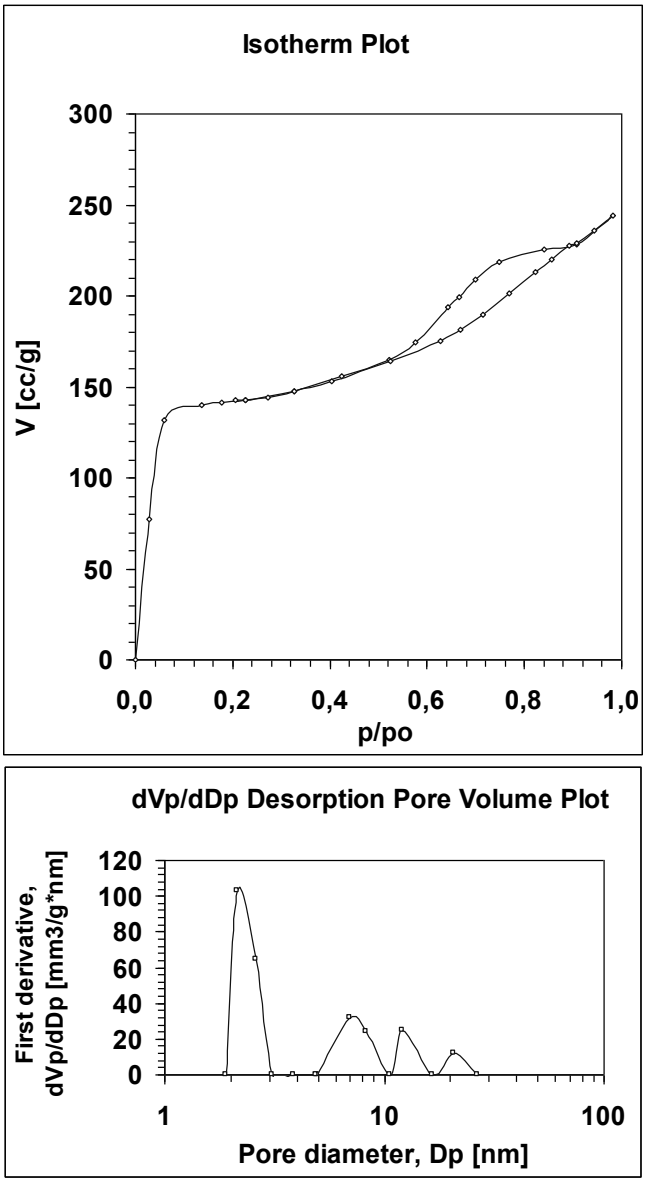

Figure II.19 *Nitrogen adsorption-desorption isotherm (a) and pore-diameter distribution (b) curves of G/SiC*

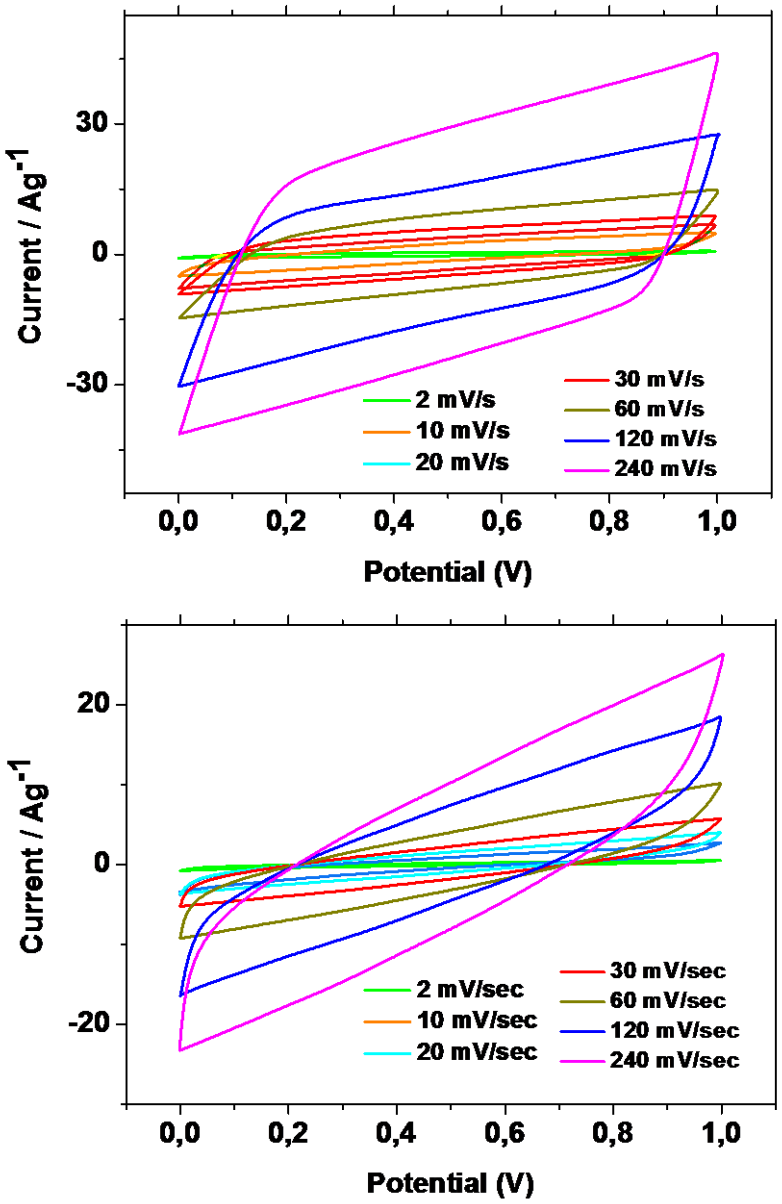

Figure II.20 *Cyclic voltammetry, in the range 0-1V, of SiC (a), G/SiC (b).*

These curves, for G/SiC, subtend a larger area and are closer to a rectangular shape than for SiC alone.

The specific capacitance was calculated from the discharge curves (Figure 21 and 22).

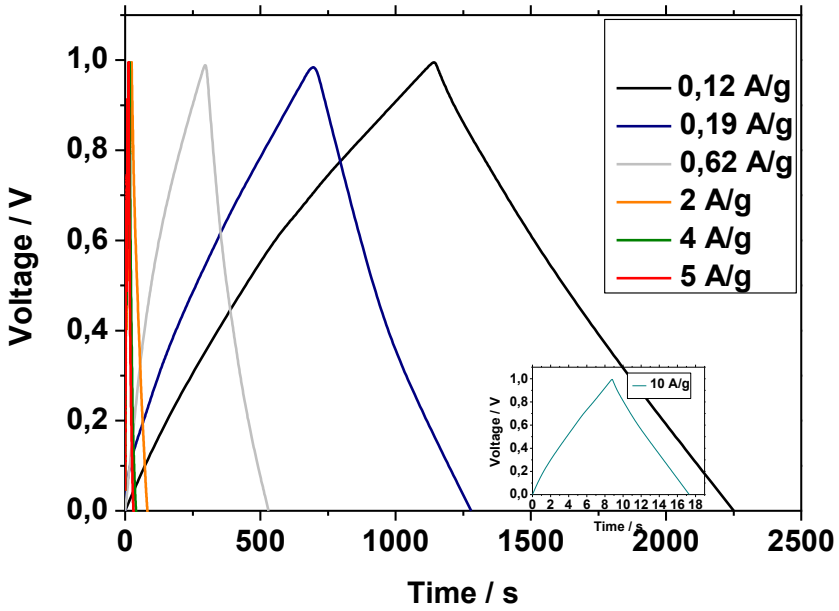

Figure II.21 *Galvanostatic charge/discharge curves of SiC (c)*

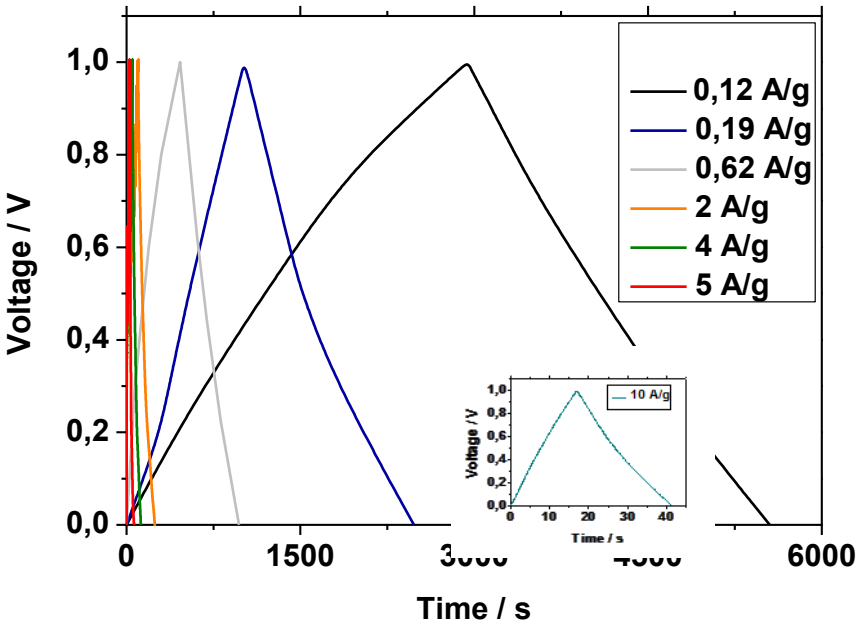

Figure II.22 *Galvanostatic charge/discharge curves of G/SiC*

In particular, the specific capacitance for G/SiC results almost three times that exhibited by SiC at the same A/g, (40 mF/cm2 (114.7 F/g) for our SiC

and 116 mF/cm2 (325.9 F/g) for G/SiC at 0.1 mA/cm2 (0.12 A/g)). The capacitances of the two electrodes at increasing current densities were shown in Figure 23.

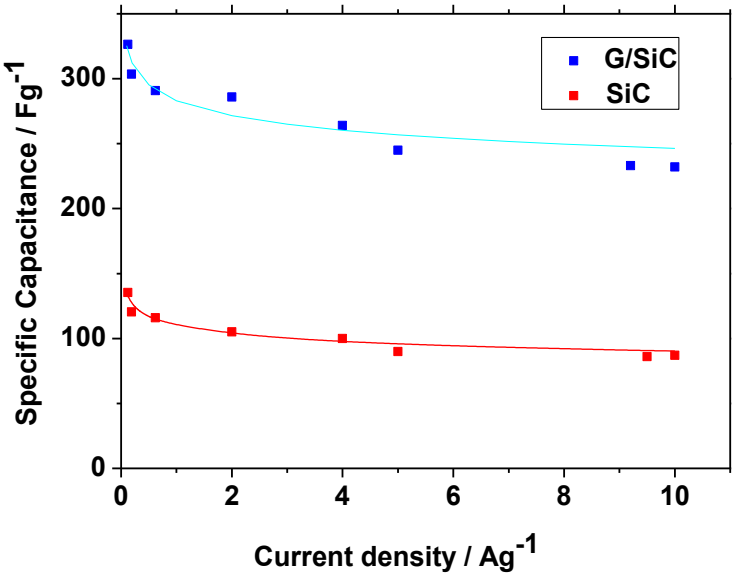

Figure II.23 Specific capacitance of SiC and G/SiC electrodes at different scan rate

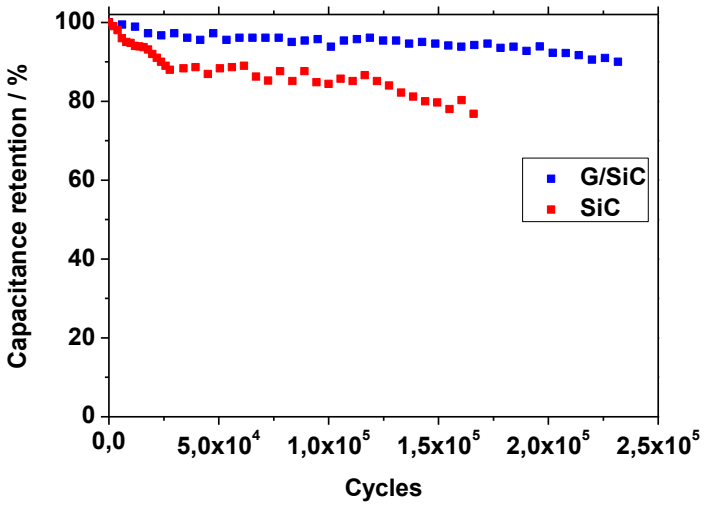

Figure II.24 *Capacitance retention at 4 A/g*

As it is expected the capacitances of both samples decrease from 0.12 A/g to 9 A/g due to the internal resistance of the electrode. On the other hand, the capacitances values are still 232 and 87 F/g for G/SiC and SiC, respectively at 10 A/g (see inserts in Figure 21 and 22). These results are probably due to a combination of factors, including: (i) the unique band gab observed for our SiC (ii) the highly graphene area exposed on the SiC filaments; (iii) the improved electrical transport and the contact interface stabilization due to graphene; (iv) the combination of micropores and mesopores, that permits the formation of EDLs and the electrolyte ions access;8 (v) an electrical coupling between the graphene and SiC.

Figure 24 shows the long cycle stability of SiC and G/SiC as evaluated at 4 A/g. After 1.2x105 cycles SiC electrode still retains about 85% of its initial capacitance showing good stability. On the other hand, G/SiC shows an improved stability.

The energy density and power densities were calculated by using the well-known equations.8 G/SiC shows very high energy density values form 91 Wh/kg to 68 Wh/kg in correspondence of a large power density range from 122 W/Kg to 5000 W/kg.

The cyclic voltammogramm (CV), in the range -0.5 - 0.5V, of G/SiC, is shows in Figure 25, giving the possibility to calculate a capacitance of 262 F/g also in this range.

Figure 25 shows the Nyquist impedance plots of SiC and G/SiC. The Nyquist plots show a straight line in the low-frequency region revealing good electrochemical capacitive properties. The 45° lines denote the feature of ion diffusion and are ascribed to the Warburg impedance. At high frequency the diameter of the semicircles correspond to polarization resistance or charge transfer resistance of the electrode, the G/SiC electrode with good conductivity shows smaller charge transfer resistance than the SiC sample. When the ordinate tend to zero, the abscissa (real part) evidences the total internal resistance, due to the electrolyte resistance, the intrinsic resistance of the active material and the contact resistances.

The ESR of G/SiC and SiC are 0.60 and 0.83 Ω, respectively.

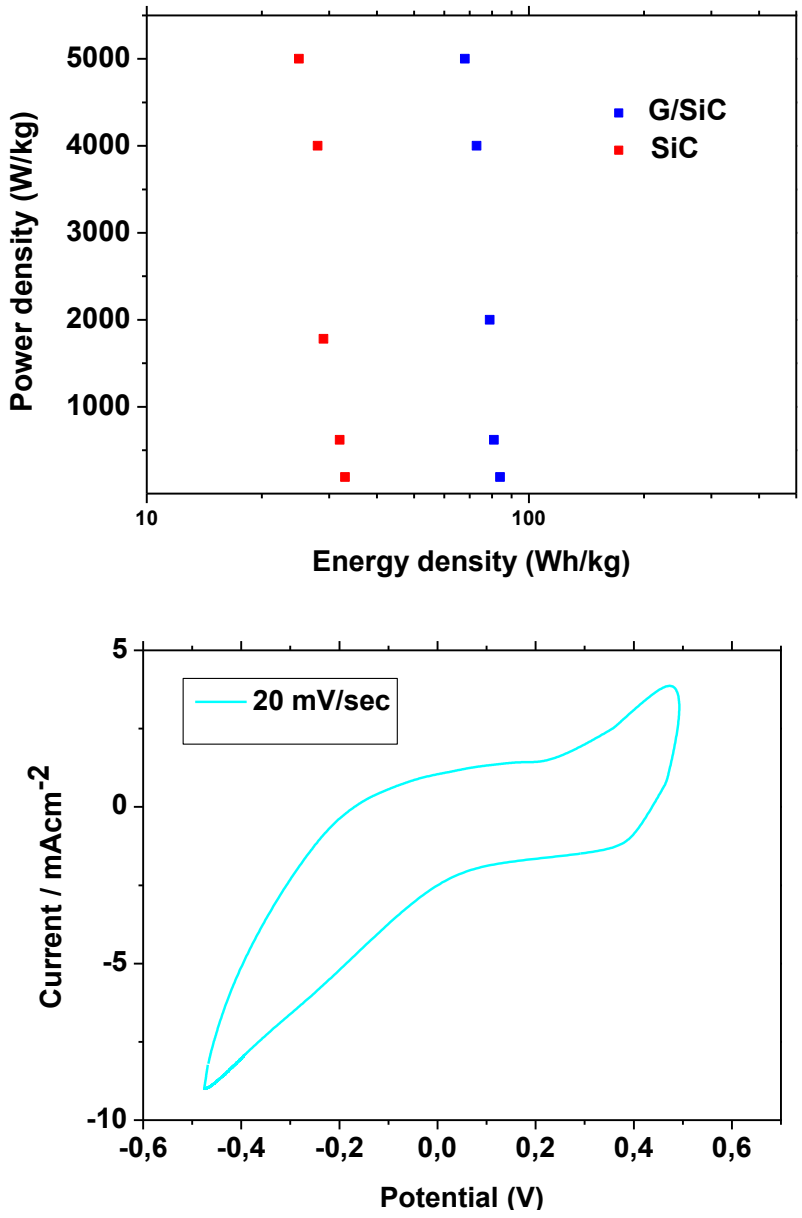

Figure II.25 *Ragone Plot for G/SiC and SiC (a). Cyclic voltammetry of G/SiC in the range -0.5-0.5 V*

Conclusion

3C-SiC powders were prepared from exhausted activated carbon and inexpensive silicon dioxide, by means of a carbothermal reduction reaction.

The nanowhiskers of SiC are about 1 μm in length and tens of nanometers in diameter, there are also a small number of larger particles. The corresponding electron diffraction pattern and the EDS spectrum confirm the cubic structure of the synthesised SiC.

Graphene and $C/SiO_2/SiC$ composite were prepared at atmospheric pressure on the 3C-SiC powders.

Graphene growth was obtained from an external sources of carbon, in particular by methane/hydrogen chemical vapour deposition (CVD). The composite $C/SiO_2/SiC$ was obtained by thermal annealing under few percents of oxygen in nitrogen. SiC powders and the advanced materials obtained were carefully characterized by the combining use of different techniques.

Three layers graphene were grown on the 3C-SiC surface, has evidenced by the TEM images and Raman Spectroscopy.

The nanofilaments after thermal annealing consist of a core shell structure with a sheath of about 20-30 nm thick. Chemical composition microanalysis, evidences the outer carbon sheath and the increased oxygen amount in the intermediate layer with respect to the core. The nanofilaments are composed of a 3C-SiC core, a SiO_2 intermediate layer, and an outer layer of graphitic carbon. Twisted graphene layers (about 13 are counted) with the typical (002) stacking of graphitic carbon are clearly visible in the outermost nanofilament layers.

Nanofilaments heterojunctions of few layer graphene/SiO2/SiC core shell structure with a sheath of about 20-30 nm thick have been prepared by a new easy designed procedure. Chemical composition microanalysis, evidences the outer carbon sheath and the increased oxygen amount in the intermediate layer with respect to the core. The nanofilaments are composed of a 3C-SiC core, a SiO_2 intermediate layer, and an outer layer of graphitic carbon. Twisted graphene layers (about 13 are counted) with the typical (002) stacking of graphitic carbon are clearly visible in the outermost nanofilament layers.

SiC powders were prepared from exhausted activated carbon and inexpensive silicon dioxide, by means of a carbothermal reduction reaction. The nanoparticles of SiC are about 1 μm in length and tens of nanometers in diameter, there are also a small number of larger particles. The corresponding electron diffraction pattern and the EDS spectrum confirm the cubic structure of the synthesised SiC. Graphene/SiC composite was prepared from external sources of carbon, at atmospheric pressure, on the SiC nanoparticles.

Three layers graphene were grown on the SiC surface, has evidenced by the TEM images and Raman Spectroscopy. The electrochemical characterization permits an efficient energy storage capability for both samples. In particular, the highly area exposed on the SiC nanofilament of the conductive graphene layer and probably an electrical coupling between graphene and SiC allow to improve the performances of the electrode.

Chapter III

Conductive carbon nanotubes for Thermal Management

Constant improvements in power electronics has generated an unavoidable increase in power density, created more waste heat, reduced the efficiency and lowered the durability. This issues become even more challenging when coupled with compact size, light weight and lower cost requirements. Planning how to manage the waste heat in the preliminary phase of board layout design appears fundamental to mitigate the effects of a non-correct thermal management. High electron mobility transistors (HEMTs) with their high-power, high frequency and high temperature applications show a temperature increase, in channel region over 100°C than ambient temperature, as also confirmed by Wang et al. (Wang et al., 2013). Often, significant thermal contact resistance at multiple interfaces from the die through the heat spreader to the heat sink remains a challenging problem. Limited cooling capabilities give rise to localized heating spots, known as hotspots, at highly active regions of a chip as confirmed by Zhang et al. (Zhang et al., 2011). So, the possibility to have a connection medium which can itself improve heat dissipation between the substrate and the heat spreader appears the best solution: chip reliability improves and the thermal crosstalk through the channel region can be reduced.

Carbon nanotubes (CNTs) have been investigated as a thermal spreader medium to balance the temperature across the chip and reduce peak temperature. Indeed CNTs have excellent characteristics, such as high current handling capability and low resistance (Horibe et al, 2004), they also exhibit high thermal conductivity (Kim et al., 2001; Shioya et al., 2007), and high aspect structure (Soga et al., 2009).

Lu et al. (Lu et al., 2012) validated the possibility to use CNTs bumps in a flip-chip configuretion to allow direct integration into devices, reducing the thermal contact resistance at interfaces and avoiding larger resistance due to defects via solders bumps. Indeed covalent bonds could improve adhesion and minimize thermal resistance, as

stated by Kaur et al. (Kaur et al., 2014). The flip-chip connection has many advantages compared to the wire bonding connections in term of thermal and electrical aspects.

Here we report an experimental, modelling and theoretical study of CNT growth and connection on a chip device with a flip chip configuretion used to improve thermal management performances, in order to elaborate board design analysis. In particular, CNTs growth by a Chemical Vapour Deposition (CVD) for the first time on an AlN substrate, typically used for microelectronic applications, was obtained, and the thermal conductivity measured. The mechanism of CNT thermal management by COMSOL modelling was explored too.

Carbon nanotubes synthesis: experimental, results and discussion.

Carbon Nanotubes forests were prepared by CVD in a continuous flow microreactor. Before the synthesis, an optimized catalytic substrate, common deposition techniques resulted in CNTs forests peeling off, was obtained by deposition of nickel ferrites nanoparticles (NPs) (Altavilla et al., 2009) on aluminium nitride. Indeed, the "wet chemistry" approach used for the synthesis of the nanoparticles results in a nanohybrid of nickel ferrites NPs covered by hydrophobic organic chains improving wettability and adhesion on the AlN substrate.

Acetylene CVD, acetylene was chosen because permits thanks to its reactivity to growth CNT at lower temperature, was carried out in a continuous flow microreactor fed by acetylene–helium gas mixture. The temperature of catalyst bed was measured with a K thermocouple located inside a third coaxial quartz tube. The reactor was heated by an electrical oven, whose temperature is controlled by a temperature programmer–controller (Eurotherm 2408). Cylinder gases (99.998 pure acetylene and 99.9990 pure helium) were mixed to obtain the stream to feed the reactor. Constant flow rate of each gas was provided by mass flow controller. The reactor temperature was increased from 298K up to 873K under helium flow and then a 200 cm^3/min flow rate of 10% acetylene in helium was introduced in the reactor during 5 min. After this time, the feed flow was stopped and the reactor was cooled down to room temperature under helium flow.

The images in Figure 1 obtained with a scanning electron microscope (SEM) LEO 420 allow the observation of nanotubes inside the forest. Their outer diameters are in the range 20-50 nm (Figure 1b), their length reached few millimetres at increasing time (Figure 1c).

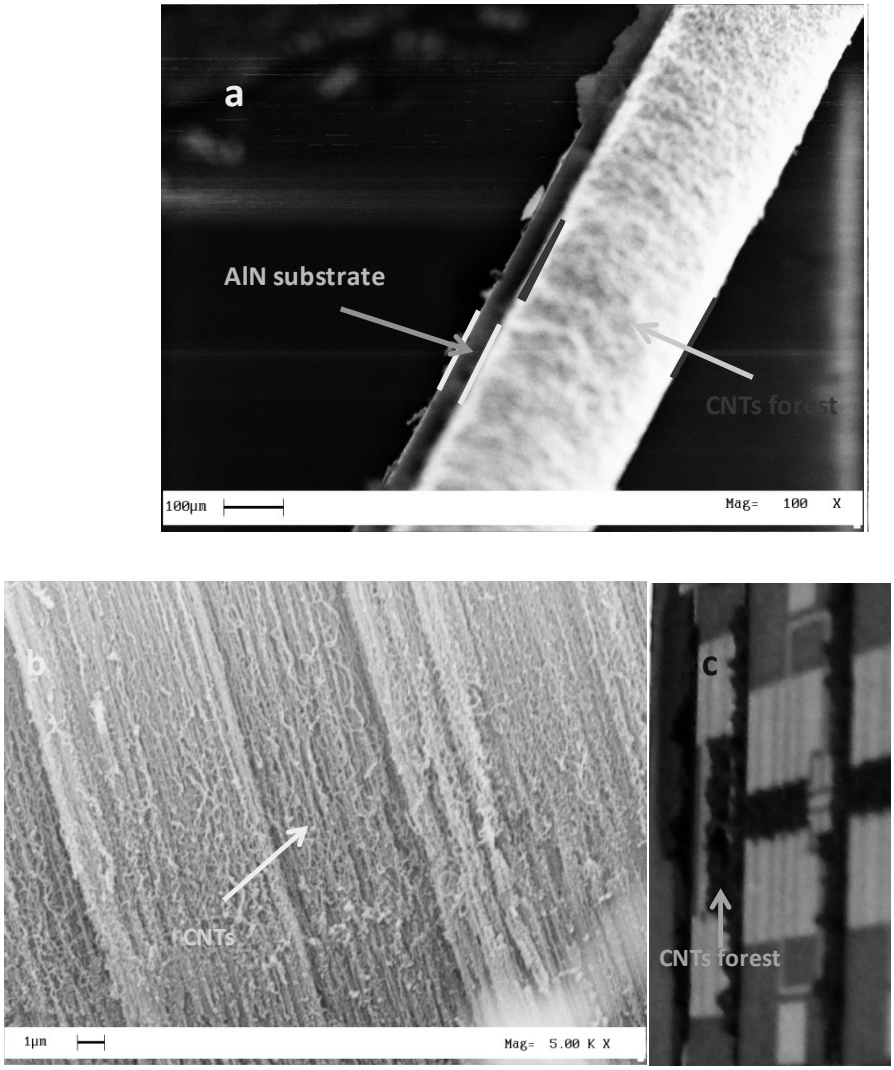

Figure III.1 *SEM image of AlN covered by a CNT forest (a, b). Photo of AlN covered by CNT forests, Au covers some areas of the devices*

In order to estimate our CNTs thermal conductivity we analyse Raman spectra finger print of an isolated CNT obtained at 873K for 5 min (Figure 2). G peak in the graphite based materials spectra manifest a strong temperature dependence and allows to monitor the local temperature change produced by the variation of the laser excitation power as stated by Balandin et al. (Balandin et al., 2008). Local temperature rise as a function of the laser power can be utilized to extract the value of the thermal conductivity. $K = 1/(2\pi h)(\Delta P/\Delta T)$, where h is CNT thickness and the local temperature rise ΔT is due to the changing heating power $\Delta P = P_2 - P_1$. Because the excitation

power levels are relatively low, the G peak position linearly depends on the sample temperature $\omega = \omega_o + x_G T$. The final expression for the thermal conductivity in the radial heat wave case can be written as:

$$K = x_G \, 1/(2h\pi)(d\omega/dP)^{-1}$$

where $d\omega$ is a small shift in the G peak position due to the variation dP in the heating power on the sample surface. We obtained a value of 1698,5 W/mK.

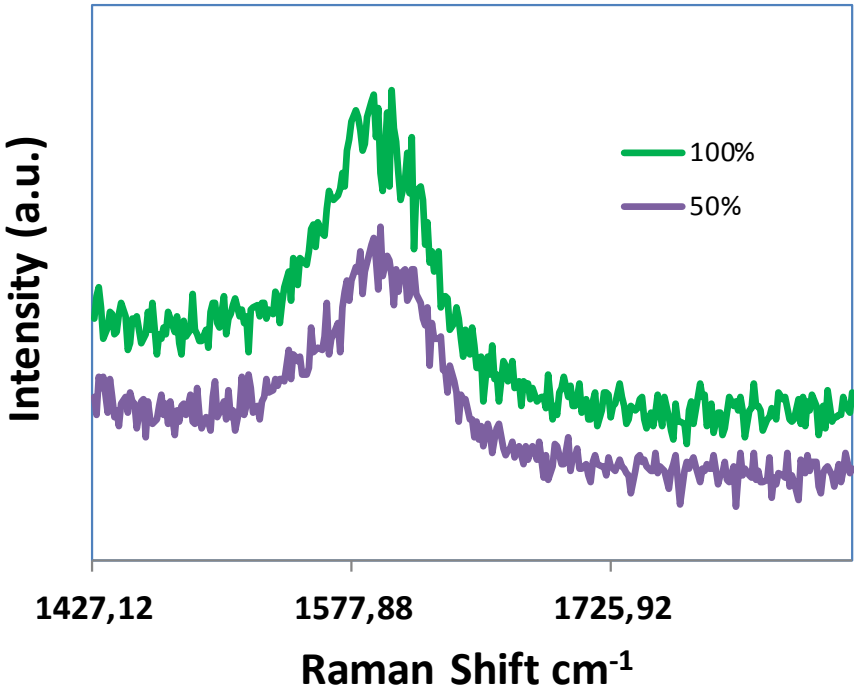

Figure III.2 *Raman spectra at two different laser power*

Numerical analysis

The numerical analysis of heat transfer in the flip-chip device has been conducted assuming the configuretion and geometrical characteristics shown in figure 3: chip layout (pHEMT FET in GaN / Sapphire technology); chip size: 1 mm x 0.8 mm x mm 0.33; gate area: 6 rectangular fingers (100 µm x 1 µm) at 50 µm distance; sapphire substrate thickness: 329 µm; FET mounted upside down, directly interconnected to the substrate through 6 bumps of carbon nanotubes: bumps dimensions are 100 x 40 µm and variable thickness: 10, 20, 30 microns; AlN substrate 1 cm x 1 cm x 0.6 mm.

As general approach, the following heat transfer equation has been considered in each subdomain:

$$\rho_i Cp_i \frac{\partial T_i}{\partial t} - \nabla \cdot (k_i \nabla T_i) = Q_i \qquad (2)$$

where the subscript i refers to the subdomain in which, time-by-time, the heat transfer equation is solved. At the boundary between two materials, continuity of temperature and heat flux has been considered. The heat source term Qi has been considered null everywhere except in the fingers.

The heat transfer equation (eq. 2) has been solved in fully 3D domain (constituted by subdomains representing the various materials involved in the flip-chip structure) and at stationary conditions, applying – as boundary conditions – a convective heat flux toward the air surrounding the flip-chip device, except for lower surface of AlN layer where a constant temperature of 313.15 K was imposed. Of course, each component has been characterized by its own thermal conductivity. In the case of fingers, a further term of heat source has been introduced, to take into account the 3 W of power generated by the fingers themselves. The set constituted by the heat transfer equation and boundary conditions equations has been compiled and solved by means of commercial package COMSOL 5.2, using a mesh discretization to solve from 46843 to 200000 degrees of freedom. The mathematical set has been solved in the fully 3D domain in order to reduce errors coming from 2D approximation in term of influence of gate width on self-heating end in terms of fingers number for the total thermal contribution (Bertoluzza et al., 2009). The three points in the figure below are used as temperature monitoring points. The positions were chosen basing on the criticality of spatial portion in order to maximize their thermal behaviour.

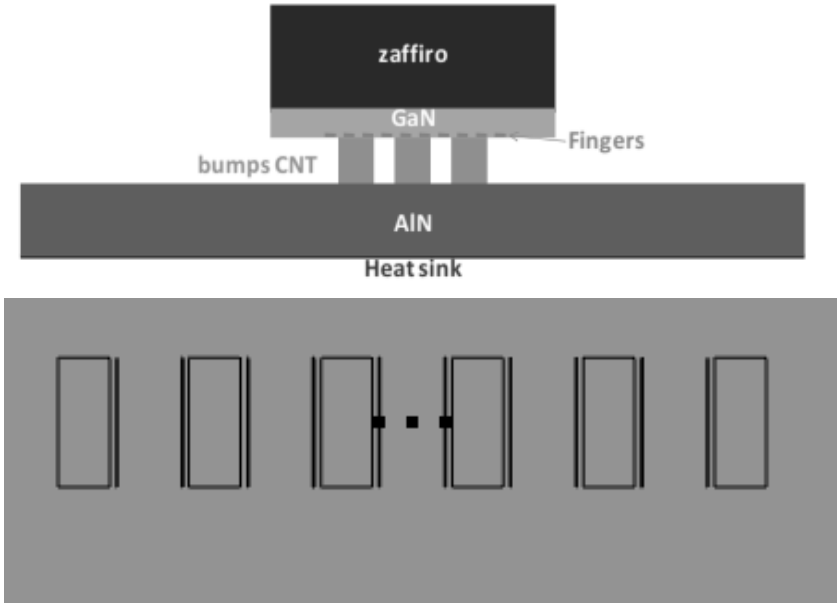

Figure III.3 *Sketch of flip-chip and planar view of the device.*

The assumptions made for the simulations were: the device DC alimented; power dissipated by fingers: 3 Watt; the heat sink was simulated by the use of a wall at constant temperature of 40°C; CNT thermal conductivity was varied in the range: 60-3000 W/(m K). Chip was installed in the centre of the package. The scope of the simulations was to verify the cooling capacity of the heat spreaders in different configuretions by monitoring chip temperature. Heat transfers through the mounted package to the surroundings for conduction and heat dissipates from all air-exposed surfaces for natural heat convection, which is modelled according to Newton law. The considered heat transfer model, based on Fourier law for heat conduiction, can efficiently and accurately describe the thermal effects at feature length scales much longer than the mean free path of phonons (i.e., 200-300 nm in silicon) as also investigated by Zhang et al. (Zhang et al., 2011).

In the nano-meter regime, where the mean free path of phonons approaches device feature scale, ballistic phonon transport is the primary heat transfer mechanism. Since the Fourier model cannot model this phenomenon accurately, other techniques such as the Gray phonon Boltzmann transport equation (BTE) under the relaxation time approximation can be used to model the nanometer device regions. On the other hand, our dimensions are larger than mean free path of phonons so the Fourier model can accurately describe our device's thermal properties.

In order to evaluate nanotubes thermal influence, we conducted four simulations set by varying the followings parameters:

- CNT's connection height,
- CNT's thermal conductivity;
- CNT number and spatial position
- device's thermal conditions.

CNT height significantly influences the capacity of heat dissipation in the various points of the channel region. Results show that the bumps of smaller thickness (10 μm) facilitate the dispersion of heat towards the substrate of aluminium nitride. Figure 4 reports the temperature results of the three configuretions (20, 30, 40 microns' bumps) along x coordinate. The figure shows the simulations conducted using a k value of 60 W/(m K). No substantial differences in term of thermal crosstalk between the different configuretions are found. The lowest temperature was recorded, as expected considering the increased conduction path, in the case in which the height of the connecting bumps is the smallest. This effect is more evident for low values of thermal conductivity (about 60 W/m K).

Increasing thermal conductivity, thermal management is improved, all the monitoring points show a smaller temperature value but this effect is mitigated after a given value of k: the temperatures reach practically constant values at a thermal conductivity of 1200 W/(m K), see Figure 4 that shows the temperature of monitoring centre point. Moreover, our simulations show that after this value, bumps thickness has no influence on the monitor points temperature. It can be seen from the figures that CNTs let the temperature decrease of about 30 °C in few microns length.

Our simulation evidences also that CNT bump width influences heat dissipation ability for low values of thermal conductivity (60 W/m K); after a value of about 1250 W/mk, a different bump's width doesn't change thermal profile.

In order to improve conduction process and prevent risk caused from negative-bias temperature instability a simulation was also performed covering all chip surface with a fine layer of gold. All temperatures are much lower than that measured during previous simulations, see Figure 5. The Au layer results able to reduce the occurrence of peak over-temperature along the chip, increasing the heat dissipation area and improving the dissipation efficiency in a simplest way than the complex 3D CNT architecture reported by Zhang et al. (Zhang et al., 2011).

For a k value of 300 W/mk, the maximum junction temperature gained in the chip is less than 85°C, see Figure 6. In all the conditions the highest temperatures were reached in the center of the package, likely due to its symmetry. Therefore the central points are the critical ones for reliability issues.

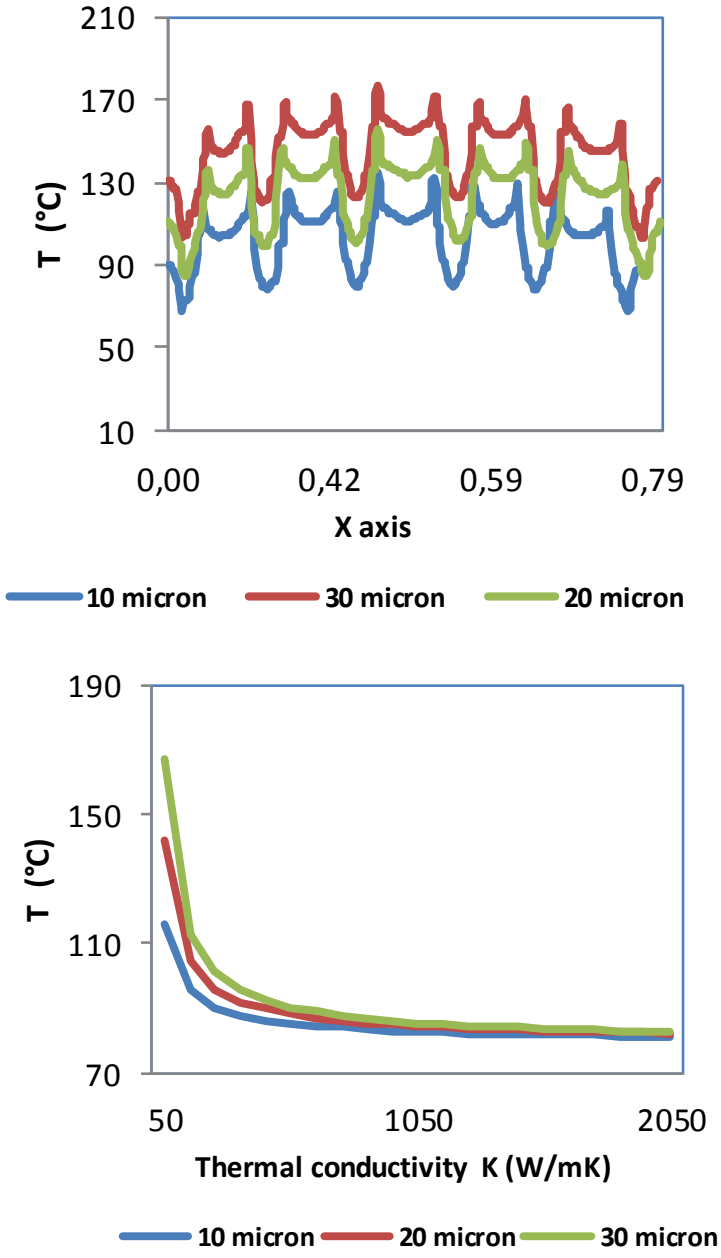

Figure III.4 *Temperature profile along x axis gained at different bumps heights and with K=60 W/mk. Temperature profile Vs thermal conductivity at the device centre for different bumps' connection height.*

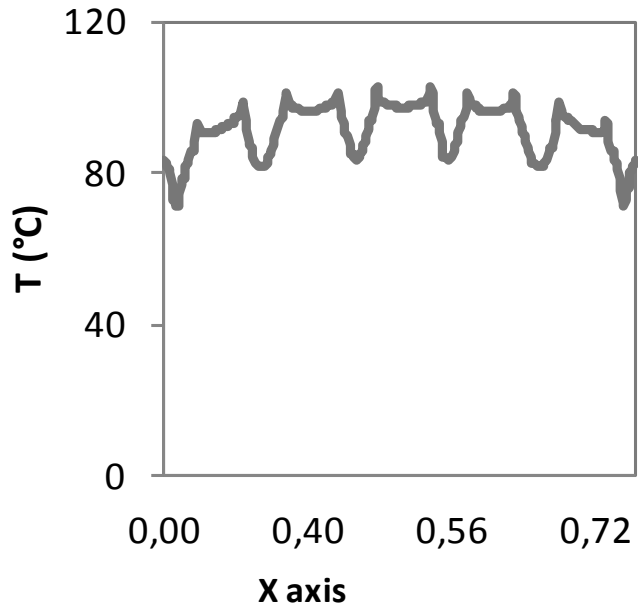

Figure III.5 *Temperature profile along x axis at bumps heights of 10 µm, with K=60W/mk and Au layer*

We also tested the introduction of a major number of CNT's bumps with a K value of 300 W/mK, see Figure 7 left side. Increasing bumps number, thermal management results improved, in terms of maximum temperature reached in the device as junction temperature and maximum temperature differences along x axis, see Figure 7 right side.

Considering the case of more devices working together, we performed also simulations in the absence of natural convection towards lateral walls of the device. We found that also in this case CNT's bumps showed improved thermal management performance also if compared with a common flip chip device, with Cu6Sn5 solders bumps in a forced convection regime, 1 m/s, of transformer oil at 273 K.

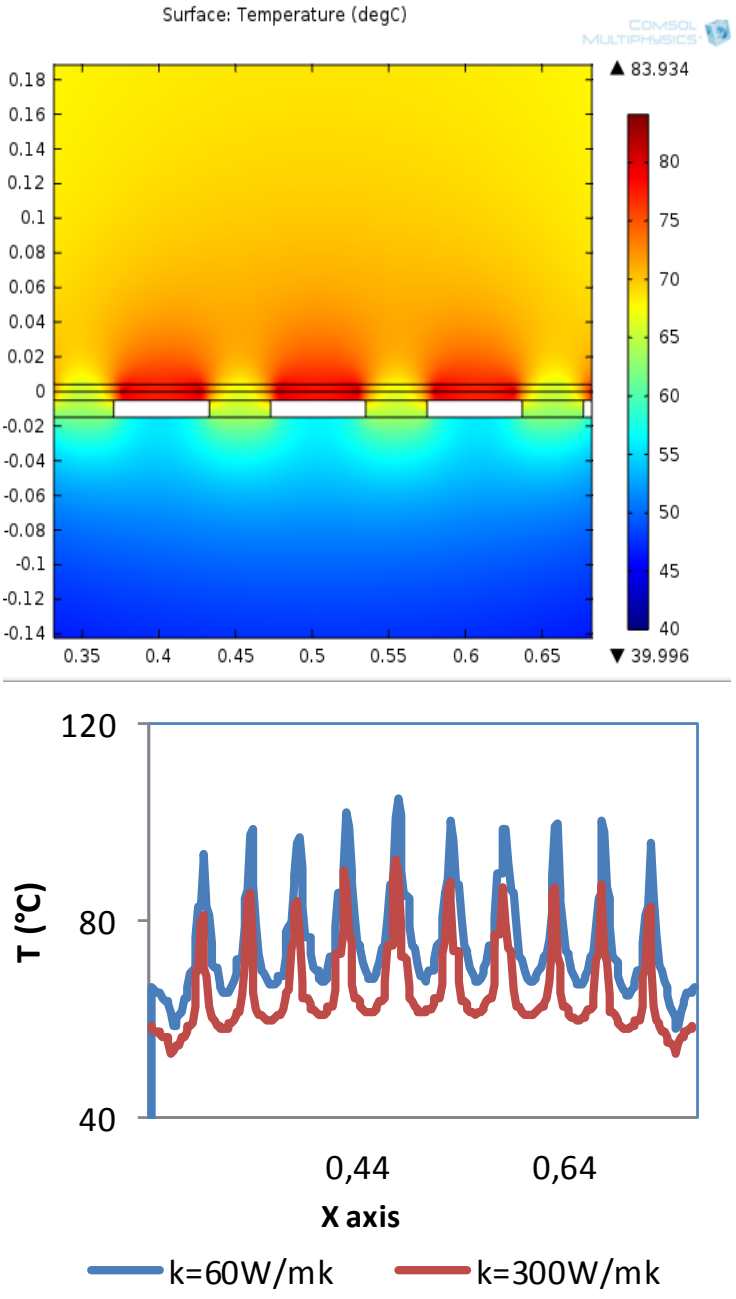

Figure III.6 Left side: device Temperature with bumps' connection height of 10 µm and with Au layer Kbumps=300 W/mk. Right side: Temperature profile along x coordinate (bumps height of 10µm).

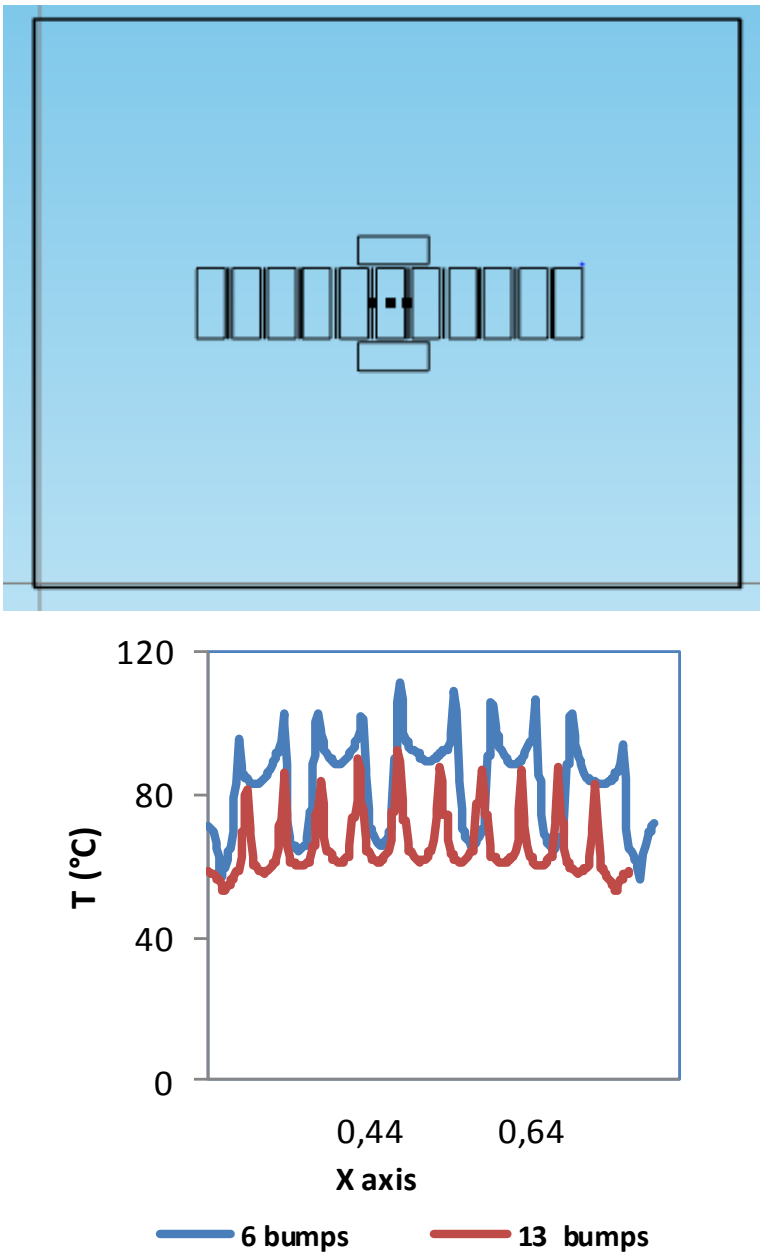

Figure III.7 *Temperature result differences between 6 and 13 bumps simulations*

Conclusions

CNTs have been successful grown on a AlN substrate and their conductivity measured with the help of Raman spectra. Simulation results showed significant temperature reduction at lower bumps height and in presence of an Au layer. From the simulations it can be stated that CNT width influences heat dissipation for low values of thermal conductivity (60 W/m K); after a value of about 1250 W/mK, different bump's width doesn't change significantly thermal profile. Increasing bumps number, thermal management is improved. Considering the case of more devices working together, our simulation demonstrate that also in this case the effect of CNT's bumps is helpful. Furthermore, the configuretion including CNT bumps gives better results than that obtained using a common flip chip device, with Cu6Sn5 solders bumps in a forced convection regime, 1 m/s, of transformer oil at 273 K. The best result was obtained in the configuretion with Au layer and 10 μm connection height CNTs, resulting in a better hotspots management.

References

- Afanasev, V.V. Bassler, M. Pensl, G. Schulz M..(1997) *Intrinsic SiC/SiO2 interface states*. Phys Status Solidi A 162 p.321-337.
- Afanasev, V.V. Stesmans, A. Bassler, M. Pensl, G. Schulz, M.J. Harris C.I..(1996) *Elimination of SiC SiO_2 interface states by preoxidation ultraviolet-ozone cleaning*. Appl Phys Lett 68 p.2141-2143.
- Alper, J. P.; Kim, M. S.; Vincent, M.; Hsia, B.; Radmilovic, V.; Carraro, C.; Maboudian, R. (2013). *Silicon carbide nanowires as highly robust electrodes for micro supercapacitors*. J. Power Sources. , 230, 298-302.
- Alper, J. P.; Vincent, M.; Carraro, C.; Maboudian, R. (2012) *Silicon carbide coated silicon nanowires as robust electrode material for aqueous micro-supercapacitor*. Appl. Phys. Lett. , 100, 163901-163904.
- Aristov, V.Y. Urbanik, G. Kummer, K.. Vyalikh, D.V. Molodtsova, O.V Preobrajenski, A.B. et al. (2010) *Graphene Synthesis on Cubic SiC/Si Wafers. Perspectives for Mass Production of Graphene-Based Electronic Devices*. Nano Lett, p.992-995
- Bechelany, M. Brioude, A. Cornu, D. Ferro, G. Miele P. (2007) *A Raman Spectroscopy study of individual SiC nanowires.* Adv Funct Mater 17 p.939-943.
- Berger C., Song Z., Li X., Wu X., Brown N., Naud C., et al.(2006) *Electronic confinement and coherence in patterned epitaxial graphene.* Science 312 p.1191-1196.
- Bertoluzza F., Delmonte N., Menozzi R., (2009), *Three-dimensional finite-element thermal simulation of GaN-based HEMTs, Microelettron. Reliab.*, p.468-473.
- Biedermann, L. B.,. Bolen M. L, Capano, M. A. Zemlyanov D., and Reifenberger, R. G. (2009) *Insights into few-layer epitaxial*

graphene growth on 4H-SiC(0001-) substrates from STM studies. Phys. Rev. B 79 125411.

- Boehm H. P., Clauss A., Hofmann U., Fischer G. O., Zeitschrift Für Naturforschung B 17 (1962) 150.
- Cai, K.F. Zhang, A.X. Yin, J.L.. 2007) *Ultra-thin and ultra-long SiC/SiO2 nanocables from catalytic pyrolysis of poly(dimethylsiloxane)*. Nanotechnology 18 509901.
- Chaika, A.N. Molodtsova, O.V. Zakharov, A.A. Marchenko, D. Sánchez-Barriga, J. Varykhalov, A. et al. (2013) *Continuous Wafer-Scale Graphene on cubic-SiC(001)*. Nano Research, p.562-570.
- Ciambelli, P. Sarno M., Gorrasi, G. Sannino, D. Tortora, M. Vittoria V..(2005) *Preparation and physical properties of carbon nanotubes-PVA nanocomposites*. J Macromol Sci B, p.779-795.
- Dai L., Chang D.W. , Ba J.B., Lu W., Small 8 (2012) 1122.
- Di Bartolomeo, A. Sarno, M. Giubileo, F. Altavilla, C. Iemmo, L. Piano S., et al. (2009) *Multiwalled carbon nanotube films as small-sized temperature sensors*. J Appl Phys, p. 064518.
- Dresselhaus, M.S.; Dresselhaus, G. and Eklund, P.C.(1996) *Science of fullerenes and carbon nanotube*, Academic Press, San Diego
- Emtsev K.V., Bostwick A., Horn, K. Jobst, J. Kellogg, G.L. Ley L., et al. (2009) *Towards wafer-size graphene layers by atmospheric pressure graphitization of silicon carbide*. Nature Mater 8 p.203-207.
- Emtsev K.V., Speck F., Seyller Th., Ley L., Riley J.D.. (2008) *Interaction, growth, and ordering of epitaxial graphene on SiC{0001} surfaces: A comparative photoelectron spectroscopy study*. Phys Rev B 77 155303.
- Feng, Z.C. Tin, C.C. Hu, R. Williams, J. (1995) *Raman and Rutherford backscattering analyses of cubic SiC thin films grown on Si by vertical chemical vapor deposition*. Thin Solid Films 266 p.1-7.
- Forbeaux I., Themlin J., Debever J., Physical Review, B 58 (1998) 16396.
- Geim, A. K., Novoselov K.S. *The Rise of Graphene*. Nat Mater 6(2007) p.183-191.
- Gu, L. Wang, Y. Lu R, Wang, W. Peng X., Sha J.,. (2015) Silicon carbide nanowires@Ni(OH)2 coreeshell structures on carbon fabric for supercapacitor electrodes with excellent rate capability. J. Power Sources. 2015, 273, 479-485.

- Gu, L.; Wang, Y.; Lu, R.; Wang, W.; Peng, X.; Sha, J. (2015) *Silicon carbide nanowires@Ni(OH)2 coreeshell structures on carbon fabric for supercapacitor electrodes with excellent rate capability*. J. Power Sources., 273, 479-485.
- Guerét C., Daroux M., Billaud F..(1997) *Methane pyrolysis: thermodynamics*. Chem Eng Sci, p.815-827.
- Guo T., Nikolaev P., Thess A., Colbert, D.T.. Smalley R.E (1995) *Catalytic growth of single-walled nanotubes by laser vaporization*, Chemical Physics Letters p 49-54.
- Handa H., Takahashi R., Abe S., Imaizumi K., Saito E., Jung M.H., et al.(2011) *Transmission Electron Microscopy and Raman-Scattering Spectroscopy Observation on the Interface Structure of Graphene Formed on Si Substrates with Various Orientations*. J J Appl Phys 50 04DH02.
- Hernandez Y., Nicolosi V., Lotya M., Blighe F.M., Sun Z., De S., et al.(2008) *High-yield production of graphene by liquid-phase exfoliation of graphite*. Nature Nanotech 3 p.563-568.
- Horibe M., Nihei M., Kondo D., Kawabata A., Awano Y.,(2004), *Influence of Growth Mode of Carbon Nanotubes on Physical Properties for Multiwalled Carbon Nanotube Films Grown by Catalystic Chemical Vapor Deposition*, Jpn. J. Appl. Phys. p.7337-7341.
- Htun M.T. Aung, J. Szmidt, M. Bakowski.(2002) *The study of thermal oxidation on SiC surface*. J Wide Bandgap Mater, p.313-318.
- Hwang J., Shields V.B., Thomas C.I., Shivaraman S., Hao D., Kim M., et al. (2010) *Epitaxial growth of graphitic carbon on C-face SiC and Sapphire by chemical vapor deposition (CVD).* J Cryst Growth 312 p.3219-3224.
- IJ Reserch, Inc. Thermal Management
- Jacobson, N.S..(1993) *Corrosion of silicon-based ceramics in combustion*. J Am Ceram Soc 76; p.3-28.
- Katharria, Y.S. Kumar, S. Prakash, R. Choudhary, R.J. Singh, F. Phase D.M., et al. (2007) *Characterizations of pulsed laser deposited SiC thin films*. J Non-Cryst Solids 353 p.4660-4665.
- Kaur S., Raravikar N., Helms B.A., Prasher R., Ogletree D.F., (2014), *Enhanced thermal transport at covalently functionalized carbon nanotube array interfaces*, Nat. Comm, p. 1-8.

- Kim P., Shi L., Majumdar A., McEuen P. L.,(2001), *Thermal Transport Measurements of Individual Multiwalled Nanotubes*, Phys. Rev. Lett., p. 215502-215506.
- Langmuir I.. *Convection and conduction of heat in gases*. (1912) Phys Rev (Series I) 34 p. 401-422.
- Li, Y. Bando, Y. Golberg. D. (2004) *SiC–SiO2–C Coaxial Nanocables and Chains of Carbon Nanotube–SiC Heterojunctions*. Adv Mater, p.93-96.
- Lu X., Shi T., Xia Q., Liao G.,(2012), *Thermal conduction analysis and characterization of solder bumps in flip chip package*, Appl. Therm. Eng., p.181-187.
- Luthra, K.L..(1991) *Some new perspectives on oxidation of silicon carbide and silicon nitride.* J Am Ceram Soc 74 p.1095-1103.
- Malard, L.M. Pimenta, M.A. Dresselhaus, G. Dresselhaus M..S.(2009) *Raman spectroscopy in graphene*. Phys Rep, p.51-87.
- Michon, A. Largeau, L. Mauguin, O. Ouerghi, A. Vezian, S. Lefebvre, D.et al. (2012) *Graphene growth using propane-hydrogen CVD on 6H-SiC(0001): temperature dependent interface and strain*. Phys Status Solidi (c) 9 p.175.
- Michon, A. Roudon, E. Portail, M. Jouault, B. Contreras, S. Chenot, S.et al. (2012) *Structural and electrical properties of graphene films grown by propane/hydrogen CVD on 6H-SiC(0001).* Mater Sci Forum 625 p.717-720.
- Michon, A. Vézian, S. Ouerghi, A. Zielinski, M. Chassagne, T. Portail. M. (2010) *Direct growth of few-layer graphene on 6H-SiC and 3C-SiC/Si via propane chemical vapor deposition*. Appl Phys Lett 97 171909.
- Michon, A. Vézian, S. Roudon, E. Lefebvre D., Zielinski, M. Chassagne, T. et al. (2013) *Effects of pressure, temperature, and hydrogen during graphene growth on SiC(0001) using propane-hydrogen chemical vapor deposition* J Appl Phys 113 203501.
- Mieskowski D.M.,. Mitchell, T.E Heuer A.H..(1984) *Bubble formation in oxide scales on SiC.* J Am Ceram Soc 67 p.C17-C18.
- Moreau, E. Ferrer, F.J. Vignaud, D. Godey S., Wallart X.. (2010) *Graphene growth by molecular beam epitaxy using a solid carbon source*. Phys Status Solidi A 207 p.300-303.
- Norimatsu W., Takada J., Kusunoki M.. (2011) *Formation mechanism of graphene layers on SiC (000¯1) in a high-pressure argon atmosphere*. Phys Rev B 84 035424.

- Ohta T., Bartelt N.C., Nie, S. Thürmer, K. Kellogg G.L.. (2010 *Role of carbon surface diffusion on the growth of epitaxial graphene on SiC*. Phys Rev B 81 121411(R).
- Ohta, T. Bostwick A., Seyller T., Horn K., Rotenberg E..(2006) *Controlling the electronic structure of bilayer graphene*. Science 313 p.951-954.
- Oliveira M.H., Schumann T., Fromm F., Koch R., Ostler M., Ramsteiner M., et al. (2013) *Formation of high-quality quasi-free-standing bilayer graphene on SiC(0001) by oxygen intercalation upon annealing in air*. Carbon 52 p.83-89.
- Oshima C., Itoh A., Rokuta E., Tanaka T., Solid State Communications 116 (2000) 37.
- Palmer, H.B. Hirt T.J. (1963) *The activation energy for the pyrolysis of methane.* J Phys Chem 67 p.709-711.
- Panda, S.K. Sengupta, J. Jacob, C. (2010) *Synthesis of Beta-SiC/SiO2 Core-Sheath nanowires by CVD technique using Ni as Catalyst*. J Nanosci Nanotech, p.3046-3052.
- Pultz W.W.,(1967) *Temperature and Oxygen Pressure Dependence of Silicon Carbide Oxidation*. J Phys Chem 71 p.4556-4558.
- Riedl C., Coletti C., Iwasaki T., Zakharov A.A., Starke U.. (2009) *Quasi-Free-Standing Epitaxial Graphene on SiC Obtained by Hydrogen Intercalation*. Phys. Rev. Lett. 103 246804.
- Riedl C., Starke U., Bernhardt J., Franke M., Heinz K..(2007) *Structural properties of the graphene-SiC(0001) interface as a key for the preparation of homogeneous large-terrace graphene surfaces*. Phys Rev B 76 245406.
- Robinson J., Weng, X. Trumbull, K. Cavalero, R., Wetherington, M. Frantz E., et al. (2010 *Nucleation of Epitaxial Graphene on SiC(0001).* ACS NANO 4 p.153-158.
- Ryoo, K.S. Kim, T.D. Kim. Y.H. (1999) *Regeneration of exhausted activated carbon by a countercurrent oxygen reaction*. Bull Korean Chem Soc, p.1447-1450.
- Sarno M., Cirillo C., Ciambelli P.. (2014) *Selective graphene covering of monodispersed magnetic nanoparticles*. Chem Eng J 246 p.27-38.
- Sarno M., Cirillo C., Piscitelli R., Ciambelli P.. (2013) *A study of the key parameters, including the crucial role of H_2 for uniform graphene growth on Ni foil.* J Mol Catal A-Chem 366 p.303–314.
- Sarno, M. Sannino, D. Leone, C. Ciambelli P.. (2012) *Evaluating the effects of operating conditions on the quantity, quality and*

catalyzed growth mechanisms of CNTs. J Mol Catal A-Chem, p.26-38.

- Sarno, M. Senatore A., Cirillo C., Petrone, V. Ciambelli P..(2014) *Oil lubricant tribological behaviour improvement through dispersion of few layer graphene oxide*. J Nanosci Nanotech 14 p.4960-4968.
- Schmeiber, D. Batchelor D.R., Mikolo, R.P. Halfmann O., Spez, A. L. (2001) *Oxide growth on SiC (0001) surfaces*. Appl Surf Sci, p.340-345.
- Science,287, 637–640.
- Shioya H., Iwai T., Kondo D., Nihei M. Awano Y.,(2007), *Evaluation of Thermal Conductivity of a Multi-walled Carbon Nanotube Using the ΔVgs Method*, Jpn. J. Appl.Phys., p.3139-3143.
- Silly. M.G.J. (2004) *Initial oxide/SiC interface formation on C-terminated β-SiC(100)c(2×2) and graphitic C-rich β-SiC(100) 1×1 surfaces*. J Vac Sci Technolog B, p.2226-2232.
- Soga I., Kondo D., Yamaguchi Y., Iwai T.,(2009), *Thermal Management for Flip-chip High Power Amplifiers utilizing Carbon Nanotube Bumps*, IEEE International Symposium on Radio-Frequency Integration Technology, p.221-224
- Song, Y. Dhar, S. Feldman, L.C. Chung, G. Williams J.R..(2004) *Modified deal and grove model for the thermal oxidation of silicon carbide.* J Appl Phys 95 p.4953-4957.
- Song, Y. Smith F.M.. (2002) *Phase diagram of the interaction of oxygen with SiC*. Appl Phys Lett 81 p.3061-3063.
- Stankovich, S. Dikin, D.A. Piner, R.D. Kohlhaas K.A., Kleinhammes, A. Y. Jia, et al.(2007) *Synthesis of graphene-based nanosheets via chemical reduction of exfoliated graphite oxide*. Carbon 45 p.1558-1565.
- Suenaga, K. Colliex, C. Demoncy, N. Loiseau, A. Pascard, H. Willaime, F. (1997) *Synthesis of Nanoparticles and Nanotubes with Well-Separated Layers of Boron Nitride and Carbon*. Science, p.653-655.
- Van Bommel A.J., Crombeen, J.E. Van Tooren A.. (1975) *LEED and Auger electron observations of the SiC(0001) surface*. Surf Sci 48 p.463-472.
- Vathulya, V.R. Wang, D.N. White, M.H..(1998) *On the correlation between the carbon content and the electrical quality of thermally grown oxides on p-type 6H–Silicon carbide*. Appl Phys Lett 73 p.2161-2163.

- Viroianadra C., Syvajarvi M., Yakimova R., Johansson L.I., Zakharov A., Balasubramanian T.. (2008) *Homogeneous large-area graphene layer growth on 6H-SiC(0001).* Phys Rev B 78 245403.
- Wang Y. H., Liang Y. C., Samundra G. S., Chang T. F., Huang G. H., Yuan L., Lo G. Q.,(2013), *Modelling temperature dependence on AlGaN/GaN power HEMT device characteristics*, Semicond. Sci. Technol. p.12, 125010
- Wang, S. Di Ventra, M. Kim, S.G. Pantelides S.T. (2001) *Atomic-scale dynamics of the formation and dissolution of carbon clusters in SiO2*. Phys Rev Lett 86 p.5946-5949.
- Yakobson, B.I. and Samsonidze, G. (2000c) Carbon,38, 1675–1680.
- Yakobson, B.I.; Brabec, C.J. and Bernholc, J. (1996a) Physical Review Letters; 76, 2511–2514.
- Yakobson, B.I.; Campbell, M.P.; Brabec, C.J. and Bernholc, J. (1997b) Comput. Mat. Sc. ,8, 341–348.
- Yang N., Zhuang, H. Hoffmann R., Smirnov W., Hees J., Jiang X. Nebel C. E., (2012) Electrochemistry of nanocrystalline 3C silicon carbide films. Chem.-Eur. J., 18, 6514-6519.
- Yoo J. J, Balakrishnan K., Huang J., Meunier V., Sumpter B. G., Srivastava, A. Conway, M. Reddy A. L. M, Yu J., Vajtai R., Ajayan P. M., (2011) Ultrathin Planar Graphene Supercapacitors. Nano Lett., 11, 1423–1427.
- Yu, M.F.; Lourie, O.; Dyer, M.; Moloni, K. and Kelly, T.(2000b)
- Zhang W., Huang J. Yang S., Gupta P.,(2011), *Case Study: Alleviating Hotspots and Improving Chip Reliability via Carbon Nanotube Thermal Interface, Design, Automation & Test* in Europe Conference & Exhibition p.1-6
- Zhang, Y. Gu, H. Suenaga, K. Iijima, S. (1997) *Heterogeneous growth of B-C-N nanotubes by laser ablation*. Chem Phys Lett, p.264-269.
- Zhang, Y. Suenaga, K. Colliex, C. Iijima S.. (1998) *Coaxial Nanocable: Silicon Carbide and Silicon Oxide Sheathed with Boron Nitride and Carbon*. Science, p.973-975.